

AperTO - Archivio Istituzionale Open Access dell'Università di Torino

The Iberia-Eurasia plate boundary east of the Pyrenees

This is a pre print version of the following article:

Original Citation:

Availability:

This version is available <http://hdl.handle.net/2318/1689817> since 2019-02-06T15:17:43Z

Published version:

DOI:10.1016/j.earscirev.2018.10.008

Terms of use:

Open Access

Anyone can freely access the full text of works made available as "Open Access". Works made available under a Creative Commons license can be used according to the terms and conditions of said license. Use of all other works requires consent of the right holder (author or publisher) if not exempted from copyright protection by the applicable law.

(Article begins on next page)

This is the author's final version of the contribution published as:

Tavani S., Bertok C., Granado P., Piana F., Salas R., Vigna B., Muñoz J.A. The Iberia-Eurasia plate boundary east of the Pyrenees. *Earth-Science Reviews*, 187 (2018), 314–337. <https://doi.org/10.1016/j.earscirev.2018.10.008>

The publisher's version is available at:

<https://www.sciencedirect.com/science/article/pii/S0012825218303040?via%3Dihub>

When citing, please refer to the published version.

Link to this full text:

<http://hdl.handle.net/2318/1689817>

The Iberia-Eurasia plate boundary east of the Pyrenees

Tavani S.¹, Bertok C.², Granado P.^{3,4}, Piana F.⁵, Salas R.^{4,6}, Vigna B.⁷, Muñoz J.A.^{3,4}

1 - Dipartimento di Scienze della Terra, dell'Ambiente e delle Risorse, Università Federico II, Napoli, Italy.

2 - Dipartimento di Scienze della Terra, Università degli Studi di Torino, Torino, Italy

3 - Departament de Dinàmica de la Terra i de l'Oceà, Universitat de Barcelona, Barcelona, Spain

4 - Institut de Recerca Geomodels, Universitat de Barcelona, Barcelona, Spain

5 - CNR-IGG Torino, Italy

6 - Departament de Mineralogia, Petrologia i Geologia Aplicada, Universitat de Barcelona, Barcelona, Spain

7 - Dipartimento di Ingegneria dell'Ambiente, del Territorio e delle Infrastrutture, Politecnico di Torino, Torino, Italy

Corresponding Author: Stefano Tavani. stefano.tavani@unina.it

Keywords: Bay of Biscay-Pyrenean Rifting; Briançonnais; Extensional deformation; Transfer zones; Plate kinematics

Highlights

The mid-Cretaceous Marguareis extensional system of the Western Alps is introduced

This system forms part of the eastern portion of the Iberia-Eurasia plate boundary

This eastern portion included structures of the SE France basin

The Early to mid-Cretaceous plate margin had a purely divergent movement

60
61
62
63 **Abstract**
64

65 In this work we provide a reappraisal of the mid-Cretaceous extensional basins located to
66
67 the east of the Pyrenean mountain ranges, from the easternmost portion of Iberia to the
68
69 Briançonnais Domain of the Western Alps fold-and-thrust belt. These features are reviewed and
70
71 compared with those of the Bay of Biscay-Pyrenean rift, with the aim of defining geometry,
72
73 kinematics, timing and lateral extent of the eastern termination of the Mesozoic Iberia-Eurasia plate
74
75 boundary. Timing and direction of extension, as well as the style of structural segmentation in the
76
77 Bay of Biscay - Pyrenean rift, are similar to those of basins exposed to the east of the Pyrenean
78
79 mountain ranges. In both areas, the divergent movement between Iberia and Eurasia caused NNE-
80
81 SSW oriented extension recorded in WNW-ESE elongated Late Jurassic to mid-Cretaceous basins,
82
83 segmented by NNE-SSW trending transfer zones.
84
85

86 In this work we also individuate and introduce the eastern termination of the Iberia-
87
88 Eurasia plate boundary. This is the Marguareis extensional system of the Briançonnais Domain of
89
90 the SW Alps. The crustal-scale Marguareis extensional system involves Paleozoic and Mesozoic
91
92 rocks and includes a tens of km long transfer fault flanking an extensional domino array that
93
94 accounted for ca. 2 km of extension along 6 km long sections. When post-Cretaceous alpine
95
96 rotation is removed, the mid-Cretaceous transfer fault and the extension direction of the Marguareis
97
98 extensional system become oriented parallel to those of the other portions of the plate boundary,
99
100 indicating its pertinence to the Bay of Biscay-Pyrenean rift system.
101
102

103 Reviewed and newly presented data about the mid-Cretaceous tectonics spanning from
104
105 the easternmost portion of Iberia to the Western Alps indicate that: (i) the Marguareis extensional
106
107 system and the extensional structures of south France constituted the easternmost portion of the
108
109 segmented and laterally terminating Bay of Biscay-Pyrenean rift system; (ii) this easternmost
110
111 portion of the Iberia-Eurasia plate boundary was characterised by a purely divergent Early to mid-
112
113 Cretaceous movement.
114
115
116
117
118

1 Introduction

1.1 The Cretaceous Iberia-Eurasia plate boundary controversy

The geometry, kinematics, and lateral extent of the Iberia-Eurasia plate boundary during the Cretaceous period remains a question of considerable debate among earth scientists. The origin of such debate goes back to the dawn of plate tectonics and underlies on the mechanism by which the Bay of Biscay opened. Indeed, during the early 70's, three main hypotheses about the opening of the Bay of Biscay were postulated (Choukroune et al., 1973). In this early work the opening of the V-shaped Bay of Biscay was described in terms of the rotation of Iberia around Eulerian poles that would have been approximately located either (i) to the east of Iberia (Fig. 1a), (ii) close to Paris (Fig. 1b), or (iii) within the Pyrenean mountain range (Fig. 1c). Each of these hypotheses has different implications for the opening mode of the Bay of Biscay and implies contrasting amounts of rotation for Iberia with respect to Eurasia: the first hypothesis entails a rift-perpendicular opening mode for the Bay of Biscay by means of an eastward diminishing divergence between Iberia and Eurasia. The second one involves a left-lateral motion of Iberia with respect to Eurasia along a dominant strike-slip transform plate boundary. The third hypothesis implies divergence between Iberia and Eurasia in the Bay of Biscay coeval with convergence between these two plates east of the Euler pole in the NE corner of Iberia (i.e., scissor-type model).

In the light of geological and geophysical research during the last 40 years, these early models have been updated and improved as shown by the works of Jammes et al. (2009) and Tugend et al. (2014) in regards of the rift-perpendicular opening mode (Fig. 1a); those of Olivet (1996) or Stampfli and Borel (2002) in relation to the strike-slip mode (Fig. 1b), or the scissor-type mode (Fig. 1c) by Sibuet et al. (2004), Vissers and Meijer (2012), and Vissers et al. (2016).

Despite the amount of data and scientific outputs, the debate is far from over. One of the main reason for this is provided by the uncertainties associated with the data constraining the Cretaceous movement of Iberia. As an example, while it is undisputed that Iberia underwent a certain amount of counter-clockwise rotation with respect to Europe coevally with the opening of

178
179 the Bay of Biscay (van der Voo, 1969), the published vertical axis rotation values span between 20°
180 to 40° (see Neres et al., 2012 and Barnett-Moore et al., 2016 for recent reviews). It is also unclear
181 whether the rotation took place during a large portion of the Cretaceous period (Galdeano et al.,
182 1989), or was only limited to the Aptian stage (Gong et al., 2008; Vissers et al., 2016). Similarly,
183 the nature and age of the Bay of Biscay floor have received different interpretations: many authors
184 support the occurrence of a large domain of exhumed subcontinental mantle in the Bay of Biscay
185 (e.g. Thinon et al., 2003; Jammes et al., 2009; Roca et al., 2011; Tugend et al., 2014; Manatschal et
186 al., 2015; Nirrengarten et al., 2017), whereas other workers lean towards a largely oceanic nature
187 (e.g. Sibuet et al., 2004; Vissers and Meijer, 2012) or a mixed model of intruded exhumed mantle
188 (Pedreira et al., 2015). These different ideas about the nature of the Bay of Biscay imply different
189 interpretations for the age and significance of some of the magnetic anomalies (Sibuet et al., 2004)
190 and, ultimately, entail different positions for Iberia at the beginning of the Bay of Biscay opening.
191 The reliability of geological data in constraining the plate tectonic evolution of this large domain
192 has also been questioned. The absence of any evidence for a mid-Cretaceous convergence stage in
193 the Pyrenean area is striking, as the Pyrenean area was experiencing a well-constrained extensional
194 regime during that time (e.g. Muñoz, 2002; Vergés et al., 2002; Jammes et al., 2009). However,
195 while many authors argue that this makes the scissor-type scenario unrealistic (e.g. Tugend et al.,
196 2014), others frame the mid-Cretaceous extension within the development of back-arc basins
197 associated with the subduction of oceanic crust (Sibuet et al., 2004). In summary, the scissor-type
198 model has its strength in the interpreted pattern of magnetic anomalies, and in the predicted amount
199 of vertical axis rotation of Iberia. However, it is not proved that all the interpreted magnetic
200 anomalies in the Bay of Biscay floor correspond to a Penrose-type oceanic crust. In addition, there
201 is no evidence for an ophiolitic sequence preserved in the Pyrenees, under the Ebro foreland basin
202 or along the Catalan Coastal Ranges. The weakest argument for the scissor-type scenario is the lack
203 of any unequivocal geological proof for mid-Cretaceous convergence in the NE Iberia. On the other
204 hand, the strike-slip scenario is consistent with the amount of vertical axis rotation documented for
205
206
207
208
209
210
211
212
213
214
215
216
217
218
219
220
221
222
223
224
225
226
227
228
229
230
231
232
233
234
235
236

237
238 Iberia as well; it partly fits with the magnetic anomalies, but the geological evidence for hundreds
239 of kilometres of left-lateral motion of Iberia during the mid-Cretaceous is missing. Therefore, the
240 rift-perpendicular solution is the most geologically-supported scenario. It is also consistent with the
241
242 rift-perpendicular solution is the most geologically-supported scenario. It is also consistent with the
243
244 pattern of magnetic anomalies for the area where no mantle exhumation is inferred. Its weakest
245
246 point though is the amount of vertical axis rotation: the coeval opening of the Bay of Biscay and the
247
248 Pyrenean arm requires, if the Iberian plate is considered rigid, a Euler pole to the east of Iberia,
249
250 which implies values of rotation of nearly 10° (Choukroune et al., 1973), largely below the
251
252 published ones (e.g. van der Voo, 1969). Another problem with the rift-perpendicular model is the
253
254 expected left-lateral movement of Iberia as the Atlantic opening progressed northward of the
255
256 Azores-Gibraltar transfer zone at Late Jurassic-Early Cretaceous times (Stampfli and Hochard,
257
258 2009). Ultimately, each of these three scenarios apparently has its strengths and weaknesses and
259
260 none of them can fully reconcile the available geological and geophysical datasets.
261
262

263
264 The key observation to solve this problem is that each of the three postulated hypotheses
265
266 implies a different style of termination for the eastern Iberia-Eurasia plate boundary (Fig. 2). In fact,
267
268 an additional controversy arises when joining the opening of the Bay of Biscay-Pyrenean rift with
269
270 the Alpine Tethys further east, in particular with the so-called Valais “ocean” (e.g. Stampfli et al.,
271
272 1998; Stampfli and Hochard, 2009; Beltrando et al., 2012). In the rift perpendicular scenario, as
273
274 proposed by Manatschal and Muntener (2009), the Bay of Biscay-Pyrenean rift and the Alpine
275
276 Tethys are diachronous and non-connected rifts, as the former is thought to terminate eastwards
277
278 around the NW continental margin of the Alpine Tethys (Fig. 2a). Coherently, the Sardinia-Corsica-
279
280 Briançonnais block is considered part of both Iberia and Eurasia. In the strike-slip type scenarios,
281
282 the left-lateral motion of Iberia with respect to Eurasia is partly or completely accommodated to the
283
284 east by the development of the Valais “ocean” (Fig. 2b). This ocean is interpreted by several authors
285
286 as a mid-Cretaceous branch of the Jurassic Alpine Tethys; it would represent a sort of dilation jog
287
288 of the North Pyrenean Fault (e.g. Stampfli and Borel, 2002; Rosenbaum and Lister, 2005; Handy et
289
290 al., 2010), establishing the connection between the Bay of Biscay-Pyrenean rift system and the
291
292
293
294
295

296
297 Alpine Tethys, and separating the Sardinia-Corsica-Briançonnais block from Eurasia. However, the
298 nature and position of the Valais “ocean” within the nearby spreading systems is significantly
299
300 nature and position of the Valais “ocean” within the nearby spreading systems is significantly
301
302 biased by the complexity of the Alpine thrust stacking and folding and associated metamorphism
303
304 (e.g., Schmid et al., 2004; Froitzheim et al., 2008). Importantly, the reported mid-Cretaceous
305
306 spreading ages for the Valais “ocean” have been challenged by U-Pb dating of magmatic zircons
307
308 which have provided disparate spreading ages, from Early Carboniferous (337 Ma; Bussy et al.,
309
310 2008), to Permian (267 and 272 Ma; Beltrando et al., 2007), or even Late Jurassic (163-155 Ma;
311
312 Liati and Froitzheim, 2006). In the scissor-type scenario, the Pyrenean arm is connected to the
313
314 Alpine Tethys as well. However, the connection is not ensured by the Valais “ocean” but, rather, the
315
316 Pyrenean arm is considered part of the Alpine Tethys undergoing north-ward subduction during the
317
318 mid-Cretaceous. The occurrence of a transform zone bounding the subduction to the east is forecast
319
320 (e.g. Advokaat et al., 2014), kinematically separating the Corsica-Sardinia-Briançonnais block from
321
322 Iberia (Fig. 2c), which implies that this block was part of Eurasia.

325 The reconstruction of the Mesozoic palaeogeography immediately east of the Pyrenees,
326
327 (Fig. 3) is not straightforward. This area has been strongly modified by the Cenozoic convergence
328
329 stage between Eurasia and Africa (e.g. Dercourt et al., 1986; Dewey et al., 1989; Mazzoli and
330
331 Helman, 1994; Handy et al., 2010; Frizon de Lamotte et al., 2011; Carminati et al., 2012; Faccenna
332
333 et al., 2014) and by the subsequent back-arc overprint associated with the late Oligocene to
334
335 Miocene opening of the Liguro-Provençal basin (e.g. Alvarez et al., 1974; Réhault et al, 1984;
336
337 Hippolyte et al., 1993; Doglioni et al, 1997; Séranne, 1999; Gattacceca et al., 2007; Bache et al.,
338
339 2010; Jolivet et al., 2015; Granado et al., 2016). As a result of this deformation history, the
340
341 Briançonnais is exposed in the Western and Central Alps, whereas relics of the Valais “ocean”
342
343 occur in the easternmost Western Alps and further east, in the Central and Eastern Alps (Schmid et
344
345 al., 2004); the Corsica-Sardinia form an independent block (Fig. 3). Albeit all these uncertainties,
346
347 information about the eastern termination of the Iberia-Eurasia plate boundary can be obtained from
348
349 the occurrence and orientation of Cretaceous extensional structures in this area, along with their
350
351
352
353
354

355
356 affinity with structures of the western and central portions of the Iberia-Eurasia plate boundary.
357
358 These features can provide robust insights on the eastern termination of the plate boundary.
359

360 The main goal of our work is to present both new information and reappraisal of published
361 data about the mid-Cretaceous geological framework of this area and evaluate its kinematic
362 compatibility with the mid-Cretaceous structures of the Pyrenean rift.
363
364
365

366 367 368 **1.2 An overview of the Cretaceous Iberia-Eurasia plate boundary**

369 The westerly Bay of Biscay arm includes a central area made of oceanic crust with an 83 Ma
370 fossil ridge, in between the northern (European) and southern (Iberian) continental margins (Tugend
371 et al., 2014, 2015). These margins are made of thinned continental crust and exhumed mantle (e.g.
372 Boillot et al., 1979; Thinon et al., 2002; Cadenas and Fernández-Viejo, 2017) (Fig. 3b). Whereas
373 the northern margin has persisted broadly undeformed since the end of rifting, the southern margin
374 has been severely deformed by Late Cretaceous to Cenozoic compressional deformation (e.g. Roca
375 et al., 2011; Pedreira et al., 2015). To the east the Mesozoic Iberia-Eurasia plate boundary continues
376 into the Pyrenean arm (Fig. 3b). The Pyrenean arm was constituted by a segmented rift system
377 formed by partly interconnected basins that have been inverted and incorporated into the Pyrenean
378 mountain belt (Fig. 3a) during the Late Cretaceous to Cenozoic convergence between Iberia and
379 Eurasia (e.g. Puigdefabregas and Souquet, 1986; Roure et al., 1989; Muñoz, 1992; Teixell, 1998;
380 Vergés et al., 2002; Mouthereau et al., 2014). Despite the significant compressional overprint, the
381 original architecture of the Pyrenean arm is still recognisable (Fig. 3b). Exposures of subcontinental
382 lithospheric mantle exhumed by the end of the Cretaceous rifting have been reported for a long time
383 in the Pyrenees (e.g. Lacroix, 1895; Vielzeuf and Kornprobst, 1984; Lagabrielle and Bodinier,
384 2008; Jammes et al., 2009; Lagabrielle et al., 2010; Masini et al., 2014; Clerc et al., 2015). These
385 exposures occur along a narrow WNW-ESE elongated ribbon (Fig. 3b), flanked to the north and to
386 the south by Late Jurassic to mid-Cretaceous basins of the European and the Iberian continental
387 margins (e.g. Souquet et al., 1985; Lanaja, 1987; Rat, 1988; Johnson and Hall, 1989; Debroas,
388
389
390
391
392
393
394
395
396
397
398
399
400
401
402
403
404
405
406
407
408
409
410
411
412
413

414
415 1990; Cámara, 1997; García-Senz, 2002; Muñoz, 2002; Vergés et al., 2002; Tavani and Granado,
416 2015; Teixell et al., 2016). To the west, these basins and the exhumed mantle exposures are
417 segmented by major transfer zones, namely the Santander and Pamplona faults (e.g. Roca et al.,
418 2011; Tugend et al., 2014) which run broadly perpendicular to the orientation of the extensional
419 basins (Fig. 3b). The eastern limit of subcontinental mantle exposures is located a few tens of
420 kilometres to the west of the Mediterranean Sea coastline, and is thus considered the eastern
421 termination of the Pyrenean Arm. Further to the east-northeast, Cretaceous extensional deformation
422 is reported in the Provence region (e.g. de Graciansky et al., 1987; Hibsich et al., 1992; Montenat et
423 al., 1997; Homberg et al., 2013). The Provence constitutes the easternmost portion of the Pyrenean
424 orogenic system (Fig. 3a). In this easterly sector, a set of inherited Paleozoic to Mesozoic NNE-
425 SSW to NE-SW striking transverse faults occur (Fig. 3b), i.e. the Cévennes, Nimes, and Durance-
426 Aix faults from west to east (Masse and Philip, 1976). During the Late Cretaceous to Cenozoic time
427 interval, these faults have provided the left-lateral transpressive junction between the E-W trending
428 and north-verging Pyrenean structures of the Pyrenees and of the Languedoc-Provence region (e.g.
429 Mauffret and Genesseeux, 1989; Séranne et al., 1995; Lacombe and Jolivet, 2005; Molliex et al.,
430 2011; Bestani et al., 2016) (Fig. 3a). Concerning the pre-contractual activity of the NNE-SSW to
431 NE-SW striking Cévennes, Nimes, and Durance-Aix faults, several authors such as de Graciansky
432 and Leimone (1988) and more recently Masse et al. (2009), have documented major WNW-ESE
433 striking Early to mid-Cretaceous normal faults bounded by NNE-SSW to NE-SW striking transfer
434 faults in the Provence region (Fig. 3). Given that the NNE-SSW to NE-SW striking transfer faults
435 of this area are oriented about parallel to the major transfer faults that segment the Bay of Biscay-
436 Pyrenean rift system (i.e., Pamplona and Santander faults), the easterly Provence region shares a
437 structural similarity with the Bay of Biscay-Pyrenean rift system. In this work we propose that this
438 series of transversal faults played a major role during rifting between Iberia and Eurasia, acting as
439 transform zones that accommodated rift segmentation, and transferred the extensional deformation
440 to the NE of the Pyrenean arm of the rift (Fig. 3c). In agreement with our working hypothesis, we
441
442
443
444
445
446
447
448
449
450
451
452
453
454
455
456
457
458
459
460
461
462
463
464
465
466
467
468
469
470
471
472

473
474 also present field survey data from an area that we consider the easternmost remanence of the
475
476 Cretaceous Iberia-Eurasia plate boundary: the Marguareis area of the Briançonnais domain.
477

478 The presentation of data in the next sections is organised as follows: we first provide a
479
480 review on the timing and kinematics of the various basins of the Pyrenean Arm (Section 2) and of
481
482 the area comprised between the easternmost portion of the Pyrenees and the Provence region
483
484 (Section 3). Finally, in Section 4, we introduce the Marguareis extensional system. The provided
485
486 comprehensive review about the Cretaceous extension recorded to the east of the Bay of Biscay-
487
488 Pyrenean rift allows us to propose that the Marguareis extensional system represents the
489
490 easternmost structure of the segmented Bay of Biscay-Pyrenean rift. At the light of the work carried
491
492 out in the Marguareis area, we discuss the three possible scenarios previously introduced for the
493
494 development of the Bay of Biscay-Pyrenean rift and its eastwards continuation during the mid-
495
496 Cretaceous.
497
498

501 **2 An overview of the Pyrenean Arm**

502 The westernmost sector of the Iberian-Eurasian plate boundary is constituted by an E-W
503
504 trending fossil oceanic ridge, located on the abyssal plain of the Bay of Biscay (Fig. 3b), and
505
506 inactive since early Campanian times (e.g. Sibuet et al., 2004; Roca et al., 2011). The oceanic ridge
507
508 is flanked to the north and to the south by Aptian-Albian to Campanian oceanic crust (Figs. 3b, 4)
509
510 (Tugend et al., 2014). The domain of oceanic crust fades out towards the north, the south, and the
511
512 east into a domain of sub-continental mantle exhumed during Barremian to Aptian times (Thinon et
513
514 al., 2003; Roca et al., 2011). The V-shaped Bay of Biscay wedges out toward the east, where it
515
516 terminates into the E-W elongated Parentis basin (Fig. 4), which is filled by as much as 8 km of
517
518 Upper Jurassic to Albian synrift sedimentary rocks (e.g. Ferrer et al., 2008). The southern margin of
519
520 the Bay of Biscay includes an emerged area with small exposures of the Upper Jurassic to Lower
521
522 Cretaceous synrift sequence (named Asturian basin by Lepvrier and Martínez-García, 1990). In
523
524 these small-sized areas, the background fracture pattern indicates a synrift NNE-SSW oriented
525
526
527
528
529
530
531

532
533 extension (Site 1 of figure 4a) (Granado et al., in press).
534

535 The Santander Transfer Fault and the Landes Plateau divide the Bay of Biscay and the
536
537 Pyrenean arms. The latter during the Cretaceous was occupying the area presently comprised
538
539 between the Santander Fault to the west and the southern prolongation of the Cévennes Faults to the
540
541 east (Fig. 4a) (e.g. Tugend et al., 2014). In this area, the Late Jurassic-Early Cretaceous extensional
542
543 structures belonging to the Pyrenean Arm of the rift have been inverted and incorporated into the
544
545 Pyrenean belt. These extensional structures include major lithospheric-scale shear zones that were
546
547 responsible for the development of the continental margin basins (e.g. Souquet et al., 1985; Rat,
548
549 1988; Debros, 1990; Muñoz, 2002; Vergés et al., 2002) and, ultimately, for the exhumation of sub-
550
551 continental lithospheric mantle (e.g. Johnson and Hall, 1989; Jammes et al., 2009; Clerc and
552
553 Lagabrielle, 2014; Tugend et al., 2014; Masini et al., 2014; Teixell et al., 2016); no oceanic crust
554
555 has ever been documented in the Pyrenean Arm. The along strike structural variations of the
556
557 Pyrenees are as well controlled by the inherited segmented configuration of the Bay of Biscay-
558
559 Pyrenean rift system, with major NNE-SSW transfer zones striking roughly perpendicular to the
560
561 main extensional basins.
562
563

564
565 Based on the lateral continuity of such extensional domains, the Pyrenean Arm has been
566
567 further divided into two portions separated by the lithospheric-scale Pamplona transfer fault (Fig. 4)
568
569 (e.g. Muñoz, 2002). The Basque-Cantabrian basin forms the westernmost portion of the Pyrenean
570
571 rift (Fig. 4a). It has an overall E-W elongated shape and it is filled by up to 10 km thick Upper
572
573 Jurassic to Albian/Cenomanian synrift infill (e.g. García-Mondéjar et al., 1986; Rat, 1988). The
574
575 Basque-Cantabrian basin is bounded to the west by the N-S trending Santander transform fault
576
577 (Roca et al., 2011) and to the east by the Pamplona fault (Fig. 4a), an inherited Paleozoic structure
578
579 that acted as a transform fault during rifting (e.g. Rat, 1988; Larrasoña et al., 2003). In the Basque-
580
581 Cantabrian basin, multiple Late Jurassic to Early Cretaceous local extension directions are recorded
582
583 by meso-structures (Tavani and Muñoz, 2012) and inferred from studies of anomaly of magnetic
584
585 susceptibility (AMS; Soto et al., 2008; Oliva-Urcia et al., 2013; Site 2 in figure 4a). The dominant
586
587
588
589
590

591
592 synrift extension direction provided by these studies is roughly NNE-SSW (Site 2 of figure 4a)
593
594 (Tavani and Muñoz, 2012), which is nearly parallel to the Santander transfer zone and
595
596 perpendicular to the elongation of the basin.
597

598
599 A few tens of km to the south of the Basque-Cantabrian basin, the Cameros basin was
600
601 forming part of a suite of Mesozoic extensional basins now exposed along the Iberian Chain (Figs.
602
603 3 and 4). These basins formed in the interior of the Iberian plate, disconnected from the Bay of
604
605 Biscay-Pyrenean rift, along the NW-SE elongated Central Iberian rift system (e.g. Álvaro et al.,
606
607 1979; Salas and Casas, 1993; Salas et al., 2001; Vergés and Garcia-Senz, 2001). The Central Iberian
608
609 Rift contributed significantly to the continental separation between Iberia and Eurasia (Salas et al.,
610
611 2001; Tugend et al., 2015). Analogously to the Basque-Cantabrian basin, extension direction
612
613 recorded by meso-structures in the Upper Jurassic to Lower Cretaceous synrift sediments of the
614
615 Cameros basin is NNE-SSW (Mata et al., 2001), whereas AMS studies provide two mutually
616
617 orthogonal directions, corresponding to NNW-SSE to NW-SE and WNW-ESE to NE-SW (e.g. Soto
618
619 et al., 2008; García-Lasanta et al., 2014) (Site 3 in figure 4a).
620
621

622
623 Immediately to the east of the Pamplona fault, the axis of mid-Cretaceous extension is
624
625 shifted northward. Intense extensional deformation is recorded in the Arzacq and Mauléon basins,
626
627 which are divided by the Grand Rieu ridge (Daignières et al., 1994; Teixell, 1988; Jammes et al.,
628
629 2009, 2010; Masini et al., 2014; Teixell et al., 2016). The northerly Arzacq basin developed on the
630
631 European plate and displays a rather simple E-W elongated sag-like geometry (e.g. Masini et al.,
632
633 2014) with a Tithonian to Albian synrift infill (Biteau et al., 2006). Extensional deformation was
634
635 more intense on the Mauléon basin to the south (e.g. Fortané et al., 1986; Johnson and Hall, 1989;
636
637 Jammes et al., 2009; Lagabrielle et al., 2010; Masini et al., 2014), where sub-continental mantle was
638
639 exhumed. The lithospheric extensional detachment system involved the Mesozoic sedimentary
640
641 succession, crustal rocks, and upper mantle lherzolites. Measured S-C structures have indicated a
642
643 top-to-the-north movement for the mantle-exhuming detachment (Lagabrielle et al., 2010) (Site 4 of
644
645 figure 4a). Mesostructures studied by Salardon et al. (2017), which affect the sedimentary cover of
646
647
648
649

650
651 the Chaînons Béarnais area in the Mauléon basin (Site 5 of figure 4a), provide a similar N-S
652 oriented extension direction for the Albian to Cenomanian interval. Similarly, Cretaceous N-S to
653 NNW-SSE extension has been documented in the same area by Olivia-Urcia et al. (2010) by means
654 of an AMS study. In the Mauléon basin, hyperextension and consequent exhumation of sub-
655 continental mantle occurred during the late Aptian to Cenomanian interval (Jammes et al., 2009;
656 Lagabrielle et al., 2010; Masini et al., 2014). The Arzacq-Mauléon system is bounded to the east by
657 the NE-SW to NNE-SSW striking Toulouse fault. Many have proposed that this fault was acting as
658 a transfer fault segmenting the Pyrenean Arm (e.g. Tugend et al., 2014), however, this is not fully
659 demonstrated, and its possible segmenting role is by far less than that of the major transfer faults of
660 the rift system. Relics of sub-continental mantle are exposed to the east and to the west of the
661 Toulouse fault, occurring aligned in a WNW-ESE direction, with no remarkable shift across the
662 fault. Domains of exhumed mantle and hyperextended crust are surrounded by Mesozoic
663 sedimentary basins that have been incorporated into the Pyrenean belt (e.g. Lagabrielle et al., 2010;
664 Tugend et al., 2014; Clerc et al., 2015). These basins, along with the Mauléon basin to the west,
665 were initially developed isolated and became connected during the Albian-Cenomanian interval to
666 form a large, WNW-ESE trending hyperextended basin (i.e. the Flysch Noir basin in figure 4) filled
667 by the syn-extensional Flysch Noir Formation (e.g. Souquet et al., 1985; Debroas, 1990). Direction
668 of mid-Cretaceous extension was N-S to NE-SW, as provided by major extensional detachments
669 exposed in the Variscan massifs of the north Pyrenean area. These massifs constitute relics of the
670 former crystalline basement of the various Cretaceous basins. In more detail, mid-Cretaceous
671 extensional detachments associated with N-S to NNE-SSW oriented stretching are exposed in the
672 Saint Barthélémy massif area (Site 6 of figure 4a) (Passchier, 1984; de Saint Blanquat et al., 1986;
673 1990) and in the Agly Massif (Site 7 of figure 4a) (Vauchez et al., 2013).

700 To the south of the Flysch Noir basin, the Organyà basin developed onto the Iberian crust.
701 The Tithonian/Berriasian to middle Albian synrift sequence of the Organyà basin exceeded 4 km
702 (Dinarès-Turell and García-Senz, 2000; Garcia-Senz, 2002), with a thickness distribution

709
710 characterised by a marked E-W to WNW-ESE elongated shape (Garcia-Senz, 2002; Mencos et al.,
711 2015). Anisotropy of magnetic susceptibility (AMS; Gong et al., 2009; Olivia-Urcia et al., 2011)
712 and meso-structural studies (Tavani et al., 2011) have been independently carried out in the area.
713
714 The AMS works provide partly contrasting results, with Gong et al. (2009) suggesting a mainly N-S
715 directed extension during rifting and Olivia-Urcia et al. (2011) recording a more scattered pattern
716 for the AMS. In agreement with Gong et al. (2009), meso- and macro-structures (including syn-
717 sedimentary faults) documented by Tavani et al. (2011) indicate N-S to NNE-SSW oriented basin-
718 scale Early Cretaceous extension (Site 8 of figure 4a), which was perpendicular to the above
719 mentioned basin axis.
720
721
722
723
724
725
726
727
728
729
730

731 **3 Cretaceous extension along the eastern portion of the Iberia-Eurasia boundary**

732
733 In this section we review the Late Jurassic to Cretaceous extensional structures reported
734 in the area comprised between the easternmost portion of the Pyrenees and the Provence belt, in
735 Sardinia, and in the European paleo-margin of the Western and Central Alps (Fig. 3a). In the
736 previous section we have illustrated extensional structures involving the basement, and thus having
737 an indisputable tectonic origin, whereas we have not included in our description the gravitational
738 structures occurring in the Pyrenean arm (López-Mir et al., 2015; Saura et al., 2016). In this section
739 we continue to report only on structures that, due to their regional size or because of the lack of
740 evaporites (or any kind of mobile unit), cannot be interpreted as gravitationally-induced.
741
742
743
744
745
746
747
748
749

750 3.1 Eastern Pyrenees

751
752 The easternmost portion of the Pyrenean mountains is characterised by the termination of
753 the Pyrenean basins (Fig. 5a). During convergence, the area around the Corbières Transfer Zone
754 (e.g. Souque et al., 2002; Luis et al., 2006; Rouvier et al., 2012) became the left-lateral transpressive
755 junction between the north-verging Pyrenean structures of the Pyrenees and the Provence region
756 (Fig. 3a), as shown by Mauffret and Gennesseaux (1989), Séranne et al. (1995), Lacombe and
757 Jolivet (2005) and more recently by Rouvier et al. (2012). Despite the contractional overprinting,
758
759
760
761
762
763
764
765
766
767

768
769 thickness variations of the Jurassic-Cretaceous sequence partly illustrate the rift architecture of the
770 area. In detail, the Boucheville, Bas Agly and St. Paull de Fenouillet synclines to the north of the
771 North Pyrenean Fault, are remanences of the easternmost mid-Cretaceous interconnected and
772 hyperextended basins of the Pyrenean Arm separating Iberia from Eurasia (e.g. Lagabrielle et al.,
773 2010; Tugend et al., 2014; Clerc et al., 2015). As previously mentioned in section 2, during the
774 Albian-Cenomanian interval these basins were forming a large WNW-ESE trending trough, filled
775 by the synrift Flysch Noir Formation (e.g. Souquet et al., 1985; Debros, 1990). Extension beneath
776 the Boucheville basin reached full crustal thinning and mantle exhumation, as indicated by the
777 occurrence of peridotite bodies and the thermal metamorphism affecting the Mesozoic prerift and
778 synrift sequences (Clerc et al., 2016). Regionally speaking, the synrift package in this area wedges
779 out northward, to the north of the North Pyrenean Fault (Figure 5a). Indeed, the Mesozoic sequence
780 in the Mouthoumet massif is represented only by postrift Upper Cretaceous strata resting on top of
781 the Paleozoic basement (Fig. 5a). To the west of the NNW-SSE striking Cévennes fault, the area
782 between the Mouthoumet and Montagne Noire massifs was also uplifted during the mid-
783 Cretaceous, as indicated by the reduced thickness or complete lack of Lower Cretaceous units (e.g.
784 Ellenberger, 1967; Souque et al., 2002). The thickness of the Lower Cretaceous is instead in the
785 order of one km in the Bas Agly syncline (Fig. 5b), where a major mid-Cretaceous N-ward directed
786 extensional detachment is exposed (Vauchez et al., 2013). Exposures of Lower Cretaceous
787 sediments continue from the Bas Agly syncline toward NE, in the La Clape area of the Corbières
788 thrust sheet (Fig. 5a), where the Mesozoic sequence is about 4 km thick, and the thickness of the
789 Lower Cretaceous sediments alone is nearly one km (Deville et al., 1994). As previously indicated,
790 such thickness decreases from the La Clape area toward the west across the south-western
791 prolongation of the Cévennes fault; this is a clear evidence of the key basin-bounding role of the
792 southern prolongation of the Cévennes fault during the mid-Cretaceous.

819
820 On the southeastern side of the Pyrenees, the Figueres-Montgrí basin is the easternmost
821 exposed Lower Cretaceous basin in the Iberian Peninsula (Fig. 5a). It is an understudied structure,
822
823
824
825
826

886
887 affect Hauterivian to Berriasian layers and are sealed by unconformable Aptian strata (Fig. 5c)
888
889 (Mató et al., 1995b). Another important unconformity is observed in the onshore Figueres area,
890
891 where Cenomanian strata are unconformable on Aptian and Albian units (Fig. 5d). Altogether, these
892
893 observations indicate that: (i) onset of extension occurred between the Barremian and Aptian age,
894
895 (ii) the oldest post rift unit is Cenomanian in age, (iii) syn-sedimentary faults (observed in the Meda
896
897 islands) point to a NW-SE oriented structural trend for the Figueres-Montgri basin.
898
899

900 3.2 SE France basin

901
902 This is the area comprised between the easternmost portion of the Pyrenees and the foreland
903
904 of the Western Alps (Fig. 6), where Late Jurassic to Late Cretaceous extensional structures are
905
906 known for a long time (e.g. Cotillon, 1968; de Graciansky and Lemoine, 1988). The SE France
907
908 basin (Fig. 6b) originated on the European continental crust during the Triassic-Jurassic interval in
909
910 response to Gondwana break-up and Alpine Tethys rifting (Lemoine, 1984; Curnelle and Dubois,
911
912 1986). Isopachs and facies distribution of Triassic, Lower and Middle Jurassic units in the basin are
913
914 NE-SW elongated. This direction is parallel to the former Tethyan palaeomargin (Curnelle and
915
916 Dubois, 1986) and defines a Triassic to Middle Jurassic through, positioned along the southwestern
917
918 prolongation of the Valais ocean; no evidence for an oceanic substratum in this area have been
919
920 reported. Starting from the Late Jurassic, the structural trend of the area became E-W. Indeed, the
921
922 observed facies distribution allowed defining two Late Jurassic to Cretaceous E-W elongated sub-
923
924 basins within the SE France basin: the Vocontian basin and the South Provence basin (Curnelle and
925
926 Dubois, 1986). These sub-basins were separated by the also E-W striking Durance Isthmus, which
927
928 became aerielly exposed during the Cenomanian (Fig. 6b).
929
930

931
932 The Vocontian basin is largely exposed, whereas the mid-Cretaceous South Provence basin
933
934 (e.g. Philip, 1970; Philip et al., 1987) has only few onshore exposures. One of them is the Beausset
935
936 syncline (Fig. 6b), where the southern boundary of the basin occurs (Hennuy, 2003). The uplift
937
938 stage which led to the division of the Vocontian and South Provence basins, commonly referred to
939
940 as the “Durance Uplift” event, has occurred in an extensional framework. This is evidenced by mid-
941
942
943
944

945
946 Cretaceous syn-sedimentary extensional faults coeval with uplift and bauxite formation and sealed
947 by Turonian strata (Guyonnet-Benaize et al., 2010). Coeval extensional faulting is documented
948 by Turonian strata (Guyonnet-Benaize et al., 2010). Coeval extensional faulting is documented
949 southward, at the southern margin of the South Provence basin. There, Cenomanian strata
950 unconformably overlie Berriasian to Albian strata defining an Albian half-graben associated with a
951 roughly E-W striking fault (Fig. 7a). However, the onset of extension in the SE France basin is
952 dated back at least at the Berriasian-Valanginian interval; this is documented by Valanginian strata
953 unconformably resting on top of Berriasian strata folded by block-tilting associated with WNW-
954 ESE striking extensional faults (Masse et al., 2009). Meso-structural data point to an extensional
955 regime for the area too, with the Late Jurassic to mid-Cretaceous interval being characterised by
956 extension directions roughly N-S to NNE-SSW and E-W to WNW-ESE oriented (e.g. Guyonnet-
957 Benaize et al., 2010; Lamarche et al., 2012; Homberg et al., 2013), with a minor strike-slip
958 contribution (e.g. Hibsich et al., 1992; Montenat et al., 1997). The link between the N-S and E-W
959 oriented extensional structures and strike-slip deformation is recognised in the whole area also at
960 more regional scale of observation (de Graciansky and Lemoine; 1988) (Fig. 6c). In agreement with
961 the data reviewed above, the structural framework reported by these authors for the Early
962 Cretaceous interval includes: major basin-scale WNW-ESE striking extensional faults associated
963 with NNE-SSW oriented extension (Sites 10 in figure 8a); secondary NNE-SSW trending
964 transverse extensional faults occurring in the hanging wall of major faults; NNE-SSW striking
965 transfer strike-slip faults. The trend of the strike-slip set recognised by de Graciansky and Lemoine
966 (1988) is parallel to the strike of the major inherited faults of the area, i.e. Cévennes, Nimes, and
967 Durance-Aix faults. Such a framework, in which the above-mentioned faults acted as transfer
968 systems, is confirmed when linking this area with the eastern Pyrenees. In this sense, during mid-
969 Cretaceous times, the Vocontian basin was clearly delimited westward by the Cévennes fault (Fig.
970 6b). The same fault seems to confine the South Provence basin too (Fig. 6b): the Bas Agly syncline,
971 which forms the easternmost relic of the suite of mid-Cretaceous basins of the Pyrenean mountains,
972 (e.g. Vauchez et al., 2013; Clerc et al., 2016), is shifted southward with respect to the South
973
974
975
976
977
978
979
980
981
982
983
984
985
986
987
988
989
990
991
992
993
994
995
996
997
998
999
1000
1001
1002
1003

1004
1005 Provence basin. The Corbières transfer zone (Fig. 5a) thus acted either as a soft- or hard-linked
1006 transfer zone (Gawthorpe and Hurst, 1993) during the mid-Cretaceous times, roughly coinciding
1007 with the SW continuation of the Cévennes fault.
1008
1009
1010

1011 3.3 Sardinia

1012
1013 In the Sardinia-Corsica block to the south of the South Provence basin (Fig. 6a), a structure
1014 similar to those described by Guyonnet-Benaize et al. (2010) for the South Provence basin also
1015 points to coeval uplift and block tilting. This structure occurs in the Olmedo area of NW Sardinia
1016 (e.g. Mameli et al., 2007) (Fig. 7b), where Coniacian strata unconformably overly a tilted sequence
1017 of Berriasian to Aptian sediments with bauxite bodies at the top. This configuration evidences
1018 tilting during mid-Cretaceous times, with the pre-unconformity monocline dipping to the SE. By
1019 removing the 95° of Cenozoic clockwise vertical axis rotation of Sardinia (Advokaat et al., 2014),
1020 this configuration corresponds to a roughly SW-dipping monocline in a Cretaceous reference
1021 framework (Site 11 in figure 8a).
1022
1023
1024
1025
1026
1027
1028
1029
1030
1031
1032

1033 3.4 Western and Central Alps

1034
1035 The Helvetic Domain of the Central Alps corresponds to the Mesozoic European continental
1036 margin of the Alpine Tethys. In this area, extensional faults postdating the Alpine Tethys rifting
1037 stage have been reported at different time intervals. Septfontaine (1995) described a Late Jurassic
1038 extensional system (Site 12 in Figure 8a) constituted by a reactivated WSW-ENE striking Early
1039 Jurassic fault that developed during Tethyan rifting. The late Jurassic reactivation of this fault is
1040 evidenced by the occurrence of an about 500 m-wide NW-ward thickening growth wedge of Upper
1041 Jurassic strata. In the same region, Cardello and Mancktelow (2014) report Cretaceous extensional
1042 structures at cm to km scales (Site 13 of figure 8a). Evidence of Late Cretaceous extensional
1043 deformation includes growth wedges, sedimentary dykes, thickness and facies variations,
1044 palaeoscarpments, and slump folds. All these features are related to km-sized SW-NE-striking
1045 faults developed in response to Santonian to early Maastrichtian NW-SE extension (Cardello and
1046 Mancktelow, 2014), oriented perpendicular to the Tethyan palaeomargin. Timing and direction of
1047
1048
1049
1050
1051
1052
1053
1054
1055
1056
1057
1058
1059
1060
1061
1062

1063
1064 extension recognised in both areas are not in line with those previously described in sections 2 and
1065
1066 3 (Fig. 8b). In addition, Cardello and Mancktelow (2014) have suggested a possible gravitational
1067
1068 origin for these structures. For those reasons, these structures are not considered as forming part of
1069
1070 the Iberia-Eurasia rift system.
1071

1072
1073 In the External Briançonnais Domain of the Western Alps, Late Jurassic to Cretaceous
1074
1075 extensional structures have been reported also (e.g. Chaulieu, 1992; Claudel et al., 1997; Claudel
1076
1077 and Dumont, 1999). A WSW-ENE striking Callovian-Oxfordian extensional fault reactivated
1078
1079 during Albian and Turonian and a NW-SE striking Albian fault were described by Claudel et al.
1080
1081 (1997) (Site 14 of Figure 8). Claudel et al. (1997) also reported the occurrence of mid-Cretaceous
1082
1083 condensed sections, stratigraphic gaps, angular unconformities and neptunian dykes; all these
1084
1085 features are evidence for mid-Cretaceous extensional tectonics in the area. Similar observations
1086
1087 have been made by Chaulieu (1992), who inferred an Albian-Turonian extensional reactivation of
1088
1089 inherited Tethyan faults based on the occurrence of chaotic breccias along with several Jurassic
1090
1091 faults. According to this, the External Briançonnais Domain of the Western Alps area (Site 14 in
1092
1093 figure 8a) recorded an extensional pulse accompanied by uplift and erosion during Aptian to
1094
1095 Turonian times. Contrary to the nearby SE France basin, Helvetic domain, and eastern Pyrenees, the
1096
1097 direction of extension is not provided for the External Briançonnais Domain of the Western Alps,
1098
1099 because this area underwent significant - and variable - counter-clockwise vertical axis rotation with
1100
1101 respect to the stable Europe framework during Cenozoic times (Collombet et al., 2002).
1102
1103

1104
1105 Finally, in the Marguareis Extensional System of the Western Alps, Bertok et al. (2012)
1106
1107 reported mid-Cretaceous extension (Site 15 in Fig. 8a). In the next section, we illustrate how the
1108
1109 Marguareis area underwent extension between the Valanginian to Aptian and the early Late
1110
1111 Cretaceous, accompanied by block tilting.
1112

1115 3.5 Summary of the eastern Iberia-Eurasia boundary

1116
1117 The link between the structures described in the eastern Iberia-Eurasia boundary and those
1118
1119
1120
1121

1122
1123 from the Bay of Biscay – Pyrenean rift system (described in section 2) is evident when comparing
1124 timing and direction of extension for both areas (Fig. 8b). Although the onset of extension in the
1125 Pyrenean Arm is slightly older, end of extension by mid-Cretaceous times is almost coeval in the
1126
1127 Pyrenean Arm to the west, in the Vocontian and South Provence basins, and in the External
1128
1129 Briançonnais of the Western Alps. It is noticeable that the Cévennes fault is almost parallel to the
1130
1131 transfer faults of the Pyrenean arm. In addition, the directions of extension to the east and to the
1132
1133 west of this fault are parallel to each other, and roughly parallel to the strike of the fault, across
1134
1135 which the mid-Cretaceous depocenters are shifted. All these features evidence that the Cévennes
1136
1137 fault acted as - or was forming the most important part of - a transfer zone during mid-Cretaceous
1138
1139 extension.

1140 1141 1142 1143 1144 1145 1146 **4. Introducing the Marguareis Extensional System**

1147
1148 The Cretaceous Marguareis extensional system is located at the SW termination of the
1149
1150 Western Alps (Ligurian Alps, Fig. 9a), in the eastern part of the External Briançonnais Domain. The
1151
1152 Briançonnais Domain is considered a major palaeogeographic domain and a tectonic unit of the
1153
1154 Western Alps (Schmid et al., 2004 and references therein) (Fig. 3b).

1155 1156 1157 **4.1 Geological overview**

1158
1159 The Western Alps formed during the collision between the Adria and the European
1160
1161 continental margins of the Alpine Tethys ocean, following the Late Cretaceous to Eocene
1162
1163 subduction of this ocean (e.g. Dercourt et al., 1986; Coward and Dietrich, 1989; Schmid and
1164
1165 Kissling, 2000; Froitzheim et al., 2008; Handy et al., 2010; Faccenna et al., 2014). In the Western
1166
1167 Alps, mountain building started during Early Eocene, when N-S convergence between Adria and
1168
1169 Europe led part of the distal European continental margin and the Alpine Tethys oceanic
1170
1171 lithosphere, i.e. the internal Alpine units, to be subducted southward below the Adriatic lithosphere,
1172
1173 reaching HP- to UHP-metamorphic conditions (Goffé and Chopin 1986; Michard et al., 2004;
1174
1175 Beltrando et al., 2007; Bousquet et al., 2008). During the Middle-Late Eocene, the metamorphosed
1176
1177 internal units were exhumed and placed on top of the European continental margin as the North
1178
1179

1181
1182 Alpine Foreland basin was formed and progressively migrated toward the external sectors of the
1183 Alpine foreland (Ford et al., 2006; Malusà et al., 2011; Schlunegger and Kissling, 2015). A major
1184 change occurred in the Early Oligocene, when the motion of Adria with respect to Europe changed
1185 from N-ward to WNW-ward (Schmid et al., 1996; Handy et al., 2010; Dumont et al., 2012). This
1186 imposed a westward indentation of Adria that in the SW Alps produced the anticlockwise rotation
1187 of the Alpine units with respect to stable European lithosphere (Thomas et al., 1999; Schmid and
1188 Kissling, 2000). In the study area such an anticlockwise rotation was up to 120° (Fig. 9a)
1189 (Collombet et al., 2002), and led to a generalised left-lateral transpressional regime (Ford et al.,
1190 2006). As a consequence, SW-ward overthrusting of the internal units onto the external ones took
1191 place (Kerckhove 1969; Merle 1982; Coward and Dietrich, 1989; Fry, 1989; Michard et al., 2004;
1192 Dumont et al., 2011, 2012), together with the left-lateral juxtaposition of units initially belonging to
1193 different tectonic domains (Lemoine et al., 2000; Ford et al., 2006; Piana et al., 2009; d’Atri et al.,
1194 2016).

1210 In the Western Alps, four adjacent Mesozoic palaeogeographic domains have been
1211 classically distinguished (Fig. 9a). From the internal (eastern in a Mesozoic reference framework) to
1212 the external (western in a Mesozoic reference framework) sectors, these domains are: the Piedmont-
1213 Ligurian Domain, corresponding to the Alpine Tethys Ocean, and the “Pre-Piemontese”,
1214 Briançonnais, and Dauphinois-Provençal domains, corresponding respectively to the distal, inner
1215 and innermost part of the European Mesozoic continental margin (Lemoine et al., 1986). The
1216 Briançonnais units exposed in this area are classically further divided into internal and external
1217 units (Fig. 9a), mainly on the basis of their metamorphic features. The internal Briançonnais units
1218 were strongly affected by Alpine metamorphism, locally reaching HP- to UHP-LT conditions
1219 (Goffé and Chopin 1986; Michard et al., 2004; Beltrando et al., 2007; Bousquet et al., 2008).
1220 Conversely, only low-grade to anchizonal metamorphism developed in the external Briançonnais
1221 units (Piana et al., 2014; d’Atri et al., 2016, and references therein), where the Marguareis
1222 extensional system is located (Fig. 9).

1240
1241 The present-day structural setting and the relationships between the different tectonic units
1242
1243 of the Marguareis area are mainly controlled by the WNW-ESE Limone-Viozene transpressive
1244
1245 shear zone (Piana et al., 2009; d'Atri et al., 2016). This zone developed during the above-mentioned
1246
1247 Alpine left-lateral strike-slip stage and produced the SW-ward transpressive re-imbrication of the
1248
1249 external Briançonnais rocks onto a stack made of the buried Dauphinois-Provençal foreland
1250
1251 succession, tectonically capped by the Helminthoides Flysch units of the internal Piedmont-
1252
1253 Ligurian Domain. The major Alpine tectonic contact of the area is a transpressive fault that put in
1254
1255 contact the Mesozoic sedimentary sequence of the Briançonnais domain to the north with the
1256
1257 Helminthoides Flysch to the south (Fig. 9b). The external Briançonnais unit to the NE of this main
1258
1259 contact is further divided into the Limone-Viozene Zone and the Marguareis Unit, to the south and
1260
1261 to the north, respectively (Fig. 9b), the boundary corresponding to the Limone-Viozene northern
1262
1263 boundary fault (d'Atri et al., 2016), hereinafter called LIVZn Fault. The Marguareis Unit in turn
1264
1265 includes a western, central and eastern domain divided by N-S striking faults, as later detailed. The
1266
1267 Limone-Viozene Zone (Piana et al., 2009; d'Atri et al., 2016) is defined as a regional WNW-ESE
1268
1269 elongated tectonic unit extending for some tens of kilometres. In the study area, such a zone
1270
1271 involves rocks of the external Briançonnais domain, and it is delimited by two main faults, namely
1272
1273 the southern and northern Limone-Viozene boundary faults (Fig. 9b). These are arranged in a
1274
1275 leading pattern, with the southern fault being the master structure dividing two different
1276
1277 palaeogeographic domains. The northern one, i.e. the LIVZn Fault, is a trailing secondary structure,
1278
1279 accounting only for less than a few km of left-lateral displacement, coherently with the fact that
1280
1281 areas to the south and to the north of this northern fault share the same stratigraphy. Flower
1282
1283 structures and highly deformed slices occur at the upper structural levels of the faults, i.e. where
1284
1285 these affect the Upper Cretaceous to Cenozoic rocks. However, the LIVZn Fault in the study area is
1286
1287 generally well-localised (as shown below), and its width spans from a few m up to some tens of m.
1288
1289 As a result, the area in between the Limone-Viozene boundary faults, albeit the occurrence of some
1290
1291 low displacement (i.e. <50 mt) faults, displays a rather simple large-scale synclinal geometry, with
1292
1293
1294
1295
1296
1297
1298

1299
1300 no significant internal deformation. In the following we will focus on the stratigraphy and structures
1301
1302 of the Briançonnais units (i.e. Limone-Viozene and Marguareis tectonic units).
1303

1304 The oldest rocks exposed in the study area are volcanic and volcanoclastic rocks of Late
1305 Carboniferous-Permian age. These are overlain by a Lower Triassic to Upper Cretaceous
1306 sedimentary succession, which is subdivided into lithostratigraphic units mostly bounded by
1307 unconformities (Vanossi, 1969, 1972; Bertok et al., 2011) (Fig. 9b). From the bottom to the top,
1308 these are: (i) The “Quarziti di Ponte di Nava” Fm. (Upper Permian?–Lower Triassic?), which is
1309 constituted by continental to littoral conglomerates and cross-bedded quartz arenites, being locally
1310 interbedded with shales. This formation is about 200 metres thick in the study area. (ii) The
1311 “Dolomie di San Pietro dei Monti” Fm. (Anisian-Ladinian), which is made up by peritidal
1312 dolostones and limestones. Its top is truncated by an erosional surface corresponding to a hiatus
1313 which spans the Upper Triassic, Lower Jurassic and part of the Middle Jurassic. The thickness of
1314 this formation is variable in the study area, ranging from less than 500 up to 900 metres. (iii) The
1315 “Calcari di Rio di Nava” Fm. (Bathonian), consisting of monotonous dark micritic limestones
1316 deposited in a restricted carbonate shelf environment; the top is truncated by an erosional surface,
1317 locally associated with a slight angular unconformity. Its thickness ranges from few tens of metres
1318 up to about 150 metres. (iv) The “Calcari di Val Tanarello” Fm. (Kimmeridgian?–Berriasian):
1319 pelagic limestones locally exhibiting a nodular Ammonitico Rosso facies in the upper part, with a
1320 total thickness of some tens of metres. (v) The “Upega” Formation (Upper Cretaceous): grey
1321 hemipelagic marly limestones, separated from the underlying “Calcari di Val Tanarello” by a black
1322 crust of Fe-Mn oxides, glauconite and phosphates containing planktic foraminiferal assemblages
1323 referable to the middle Albian (Bertok et al., 2011). This mineralised hardground documents a
1324 prolonged hiatus encompassing the Valanginian-Aptian interval. The top of the Mesozoic
1325 succession is truncated by a regional unconformity, overlain by a Middle Eocene-Lower Oligocene
1326 Alpine Foreland succession, here composed of massive bioclastic limestones up to 30 metres thick,
1327 overlain by dark shales with interbedded turbiditic sandstone layers (d’Atri et al., 2016). In the
1328
1329
1330
1331
1332
1333
1334
1335
1336
1337
1338
1339
1340
1341
1342
1343
1344
1345
1346
1347
1348
1349
1350
1351
1352
1353
1354
1355
1356
1357

1358
1359 northeastern part of the Marguareis area the Cenozoic sediments directly rest on top of Jurassic
1360
1361 limestones through an erosional surface. The Upper Cretaceous deep-water Upega Fm. is locally
1362
1363 affected by a pervasive foliation, particularly nearby the Limone-Viozene boundary faults, which
1364
1365 documents a strong localization of the deformation in anchizonal metamorphic conditions (Piana et
1366
1367 al., 2014). Instead, the Permian-Jurassic stratigraphic succession experienced much less internal
1368
1369 deformation, allowing for the preservation of most of the primary stratigraphic features (Piana et al.,
1370
1371 2009; Bertok et al., 2011, 2012; Martire et al., 2014).

1374 **4.2 Main faults of the Marguareis area**

1375
1376 Three major faults affect the Briançonnais units of the study area. The E-W-striking LIVZn
1377
1378 Fault divides the Limone-Viozene zone to the south, where strata are SW-dipping, from the
1379
1380 Marguareis Unit to the north. The latter unit is subdivided into the western, central and eastern
1381
1382 domains, which are separated from each other by the N-S striking and E-dipping Colle del Pas and
1383
1384 Passo delle Saline normal faults (Fig. 9b). Both faults extend for several kilometres and clearly abut
1385
1386 upon the LIVZn Fault. The E-W striking LIVZn Fault in the western portion of the study area is
1387
1388 near vertical and has W-dipping Mesozoic carbonates in the northern block and SSW-dipping to
1389
1390 near vertical Permian volcanites and Triassic sediments in the southern block, respectively (Fig.
1391
1392 10a-c). The Principal Displacement Zone (PDZ; Tchalenko, 1970) is exposed to the NE of the
1393
1394 Carnino Village (Fig. 10c-e), where the Middle Triassic “Dolomie di San Pietro dei Monti” Fm. is
1395
1396 in contact with the Permian volcanites (Fig. 10c-d). The PDZ displays a left-lateral strike-slip
1397
1398 kinematics (Fig. 10d, e). To the west, the LIVZn Fault has a N-ward dip of about 60°-70° and the
1399
1400 PDZ is no longer well-exposed (Fig. 11). There the fault juxtaposes Cenozoic, Upper Cretaceous,
1401
1402 and Jurassic rocks of the northern block, with Triassic and Jurassic to lowermost Cretaceous rocks
1403
1404 of the southern block (Fig. 11a, b). At places the southern and northern blocks are 20-30 m apart, in
1405
1406 other areas the LIVZn Fault is constituted by an up to 200 m wide zone including decametre- to
1407
1408 hectometre-sized fault-bounded slices of Upper Cretaceous and Cenozoic rocks, arranged in an
1409
1410 anastomosed geometry and stretched along an WNW-ESE direction. The southern block in this
1411
1412
1413
1414
1415
1416

1417
1418 western area is composed of a SSW-dipping monocline, which to the west is affected by left-
1419 stepping NW-SE striking and NE-dipping normal faults abutting on the LIVZ Fault (Fig. 11a, b),
1420 and showing displacement up to few tens of metres (Fig. 6a). In the northern block of the LIVZn
1421 Fault, a few tens of m apart from the fault itself, a Cretaceous E-W oriented palaeoescarpment has
1422 been documented by Bertok et al. (2012). This palaeoescarpment is evidenced by the occurrence of
1423 an irregular erosional surface incised within the Upper Jurassic - lowermost Cretaceous limestones
1424 of the Calcari di Val Tanarello Fm., locally covered by patches of a mineralised crust bearing
1425 planktic foraminifers assemblages referable to the Albian, and overlapped by the Upper Cretaceous
1426 sediments of the Upega Fm. (Fig. 11c-d). Close to the palaeoescarpment, metre- to decametre-sized
1427 olistoliths of Calcari di Val Tanarello limestones occur, completely embedded within the deep-
1428 water sediments of the Upper Cretaceous Upega Fm. (Bertok et al., 2012). It is worth noting that the
1429 palaeoescarpment does not correspond to the Cretaceous LIVZn Fault, as these structures have
1430 some orders of magnitude of difference: the LIVZn Fault affects the upper crust while the
1431 palaeoescarpment evidencing sub ordered faulting with less than a few tens of metres of
1432 displacement. The importance of the palaeoescarpments lies in the fact that they allow to constrain
1433 the age of the onset of extensional deformation.

1434
1435 The Passo delle Saline Fault, located in the eastern portion of the study area, runs almost N-
1436 S and abuts on the LIVZn Fault (Figs. 9b, 12a). The stratigraphic displacement of this fault is in the
1437 order of some hundreds of metres and the dip of the fault is 30° to 40° toward the east. Units
1438 exposed in both the hanging wall and the footwall dip toward the west. The Cenozoic sediments are
1439 not affected by extensional faults and in the hanging wall of the Passo delle Saline fault, they
1440 unconformably overlie the Triassic to Cretaceous sediments (Fig. 12a). N-S oriented extensional
1441 structures occur at different scales in the area. They span from the tens of km long Passo delle
1442 Saline and Colle del Pas faults, to the hundreds of m long extensional faults exposed in the hanging
1443 wall of the former fault (Fig. 12a) and includes also N-S striking background veins and joints,
1444 which are widespread in the Triassic and Jurassic carbonate beds (Fig. 12b).

1476
1477 To the west, the other N-S striking and E-dipping fault is the Colle del Pas Fault (Fig. 13).
1478
1479 In its hanging wall, W-dipping Triassic and Jurassic carbonates are exposed. The footwall is made
1480
1481 up of Permian to Jurassic rocks, dipping toward the west and, in the southern part, toward the south.
1482
1483 Along the fault, the occurrence of sedimentary breccias unconformably resting on Permian volcanic
1484
1485 rocks of the footwall, and overlapped by Upper Cretaceous sediments (Bertok et al., 2012) (Fig.
1486
1487 13b,c), evidence a Cretaceous normal displacement in the order of many hundreds of metres.
1488
1489 Although most of the displacement has occurred before the deposition of the Upega Fm., the Colle
1490
1491 del Pas Fault was still active at the beginning of the Late Cretaceous, as indicated by growth
1492
1493 geometries in the lowermost portion of the Upega Fm. (Fig. 13d). Along the southern portion of the
1494
1495 Colle del Pas Fault, the Piaggia Bella karstic system provides additional data about the fault
1496
1497 geometry at depth (Fig. 13a). The karstic system is developed within the Mesozoic carbonates
1498
1499 located on the hanging wall, which are juxtaposed to the impermeable base of the system,
1500
1501 represented by the Permo-Triassic quartz arenites and shales of the Quarziti di Ponte di Nava Fm.
1502
1503 and the Permian volcanic rocks, at the footwall. This tectonic contact between hanging wall
1504
1505 carbonates and the impermeable base of the footwall is observed at several places along the karstic
1506
1507 system (Fig. 14), and the corresponding XYZ coordinates are available. This subsurface dataset has
1508
1509 been used for constructing the cross sections in figure 15.
1510
1511
1512
1513
1514

1515 **4.3 The 3D architecture of the Marguareis extensional system**

1516

1517 Field measurements of bedding, 5-m-resolution digital terrain model (DTM ICE 2009-2011
1518
1519 by Regione Piemonte), 0.5 m/px orthophotos (Orthoimages ICE 2009-2011 by Regione Piemonte),
1520
1521 subsurface geological data from the Piaggia Bella karstic system, and geological maps by Vanossi
1522
1523 (1972) and Bertok et al. (in Press), were integrated in the Midland Valley 3D Move software, in
1524
1525 order to build a 3D model of the area. Ten representative vertical sections - six E-W and four N-S
1526
1527 striking - are used to illustrate the 3D structure of the area (Fig. 15). All the E-W striking sections
1528
1529 are from the northern block of the LIVZn Fault, and for all of them we reported: the distance
1530
1531 between two pin lines placed at the edge of the section (computed at the top of Jurassic to
1532
1533
1534

1535
1536 lowermost Cretaceous Calcari di Val Tanarello Fm.), the length of the unfaulted top of the Jurassic
1537
1538 to lowermost Cretaceous, and the derived amount of extension. The amount of extension computed
1539
1540 along all the E-W sections (including those in the 3D move file in the supplementary material) is
1541
1542 also reported in the map on figure 15. A one-km long bar is provided for those sectors of the
1543
1544 sections where, in 3D, the dip-direction of layers runs roughly parallel to the section, and its base is
1545
1546 pinned at the base of the Quarziti di Ponte di Nava Fm. This bar thus serves to illustrate
1547
1548 sedimentary thickness variations.
1549

1550
1551 The E-W oriented sections to the north of the LiVZ are characterised by a domino pattern,
1552
1553 with three main W-dipping blocks being bounded by the two major E-dipping Colle del Pas and
1554
1555 Passo delle Saline extensional faults. In detail, the eastern and central tilted blocks dip about 20°,
1556
1557 while the western one dips 30° (as seen in sections EW13, EW15, and EW17). The dip of N-S
1558
1559 striking extensional faults, including the secondary ones, ranges between 30° and 45°, as seen also
1560
1561 at depth along the Piaggia Bella Karstic system (Fig. 14), and their cutoff angles range between 50°
1562
1563 and 60°. The amount of E-W extension to the north of the LIVZn Fault increases northward, being
1564
1565 21% close to the fault, and 38% in the northernmost E-W section. The extension is mostly achieved
1566
1567 by slip along the two major faults, with a minor contribution from the other extensional structures.
1568
1569 The slip along the Passo delle Saline Fault is roughly constant along its strike, whereas
1570
1571 displacement along the Colle del Pas fault increases northward. The latter fault is thus responsible
1572
1573 for the northward-increasing cumulative extension.
1574
1575

1576
1577 A first structural observation concerns the occurrence of a large anticline striking about
1578
1579 WNW-ESE. To the west, in sections NS1 and NS4 of figure 15, the axis of the anticline is in the
1580
1581 northern block of the LIVZn Fault. The northern limb of the anticline is tilted slightly, so the pre-
1582
1583 folding geometries remain largely preserved. The anticline and the LIVZn Fault run oblique to each
1584
1585 other and further to the east, along sections NS7 and NS10 of figure 15, the anticlinal axial surface
1586
1587 is no longer occurring. The LIVZn Fault in this eastern area is near-vertical and displays a cutoff
1588
1589 angle of about 90° with layers of its northern block. Cutoff angles with the folded layers of the
1590
1591
1592
1593

1594
1595 southern block range instead from 20° to 40°. The Quarziti di Ponte di Nava Fm. is about 150 to
1596
1597 200 m-thick in the entire area, with a couple of sections (western block of sections EW13 and EW7)
1598
1599 in which its thickness reaches almost 300 m. A significant thickness variation of the Triassic
1600
1601 Dolomie di San Pietro dei Monti Fm. is instead observed across the LIVZn Fault, being constantly
1602
1603 below 600 m to the north and roughly 800-850 m to the south. Such a thickness variation is not
1604
1605 accompanied by any remarkable structural repetition of the sequence, thus indicating its
1606
1607 sedimentary origin. The total thickness of the Jurassic-lowermost Cretaceous formations spans
1608
1609 between 150 and 250 m in the entire area. The original stratigraphic thickness of the Upega Fm. is
1610
1611 hardly to assess due to the scarcity of outcrops of its upper boundary with the overlying Cenozoic
1612
1613 sediments, the erosional nature of such boundary locally incising down to the Jurassic formations,
1614
1615 and even because of the high finite strain affecting the Upega Fm. itself. Nevertheless, the
1616
1617 geological map evidences that it is mainly preserved close to the N-S striking, E-dipping faults
1618
1619 bounding westward the three main W-dipping blocks, and that it roughly wedges out toward the
1620
1621 tilted blocks' culminations.
1622
1623

1624 1625 **4.4 The Cretaceous structural framework** 1626 1627

1628
1629 Observations provided in this work support the activity of the Colle del Pas and Passo delle
1630
1631 Saline N-S striking normal faults during the Cretaceous. These faults form part of an extensional
1632
1633 array that started to develop in the Valanginian-Aptian time interval, as indicated by Albian
1634
1635 palaeoescarpments incised within the Upper Jurassic - lowermost Cretaceous limestones (Fig. 11c-
1636
1637 d) (Bertok et al., 2012). The Upega Fm. mostly seals the extensional faults; however, we have
1638
1639 documented that the lowermost portion of this unit includes growth geometries (Fig. 13d). Based on
1640
1641 these observations, we deduce that extensional tectonics in the area spanned from the Valanginian-
1642
1643 Aptian up to the early Late Cretaceous. The occurrence of metre- to tens of metres-sized olistoliths
1644
1645 of Triassic dolostones and Jurassic limestones embedded within the Upper Cretaceous sediments,
1646
1647 provide additional evidence for the Cretaceous extensional tectonics, as these features are coherent
1648
1649 with the development of Cretaceous topographic highs and depocentres associated with extensional
1650
1651
1652

1653
1654 tectonics. Along the Colle del Pas Fault, the Upper Cretaceous sediments locally onlap sedimentary
1655 breccias directly resting on an erosional surface incised within tilted Permian rocks (Fig. 13b,c).
1656
1657 This documents a minimum normal displacement of the Cretaceous fault of about 700 metres,
1658
1659 which is roughly equivalent to the present-day displacement. This demonstrates a roughly
1660
1661 negligible Alpine overprint along this fault and suggests a similar framework for the Passo delle
1662
1663 Saline Fault, where no evidence of inversion occurs. The domino pattern presently characterizing
1664
1665 the area to the north of the LIVZn Fault is also interpreted as Cretaceous, as indicated by the breccia
1666
1667 body resting on top of the Colle del Pas Fault. The fault is in fact dipping 30° eastward and has a
1668
1669 cutoff angle of about 50-60°, assuming a Cenozoic tilting of the footwall of the Colle del Pas fault
1670
1671 would require a Cretaceous breccias depositional angle of about 60 degrees, which is impossible.
1672
1673
1674

1675 The LIVZn Fault is characterised by an Alpine left-lateral displacement in the order of less
1676
1677 than a few km. This value is suggested by scaling relationships between fault displacement and
1678
1679 length (e.g. Cowie and Scholz, 1992; Kim and Sanderson, 2005). Indeed, these relationships point
1680
1681 to less than a few km of displacement for a fault strand long less than a few tens of km, like the
1682
1683 LIVZn. The marked thickness change of the Triassic sequence across it, indicates an at least
1684
1685 Triassic origin, thus this fault was already formed during the Cretaceous. However, no direct
1686
1687 observations on the Cretaceous kinematics and displacement of the WNW-ESE striking LIVZn
1688
1689 Fault are presently possible, because of the above mentioned Alpine transpressive tectonics. The N-
1690
1691 S striking Colle del Pas and Passo delle Saline faults abut against it and no N-S striking fault occur
1692
1693 southward of the LIVZn Fault. These features support a kinematic relationship between the E-W
1694
1695 striking LIVZn Fault and the Cretaceous N-S striking normal faults. As illustrated in figure 16, at
1696
1697 Cretaceous times the restored NNE-SSW striking (once removed the 120° counter-clockwise
1698
1699 rotation, Collombet et al., 2002), steeply dipping LIVZn Fault would have divided a westerly
1700
1701 unfaulted block from an easterly faulted and southward translating extended block. This
1702
1703 configuration implies that the LIVZn Fault was forming a hard-linked transfer fault (e.g., Gibbs,
1704
1705 1984; Morley et al., 1990; Gawthorpe and Hurst, 1993), with a right-lateral component as shown in
1706
1707
1708
1709
1710
1711

1712
1713 figure 16. Such transfer fault should extend much further the study area, as documented by the
1714
1715 occurrence of other N-S striking faults (in present day orientation), both to the east (Mongioie Fault,
1716
1717 Bertok et al., 2012) and to the west (Michard and Martinotti, 2002). Accordingly, we propose that
1718
1719 during the Cretaceous the LIVZn Fault reached a total length of several tens of kms; however, no
1720
1721 trustworthy information about the Cretaceous kinematics is available for this fault. Nevertheless, a
1722
1723 series of NW-SE striking faults arranged in an en echelon pattern occurring in the western portion
1724
1725 of the study area (Fig. 11a,b) could be taken as indicative for a Cretaceous right-lateral activity of
1726
1727 the fault, albeit the timing of these en echelon faults is not constrained.
1728
1729

1730 The last important observation concerns the sediments deposited during and after the faults
1731
1732 activity. To the north of the LIVZn fault Upper Cretaceous sediments are mostly preserved within
1733
1734 semi-graben basins related to the N-S striking faults. Their maximum thickness does not exceed 200
1735
1736 metres and they roughly wedge out toward the footwall scarp and the tilted blocks' culmination,
1737
1738 where Cenozoic strata even directly rest on top of Jurassic carbonates. Olistoliths made up of
1739
1740 Triassic and Jurassic carbonatic rocks occur embedded both within Upega Fm. and Cenozoic
1741
1742 succession, thus proving that Late Cretaceous semi-graben basins were still under-filled in the Late
1743
1744 Eocene.
1745
1746

1747 Summarizing, the Valanginian-Aptian to early Late Cretaceous extensional system of the
1748
1749 Marguareis area was characterised by a tens of kilometres long near vertical right-lateral fault
1750
1751 (reactivating an inherited Triassic fault), whose strike was nearly NNE-SSW, having associated a
1752
1753 set of normal faults, which accommodated an amount of SSW-directed extension in the order of
1754
1755 some kilometres.
1756
1757

1758 **5 Discussion**

1759
1760 Information provided in this work indicates that the Cretaceous structures of the Marguareis
1761
1762 extensional system and the SE France basin are kinematically similar, and coeval to that of the Bay
1763
1764 of Biscay - Pyrenean rift system. Our conclusion arises from the kinematic observations illustrated
1765
1766
1767
1768
1769
1770

1771
1772 above, coupled with information about timing of major geodynamic events. Data about the
1773
1774 extension directions, the basins' shape and extensional domains, the orientation of transfer faults,
1775
1776 and the timing of major tectonic events - i.e. basins formation and mantle exhumation - provide a
1777
1778 consistent picture for a dominantly NNE-SSW oriented divergent movement along the Iberia-
1779
1780 Eurasia plate boundary (Fig. 17). As discussed below, the plate boundary was formed by the Bay of
1781
1782 Biscay and Pyrenean arms and, to the east of the Pyrenees, by the SE France Arm (made by the
1783
1784 Figueres-Montgrí, South Provence, and Vocontian basins) and the Briançonnais Arm (made by the
1785
1786 Marguareis extensional system) (Fig. 17b).
1787
1788

1789
1790 Transfer faults running perpendicular to major extensional faults and accommodating the
1791
1792 connection between individual fault segments, faults, or extensional basins, are constitutive features
1793
1794 of extensional systems (e.g. Gibbs, 1984; Morley et al., 1990; Lister et al., 1991; Gawthorpe and
1795
1796 Hurst, 1993; Faulds and Varga, 1998), and include transform faults segmenting the actively
1797
1798 spreading oceanic ridges (Wilson, 1965). A noticeable kinematic constraint at the Iberia-Eurasia
1799
1800 plate boundary is provided by this kind of faults. All the major transfer faults segmenting the rift
1801
1802 (i.e., Santander, Pamplona, Cérvennes, Durance-Aix, Nimes, and LIVZn faults) are roughly
1803
1804 perpendicular to the WNW-ESE elongated Parentis, Basque-Cantabrian, Arzacq-Mauléon, Flysch
1805
1806 Noir, Organyà, Vocontian, South Provence, and Marguareis basins, and are roughly parallel to the
1807
1808 mid-Cretaceous extension directions recognised in all these areas (Fig. 17). This configuration
1809
1810 admits very little, if any, obliquity in the rift system.
1811
1812

1813
1814 Timing of major events along the rift is slightly diachronic, overall pointing to an eastward
1815
1816 propagation of the rift. The base of the synrift infill is Kimmeridgian in the Basque-Cantabrian
1817
1818 basin (e.g. García-Mondéjar et al., 1986; Rat, 1988), Tithonian in the Arzacq basin (Biteau et al.,
1819
1820 2006), and Tithonian-Berriasian in the Organyà basin (Dinarès-Turell and García-Senz, 2000;
1821
1822 García-Senz, 2002) (Fig. 17b). The first evidence of extensional deformation to the east of the
1823
1824 Cévennes fault is instead Early Cretaceous. In detail, it is Hauterivian to Berriasian in the Figueres-
1825
1826 Montgrí basin (Mató et al., 1995b) and Berriasian-Valanginian in the SE France basin (Masse et al.,
1827
1828
1829

1830
1831 2009). In the Marguareis system to the east, onset of extension occurred between Valanginian and
1832
1833 Aptian times. During the Albian-Cenomanian interval, the synrift stage ended in all the reviewed
1834
1835 basins and hyperextension followed by the consequent exhumation of sub-continental mantle
1836
1837 occurred in the Mauléon basin (Jammes et al., 2009; Lagabrielle et al., 2010; Masini et al., 2014).
1838
1839 As already pointed out, the structures from the Central Alps have different timing and orientations
1840
1841 instead (Fig. 8), and therefore may pertain to a different geodynamic framework, including
1842
1843 gravitationally-induced deformation along the passive European margin of the Alpine Tethys ocean.
1844
1845

1846 The kinematics, timing, and synchronicity of extensional deformation in the area extending
1847
1848 from the Bay of Biscay to the External Briançonnais Domain, have major geodynamic implications
1849
1850 for the long debated opening mode of the Bay of Biscay. The occurrence of roughly E-W elongated
1851
1852 mid-Cretaceous basins to the east of the Cévennes fault, i.e., the Figueres-Montgrí, Vocontian,
1853
1854 South Provence, and Marguareis basins, is incompatible with the scissor-type opening mode for the
1855
1856 Bay of Biscay (Fig. 2). In that model, the mid-Cretaceous basins of the Pyrenees have been
1857
1858 interpreted as back-arc structures (e.g. Sibuet et al., 2004). According to Advokaat et al. (2014), the
1859
1860 mid-Cretaceous northward subduction of Iberia was confined eastward by a major N-S striking
1861
1862 transform, located to the west of Sardinia (Fig. 2c). Such configuration cannot explain the
1863
1864 occurrence of extensional deformation coeval with that of the Pyrenean arm, and to the east of the
1865
1866 subduction termination. As mentioned in the introduction, the strike-slip opening mode assumes
1867
1868 mid-Cretaceous transform plate boundary located along the North Pyrenean Fault. Eastward
1869
1870 translation of Iberia would have accommodated to the east by the opening of the Valais ocean (e.g.
1871
1872 Stampfli and Borel, 2002; Handy et al., 2010), which would represent a sort of dilation jog placed at
1873
1874 the termination of a left-lateral transform fault. The mid-Cretaceous age of the Valais “ocean” is
1875
1876 questionable in the light of U-Pb dating providing Early Carboniferous (Bussy et al., 2008),
1877
1878 Permian (Beltrando et al., 2007), or even Late Jurassic (Liati and Froitzheim, 2006) ages. Moreover,
1879
1880 the hypothesis of a mid-Cretaceous dilation jog of a hypothetical North Pyrenean transform fault is
1881
1882 not supported by the data presented here and discussed as follows: after restoring the Corsica-
1883
1884
1885
1886
1887
1888

1889
1890 Sardinia block to its position before the opening of the Liguro-Provençal basin (Bache et al., 2010)
1891
1892 (Figs. 3b, 6a), the block must be shifted southward tens of km to remove the Pyrenean shortening.
1893
1894 Bestani et al. (2016) propose that Sardinia and Provence were 140 km apart before onset of
1895
1896 Pyrenean convergence. Such a great distance allows placing a hyperextended continental crust or
1897
1898 exhumed mantle domain, or even oceanic crust, in between. Indeed, many authors support the
1899
1900 occurrence of a suture zone between the Provence region and the Sardinia-Corsica block, whose
1901
1902 remnants are presently underneath the Provence crust (e.g. Lacombe and Jolivet, 2005; Bestani et
1903
1904 al., 2016). For the Early to mid-Cretaceous deformation history of Sardinia and Corsica, the only
1905
1906 available datum is represented by the work of Mameli et al., (2007) and is illustrated in figure 7b.
1907
1908 However, the structure described by these authors for the Sardinia-Corsica block, together with data
1909
1910 from the South Provence basin, the Vocontian basin, and the Marguareis system, all point to an
1911
1912 Early to mid- Cretaceous N-S to NE-SW directed extension. The N-S to NE-SW extension direction
1913
1914 is consistent with the extensional structures of the Pyrenean arm and rules out the hypothesis of a
1915
1916 North Pyrenean Fault-Valais strike-slip system. In such a strike-slip system, the Valais dilation jog
1917
1918 should open to accommodate the left-lateral motion of Iberia along the North Pyrenean Fault. As a
1919
1920 result, the extension direction in the Valais ocean should have formed an angle from 0° to 45° (e.g.
1921
1922 Sylvester, 1988) with the plate boundary. Conversely, we have documented in this work that
1923
1924 extension was almost perpendicular to the plate boundary, making the strike-slip scenario not
1925
1926 supported by geological data and hence, not kinematically admissible. In addition, the idea that
1927
1928 Pyrenean rift basins could have developed as pull apart structures that eventually became linked is
1929
1930 to be discarded for the following arguments. The hyperextended domain of the eastern Pyrenees, the
1931
1932 South Provence basin, the Vocontian basin, and the Marguareis structure form a gross left-stepping
1933
1934 system, but not consistent with left-lateral strike-slip tectonics. Data presented in our work indicates
1935
1936 that, if any, the hyperextended domain between the Sardinia-Corsica block and the South Provence
1937
1938 basin was WNW-ESE elongated and represented the eastern prolongation of the Pyrenean arm. In
1939
1940 conclusion, data to the east of the Pyrenees indicate that a plate boundary extended westward from
1941
1942
1943
1944
1945
1946
1947

1948
1949
1950
1951
1952
1953
1954
1955
1956
1957
1958
1959
1960
1961
1962
1963
1964
1965
1966
1967
1968
1969
1970
1971
1972
1973
1974
1975
1976
1977
1978
1979
1980
1981
1982
1983
1984
1985
1986
1987
1988
1989
1990
1991
1992
1993
1994
1995
1996
1997
1998
1999
2000
2001
2002
2003
2004
2005
2006

the Bay of Biscay to the Briançonnais domain to the east and had a purely divergent movement during the Early to mid-Cretaceous time interval. In agreement with the lateral evolution of magma-poor rifting (Manatschal, 2004), the Bay of Biscay floored by oceanic crust is the more evolved portion of the rift, the Pyrenean arm, where mantle exhumation is documented, is the intermediate stage, whereas the SE France-Marguareis areas form the less evolved portion of the rift system; such arrangement is coherent with an eastward diminishing amount of divergence. For this long list of evidence, the mid-Cretaceous left-lateral transform model for the Iberia-Eurasia margin should be definitively abandoned. This model has been the paradigm, especially among geologists, for explaining the rotation of Iberia for a very long time (e.g. Souquet et al., 1985; Debroas, 1990; Choukroune, 1992; Olivet, 1996). However, after tens of years of field studies, at the best only equivocal and ambiguous arguments support it. A certain variability of the local extension direction has been documented in the various Cretaceous basins of the margin (e.g. Soto et al., 2008; Olivia-Urcia et al., 2011). The extension is mostly arranged in two mutually perpendicular directions, which is a normal behaviour for extensional systems (e.g. Destro, 1995): such complexity cannot be interpreted as strike-slip tectonics if no evidence for strike-slip motion occurs. Also, the evidence for initially isolated basins that become linked and interconnected, cannot be taken by any reason as an evidence of a pull apart origin. The pattern of faults, and in particular the angular relationships among them and their interpretation according to a Riedel's pattern (Riedel, 1929), has been also invoked as an evidence for the left-lateral strike-slip mid-Cretaceous tectonics (e.g. García-Mondéjar, 1996). However: (1) evidence for left-lateral strike slip striations in such Riedel fault pattern has never been reported in the literature, (2) the occurrence of Variscan and Permo-Triassic inheritances, along with the Upper Cretaceous to Cenozoic reactivation of many of these faults, makes the analysis of the angular relationships alone questionable, as its best. In summary, along the Pyrenees no unequivocal evidence for a Cretaceous lithospheric strike-slip system, comparable for size and displacement to the North Anatolian or San Andrea faults, has ever been provided.

Having demonstrated the incompatibility between the Cretaceous geological record of the

2007
2008 Iberia-Eurasia plate boundary and both the strike-slip and the scissor type models, a major plate
2009 kinematics issue is to be addressed, as introduced at the beginning of this work, magnetic anomalies
2010 showing a diachrony in the opening of the northern Atlantic (e.g. Sibuet et al., 2004; Vissers and
2011 Meijer, 2012) and paleomagnetic data about the rotation of Iberia (e.g. Barnett-Moore et al., 2016),
2012 are apparently at odds with the divergent model proposed here. This is something known for a long
2013 time (Fig. 1): as already pointed out by Choukroune et al. (1973), if a rigid plate behaviour is
2014 assumed for the Iberia plate, in order to form the Bay of Biscay with coeval extension in the
2015 Pyrenees, the divergent scenario requires an Euler pole to the east of the rift's termination, i.e. to the
2016 east of the Briançonnais Domain. Such pole would be able to account for less than 10° of rotation,
2017 instead of the documented > 30° counter-clockwise rotation (Barnett-Moore et al., 2016, and
2018 references therein). In our view, the key to resolve this apparent discrepancy is the wrong
2019 assumption of a rigid behaviour for the Iberian plate during the Cretaceous divergence, which is all
2020 but certain as it is generally assumed for the sake of simplicity. The importance of intraplate
2021 structures during the separation between Iberia and Eurasia has been recently recalled by Tugend et
2022 al. (2015) but Late Jurassic to Early Cretaceous extension – coeval with the opening of the Bay of
2023 Biscay - focused along the NW-SE striking intra-plate Central Iberian rift is known for a long time
2024 (e.g. Álvaro et al., 1979; Salas and Casas, 1993; Salas et al. 2001). In the Central Iberian rift system,
2025 no mantle exhumation has been reported but evidence for Late Jurassic to mid-Cretaceous extreme
2026 crustal thinning has been provided in its three large depocentres (Fig. 17): the Cameros basin to the
2027 NW (Mata et al., 2001; Salas et al., 2001; Omodeo-Salé et al., 2017), the Maestrat basin to the SE
2028 (e.g. Salas et al., 2001), and the offshore Columbretes basin further to the SE (e.g. Ayala et al.,
2029 2003), where Granado et al. (2016) have even provided evidence for hyper-thinning of the lower
2030 crust and associated mantle faulting. Remarkable extensional deformation, reaching the hyper-
2031 thinning and mantle faulting, implies that the Central Iberian rift could have partially decoupled the
2032 Ebro Block to the NE from the western Iberia to the west (Fig. 17b). Indeed, these two blocks have
2033 a similar amount of Cretaceous counter-clockwise vertical axis rotation but there is no geological
2034
2035
2036
2037
2038
2039
2040
2041
2042
2043
2044
2045
2046
2047
2048
2049
2050
2051
2052
2053
2054
2055
2056
2057
2058
2059
2060
2061
2062
2063
2064
2065

2066
2067 reason, at present, for assuming that these formed a unique rigid block rotating around a unique
2068 Eulerian pole. Such partial decoupling of the Ebro block is in line with the observation that in non-
2069 oceanic frameworks plates may not behave as rigid objects (Molnar, 1988). This fully applies to the
2070 Bay of Biscay-Pyrenean rift system, which displays an increasingly de-localised nature toward its
2071 eastern - non-oceanic - termination (Fig. 17b): as said, to the east of the Basque-Cantabrian basin,
2072 where no oceanic crust occurs, the rift system splits along two arms: the Pyrenean Arm and the
2073 Central Iberian rift, with the Ebro block in between. Further towards its eastern termination, the
2074 number of basins progressively increases to the east of the Cévennes transfer fault, where the area
2075 undergoing extension reaches a width comparable to that of the entire Iberian plate. In conclusion,
2076 if the eastern portion of the Bay of Biscay – Pyrenean rift is considered as a diffuse divergent plate
2077 boundary, geological and geophysical observations can be reconciled: the first one indicating
2078 extension along the entire length of the rift system during the Early Cretaceous; the second allowing
2079 to model the bulk of the movement of the western portion of the Iberian plate by means of counter-
2080 clockwise rotation about a pole most likely located in the eastern portion of the Pyrenees.
2081
2082
2083
2084
2085
2086
2087
2088
2089
2090
2091
2092
2093
2094
2095
2096
2097
2098

2099 **6. Conclusions**

2100
2101 In this work we have presented a throughout revision of geological data in the Cretaceous basins to
2102 the east of the Pyrenees, in the area comprised between the easternmost portions of the Pyrenees
2103 and the Western Alps. Our work evidences that, from the Late Jurassic to the mid-Cretaceous times,
2104 the Pyrenean Arm of the rift was undergoing NNE-SSW-directed extension and it was delimited to
2105 the east by the NNE-SSW striking Cévennes fault. To the east of this transfer fault, synrift Late
2106 Jurassic to mid-Cretaceous N-S extension is documented in the three major E-W elongated
2107 extensional basins forming the SE France Arm of the rift system: the Vocontian and South
2108 Provence basins, presently exposed in the north-verging portion of the Provence fold-and-thrust
2109 belt, and the Figueres-Montgrí basin, which is partly exposed in the easternmost sector of the south-
2110 verging portion of the Pyrenees fold-and-thrust belt. In between these basins, an E-W elongated
2111
2112
2113
2114
2115
2116
2117
2118
2119
2120
2121
2122
2123
2124

2125
2126 domain of hyperextended continental crust can be hypothesised. To the east of the SE France Arm,
2127
2128 evidence of an even easternmost arm of the rift – i.e. the Briançonnais Arm - occurs in the
2129
2130 Marguareis extensional system of the Western Alps. This extensional system holds evidence of N-S
2131
2132 extension and it was delimited to the west by a N-S striking transfer fault.
2133

2134
2135 We conclude that the SE France and Briançonnais arms share the same timing and
2136
2137 direction of extension with those documented in the Bay of Biscay - Pyrenean rift. Reviewed data
2138
2139 along with that presented in this study constrain the Early to mid-Cretaceous divergent movements
2140
2141 in the easternmost portion of the of Iberia-Eurasia plate boundary, and support a purely divergent
2142
2143 kinematics for the entire plate boundary.
2144

2145 2146 2147 2148 2149 **Acknowledgements**

2150
2151 We thank two anonymous reviewers for helping improve an early version of the manuscript. The
2152
2153 geological cross sections presented in this work were constructed using the Midland Valley 3D
2154
2155 Move software.
2156
2157
2158
2159
2160
2161
2162
2163
2164
2165
2166
2167
2168
2169
2170
2171
2172
2173
2174
2175
2176
2177
2178
2179
2180
2181
2182
2183

2184
2185
2186
2187 **Figure 1**
2188

2189 Kinematic models proposed in the early 70's to explain the opening of the Bay of Biscay. The
2190 motion of Iberia with respect to fixed Eurasia is described by its rigid rotation about a Euler's pole
2191 located: (A) to the east of Iberia, (B) near Paris, (C) in the Pyrenean mountain range. Modified from
2192 Choukroune et al. (1973)
2193
2194
2195
2196
2197
2198
2199

2200 **Figure 2**
2201

2202 Reconstructions of the Iberia-Eurasia margin and surrounding regions at the mid-Cretaceous time.
2203 (A) Rift-perpendicular scenario, after Manatschal and Müntener (2009). (B) Strike-slip scenario,
2204 after Stampfli and Borel (2002). (C) Scissor scenario, after Advokaat et al., (2014).
2205
2206
2207
2208
2209

2210 **Figure 3**
2211

2212 Tectonic map of the westernmost Europe, with Late Cretaceous - Cenozoic belts and basins (A),
2213 and Mesozoic domains (B), with focus on the architecture of the Bay of Biscay – Pyrenean rift
2214 system. The distribution of Mesozoic domains is modified after Tugend et al. (2015) for the Bay of
2215 Biscay-Pyrenean area, and from Handy et al., (2010) for the Alps-Appennines area. The position of
2216 the Corsica-Sardinia block before the opening of the Liguro-Provençal basin is from Bache et al.,
2217 (2010). (C) Reconstruction of the Iberia-Eurasia margin and surrounding domains in the mid-
2218 Cretaceous, modified from Manatschal and Müntener (2009)
2219
2220
2221
2222
2223
2224
2225
2226
2227
2228
2229

2230 **Figure 4**
2231

2232 Cretaceous extensional structures in the Pyrenean Arm. (A) Detail of the map in figure 3b in the
2233 Pyrenean area, with orientation of Cretaceous extension indicated. (B) Table illustrating the timing
2234 of major events and the direction of extensional structures in the different domains of the Pyrenean
2235 Arm and surrounding areas. References cited in the text and/or indicated in the figure are: Tugend
2236
2237
2238
2239
2240
2241
2242

2243
2244 et al. (2014) for the age of the oceanic crust in the Bay of Biscay. Thinon et al. (2003) and Roca et
2245
2246 al. (2011) for the age of mantle exhumation in the Bay of Biscay. Ferrer et al. (2008) for the age of
2247
2248 extension and hyperextension in the Parentis basin. García-Mondéjar et al. (1986) and Rat (1988)
2249
2250 for the age of extension in the Basque-Cantabrian basin. Biteau et al. (2006) for the age of extension
2251
2252 in the Arzacq basin. Jammes et al. (2009), Lagabrielle et al. (2010), and Masini et al. (2014) for the
2253
2254 age of hyperextension and mantle exhumation in the Mauléon basin. Souquet et al. (1985) and
2255
2256 Debros (1990) for the age of extension and hyperextension in the Flysch Noir basin. Dinarès-
2257
2258 Turell and García-Senz (2000) and García-Senz (2002) for the age of extension in the Organyà
2259
2260 basin. Granado et al. (In press) for the extension direction (meso-structural data) in the Asturian
2261
2262 basin (indicated as site 1). Soto et al. (2008) and Oliva-Urcia et al. (2013) (AMS data), and Tavani
2263
2264 and Muñoz (2012) (meso- and macro-structural data) for the extension direction in the Basque-
2265
2266 Cantabrian basin (indicated as site 2). Soto et al. (2008) and García-Lasanta et al. (2014) (AMS),
2267
2268 and Mata et al. (2001) (meso-structural data) for the extension direction in the Cameros basin
2269
2270 (indicated as site 3). Lagabrielle et al. (2010) for the extension direction (meso-structural data) in
2271
2272 the Mauléon extensional detachment (indicated as site 4). Salardon et al. (2017) (meso-structural
2273
2274 data) and Oliva-Urcia et al. (2010) (AMS) for the extension direction in the Mauléon basin
2275
2276 (indicated as site 5). Passchier (1984) and de Saint Blanquat et al. (1986 and 1990) for the extension
2277
2278 direction (meso-structural data) in the Saint Barthélémy massif extensional detachment (indicated
2279
2280 as site 6). Vauchez et al. (2013) for the extension direction (meso-structural data) in the Agly massif
2281
2282 extensional detachment (indicated as site 7). Gong et al. (2009) and Oliva-Urcia et al. (2011) (AMS
2283
2284 data), and Tavani et al. (2011) (meso- and macro-structural data) for the extension direction in the
2285
2286 Organyà basin (indicated as site 8).
2287
2288
2289
2290
2291
2292

2293 **Figure 5**

2294 (A) Geological map of the eastern Pyrenees. (B) Cross section across the Bas Agly syncline (after
2295
2296 Vauchez et al., 2013). (C) Cross section across the Meda Islands of the Montgrí area (after Mató et
2297
2298
2299
2300
2301

2302
2303 al., 1995b). (D) Geological map of the Figueres area.
2304
2305
2306

2307 **Figure 6**
2308

2309 (A) Detail of the map in figure 3b, showing the location of the Late Jurassic - Cretaceous
2310 extensional structures developed on the European margin of the Alpine Tethys, and presently
2311 exposed in the Western Alps, in the Languedoc-Provence region of the Pyrenean System, and in
2312 Sardinia (B) Facies distribution in the SE France basin, from Triassic to mid-Cretaceous (after
2313 Curnelle and Dubois, 1986). (C) Simplified Early Cretaceous structural scheme of the SE France
2314 basin, with major faults indicated (after de Graciansky and Lemoine, 1988).
2315
2316
2317
2318
2319
2320
2321
2322
2323

2324 **Figure 7**
2325

2326 (A) Schematic cross-section of the southern margin of the South Provence basin (after Philip et al.
2327 (1987). (B) Cross-section of the Olmedo area in Sardinia (after Mameli et al., 2007).
2328
2329
2330
2331
2332

2333 **Figure 8**
2334

2335 Cretaceous extensional structures in eastern Pyrenees and SE France basin. (A) Detail of the map in
2336 figure 3b in the area, with orientation of Cretaceous extension indicated. (B) Table illustrating the
2337 timing of major events and the direction of extensional structures in the different domains, with data
2338 from the Bay of Biscay - Pyrenean Arm in transparency. References cited in the text and/or
2339 indicated in the figure are: Saula et al. (1994) and Mató et al. (1995a, 1995b) for the age of
2340 extension in the Figueres-Montgrí basin. Guyonnet-Benaize et al. (2010) and Masse et al (2009) for
2341 the age of extension in the Vocontian and South Provence basins. Mameli et al. (2007) for the age
2342 of extension in the Olmedo area of Sardinia. Mató et al. (1995b) for the extension direction (syn-
2343 sedimentary faults orientation) in the Figueres-Montgrí (indicated as site 9). Guyonnet-Benaize et
2344 al. (2010), Lamarche et al. (2012), and Homberg et al. (2013) (meso-structures), and de Graciansky
2345 and Lemoine (1988) (major faults) for the extension direction in the Vocontian and South Provence
2346
2347
2348
2349
2350
2351
2352
2353
2354
2355
2356
2357
2358
2359
2360

2361
2362 basins (both indicated as site 10). Mameli et al. (2007) (orientation of an extensional fold) for the
2363 extension direction in the Olmedo area of Sardinia (indicated as site 11). Septfontaine (1995) for the
2364 age and direction (orientation of major fault) of extension in the Helvetic domain (indicated as site
2365 12). Cardello and Mancktelow (2014) for the age and direction (meso- and macro-structures) of
2366 extension in the Helvetic domain (indicated as site 13), notice that this could be a gravitational-
2367 structure. Chaulieu (1992), Claudel et al. (1997), and Claudel and Dumont (1999) for the age of
2368 extension in the external Briançonnais Domain of the Western Alps (indicated as site 14).
2369
2370
2371
2372
2373
2374
2375
2376
2377
2378

2379 **Figure 9**

2380 Geological maps of the study area. (A) Map of the Western Alps (modified from d’Atri et al.,
2381 2016), with inset showing the location of figure 9b. The arrows indicate counter-clockwise rotations
2382 about vertical axes (from Collombet et al., 2002). (B) Map of the Marguareis area, with structural
2383 scheme
2384
2385
2386
2387
2388
2389
2390
2391

2392 **Figure 10**

2393 Limone-Viozene northern (LIVZn) Fault in the eastern portion of the study area. (A) Panoramic
2394 view, from the west, of the LIVZn Fault, showing south-dipping Permo-Triassic rocks exposed in
2395 the southern block, and Triassic to Jurassic carbonates of the northern block, faulted by the Passo
2396 delle Saline Fault. (B) Orthophoto with structural scheme of the area and location of photographs
2397 and E-W and N-S oriented geological cross-sections (C) Panoramic view of the northern block of
2398 the LIVZn Fault: W-dipping Triassic and Jurassic carbonates are in the hanging wall of the E-
2399 Dipping Passo delle Saline Fault, which abut onto the LIVZn Fault. (D) Principal displacement
2400 zone of the LIVZn Fault, with Permian Volcanites and Triassic dolostones in the southern and
2401 northern block, respectively. (E) Detail of the fault, showing calcite slicken-fibers indicating a left-
2402 lateral kinematics.
2403
2404
2405
2406
2407
2408
2409
2410
2411
2412
2413
2414
2415
2416
2417
2418
2419

2420
2421 **Figure 11**
2422

2423 Details of the Limone-Viozene northern (LIVZn) Fault in the western portion of the study area. (A)
2424 View from the north of the fault (for location of the photograph see Fig. 11b), with inset photograph
2425 showing a NW-SE striking normal fault in the southern block of the fault. (B) Orthophoto with
2426 structural scheme of the area and location of photographs. (C) and (D) E-W striking faults
2427 palaeoescarpment in Jurassic carbonates covered by patches of mid-Cretaceous sediments.
2428
2429
2430
2431
2432
2433
2434
2435

2436 **Figure 12**
2437

2438 (A) Orthophoto with structural scheme of the Passo delle Saline Fault area, showing hundreds of
2439 metres long N-S striking extensional faults. (B) N-S striking veins affecting Jurassic carbonates
2440
2441
2442
2443

2444 **Figure 13**
2445

2446 (A) Orthophoto with structural scheme of the Colle del Pas Fault area. (B) View from the south of
2447 the fault, with W-dipping Permo-Triassic rocks in the footwall and sub-horizontal to slightly W-
2448 dipping Upper Cretaceous and Cenozoic rocks in the hanging wall. (C) Detail of the fault showing
2449 Permian volcanites underlying a 5-m thick breccia, which in turn is overlapped by Upper Cretaceous
2450 marls of the Upega Fm. (D) Three-dimensional virtual outcrop model of the lower portion of the
2451 Upega Fm., built by means of multi-view photographs (see Tavani et al., 2016 details). The model
2452 is seen in orthographic view along a direction perpendicular to bedding, thus representing a
2453 distortion-free properly oriented cross-section of the outcrop, and shows a growth wedge of 15° in
2454 the lowermost portion of the Upega Fm.
2455
2456
2457
2458
2459
2460
2461
2462
2463
2464
2465
2466
2467

2468 **Figure 14**
2469

2470 Photograph of Colle del Pas Fault plane as seen in the Piaggia Bella Karstic system
2471
2472
2473

2474 **Figure 15**
2475
2476
2477
2478

2479
2480 E-W and N-S oriented cross-sections across the Marguareis extensional system. See text for details.
2481
2482
2483

2484 **Figure 16**
2485

2486 3D scheme illustrating the geometry of the Marguareis Extensional System at early Late
2487 Cretaceous.
2488
2489

2490
2491
2492 **Figure 17**
2493

2494 (A) Table illustrating the timing of major events and the direction of extensional structures in the
2495 different domains of the study area. (B) Reconstruction of the Iberia-Eurasia margin and
2496 surrounding areas in the mid-Cretaceous times, with major basins, transform faults, and crustal
2497 domains indicated.
2498
2499
2500
2501
2502
2503
2504
2505
2506
2507
2508
2509
2510
2511
2512
2513
2514
2515
2516
2517
2518
2519
2520
2521
2522
2523
2524
2525
2526
2527
2528
2529
2530
2531
2532
2533
2534
2535
2536
2537

2538
2539 **REFERENCES**
2540

- 2541 Advokaat, E. L., van Hinsbergen, D. J., Maffione, M., Langereis, C. G., Vissers, R. L., Cherchi, A.,
2542
2543 Schroeder, R., Madani, H., Columbu, S. (2014). Eocene rotation of Sardinia, and the
2544
2545 paleogeography of the western Mediterranean region. *Earth and Planetary Science Letters*,
2546
2547 401, 183-195.
2548
- 2549 Alvarez, W., Coccozza, T., Wezel, F.C., 1974. Fragmentation of the Alpine orogenic belt by
2550
2551 microplate dispersal. *Nature*, 248, 309-314.
2552
- 2553 Álvaro, M., Capote, R., Vegas, R. (1979). Un modelo de evolución geotectónica para la Cadena
2554
2555 Celtibérica. *Acta Geológica Hispánica*, 14, 172-177.
2556
2557
- 2558 Ayala, C., Torné, M., Pous, J. (2003). The lithosphere-asthenosphere boundary in the western
2559
2560 Mediterranean from 3D joint gravity and geoid modelling: tectonic implications. *Earth and*
2561
2562 *Planetary Science Letters*, 209, 275-290
2563
- 2564 Bache, F., J. L. Olivet, C. Gorini, D. Aslanian, C. Labails, and M. Rabineau (2010), Evolution of
2565
2566 rifted continental margins: The case of the Gulf of Lions (Western Mediterranean Basin),
2567
2568 *Earth Planet. Sci. Lett.*, 292(3–4), 345–356, doi:10.1016/j.epsl.2010.02.001.
2569
2570
- 2571 Barbarand, J., Lucazeau, F., Pagel, M., Séranne, M. (2001). Burial and exhumation history of the
2572
2573 south-eastern Massif Central (France) constrained by apatite fission-track thermochronology.
2574
2575 *Tectonophysics*, 335, 275-290.
2576
- 2577 Barnett-Moore, N., M. Hosseinpour, and S. Maus (2016), Assessing discrepancies between
2578
2579 previous plate kinematic models of Mesozoic Iberia and their constraints, *Tectonics*, 35, 1–20,
2580
2581 doi:10.1002/(ISSN)1944-9194.
2582
- 2583 Beltrando, M., D. Rubatto, R. Compagnoni, G. Lister (2007), Was the Valaisian basin floored by
2584
2585 oceanic crust? Evidence of Permian magmatism in the Versoyen unit (Valaisian domain, NW
2586
2587 Alps), *Ophioliti*, 32, 85-99.
2588
2589
- 2590 Beltrando, M., G. Frasca, R. Compagnoni, and A. Vitale-Brovarone (2012), The Valaisian
2591
2592 controversy revisited: Multi-stage folding of a Mesozoic hyper-extended margin in the Petit
2593
2594
2595
2596

2597
2598 St. Bernard pass area (Western Alps), *Tectonophysics*, 579, 17–36,
2599
2600 doi:10.1016/j.tecto.2012.02.010.
2601

2602 Bertok, C., L. Martire, E. Perotti, A. D'Atri, and F. Piana (2011), Middle-Late Jurassic
2603 syndepositional tectonics recorded in the Ligurian Briançonnais succession (Margarais–
2604 Mongioie area, Ligurian Alps, NW Italy), *Swiss J. Geosci.*, 104(2), 237–255,
2605
2606 doi:10.1007/s00015-011-0058-0.
2607
2608

2609 Bertok, C., L. Martire, E. Perotti, A. D'Atri, and F. Piana (2012), Kilometre-scale
2610 palaeoscarpments as evidence for Cretaceous synsedimentary tectonics in the External
2611 Briançonnais Domain (Ligurian Alps, Italy), *Sediment. Geol.*, 251–252, 58–75,
2612
2613 doi:10.1016/j.sedgeo.2012.01.012.
2614
2615

2616 Bertok, C., Musso, A., d'Atri, A., Martire, L., Piana, F. (In press). Geology of the Colle di Tenda –
2617 Monte Marguareis area (Ligurian Alps, NW Italy). *Journal of Maps*.
2618
2619 doi:10.1080/17445647.2018.1500497
2620
2621

2622 Bestani, L., N. Espurt, J. Lamarche, O. Bellier, and F. Hollender (2016), Reconstruction of the
2623 Provence Chain evolution, southeastern France, *Tectonics*, 35(6), 1506–1525,
2624
2625 doi:10.1002/2016TC004115.
2626
2627

2628 Biteau, J. J., Le Marrec, A., Le Vot, M., Masset, J. M. (2006). The Aquitaine Basin. *Petroleum*
2629
2630 *Geoscience*, 12, 247-273.
2631
2632

2633 Boillot, G., Dupeuble, P.A. & Malod, J. (1979) Subduction and tectonics on the continental margin
2634
2635 off northern Spain. *Mar. Geol.*, 32, 53–70.
2636
2637

2638 Bott, M. H. P. (1981). Crustal doming and the mechanism of continental rifting. *Tectonophysics*,
2639
2640 73(1-3), 1-8.
2641
2642

2643 Bousquet, R., R. Oberhänsli, B. Goffé, M. Wiederkehr, F. Koller, S. M. Schmid, R. Schuster, M.
2644
2645 Engi, A. Berger, and G. Martinotti (2008), Metamorphism of metasediments at the scale of an
2646
2647 orogen: a key to the Tertiary geodynamic evolution of the Alps*, *Geol. Soc. London, Spec.*
2648
2649 *Publ.*, 298(1), 393–411, doi:10.1144/SP298.18.
2650
2651
2652
2653
2654
2655

- 2656
2657 Bussy, M.H., M. Eichenberger, N. Giroud, C. Meilhac, S. Presniakov (2008), Early Carboniferous
2658
2659 age of the Versoyen ophiolites and consequences: non-existence of a “Valais ocean” (Lower
2660
2661 Penninic, western Alps), *Bulletin de la Société Géologique de France*, 179, 337-355.
2662
2663
2664 Cadenas, P., & Fernández-Viejo, G. (2017). The Asturian Basin within the North Iberian margin
2665
2666 (Bay of Biscay): seismic characterization of its geometry and its Mesozoic and Cenozoic
2667
2668 cover. *Basin Research*.
2669
2670 Cámara, P. (1997), The Basque-Cantabrian basin’s Mesozoic tectono-sedimentary evolution,
2671
2672 *Mémoires la Société Géologique Fr.*, 171, 187–191.
2673
2674 Cardello, G.L., Mancktelow, N.S. (2014). Cretaceous syn-sedimentary faulting in the Wildhorn
2675
2676 Nappe (SW Switzerland). *Swiss Journal of Geosciences*, 107, 223-250.
2677
2678
2679 Carminati, E., M. Lustrino, and C. Doglioni (2012), Geodynamic evolution of the central and
2680
2681 western Mediterranean: Tectonics vs. igneous petrology constraints, *Tectonophysics*, 579,
2682
2683 173–192, doi:10.1016/j.tecto.2012.01.026.
2684
2685 Chaulieu, P. *La sédimentation détritique sur la marge nord-téthysienne témoin de l'évolution*
2686
2687 *géodynamique des Alpes occidentales*. PhD thesis, Université Joseph-Fourier - Grenoble I,
2688
2689 1992.
2690
2691 Choukroune, P., Le Pichon, X., Seguret, M., Sibuet, J. C. (1973). Bay of Biscay and Pyrenees.
2692
2693 *Earth and Planetary Science Letters*, 18, 109-118.
2694
2695 Choukroune P. (1992). Tectonic evolution of the Pyrenees. *Ann. Rev. Earth planet. Sci.*, 20, 143-
2696
2697 158
2698
2699
2700 Claudel, M. E., Dumont, T., & Tricart, P. (1997). Une preuve d'extension contemporaine de
2701
2702 l'expansion océanique de la Téthys ligure en Briançonnais: les failles du Vallon Laugier.
2703
2704 *Comptes Rendus de l'Académie des Sciences-Series IIA-Earth and Planetary Science*, 325(4),
2705
2706 273-279.
2707
2708 Claudel, M., and Dumont, T., (1999). A record of multistage continental break-up on the
2709
2710 Briançonnais marginal plateau (Western Alps): Early and Middle-Late Jurassic rifting.
2711
2712
2713
2714

2715
2716 *Eclogae Geologicae Helvetiae*, 92(1), 45-61.
2717

2718 Clerc, C., Lagabrielle, Y. (2014). Thermal control on the modes of crustal thinning leading to
2719 mantle exhumation: Insights from the Cretaceous Pyrenean hot paleomargins. *Tectonics*, 33,
2720 1340-1359.
2721
2722

2723
2724 Clerc, C., A. Lahfid, P. Monié, Y. Lagabrielle, C. Chopin, M. Pujol, P. Boulvais, J.-C.
2725 Ringenbach, E. Masini, and M. de St Blanquat (2015), High-temperature metamorphism
2726 during extreme thinning of the continental crust: a reappraisal of the North Pyrenean passive
2727 paleomargin, *Solid Earth*, 6(2), 643–668, doi:10.5194/se-6-643-2015.
2728
2729

2730
2731 Clerc, C., Lagabrielle, Y., Labaume, P., Ringenbach, J. C., Vauchez, A., Nalpas, T., Bousquet R.,
2732 Ballard J.F., Lahfid A., Fourcade, S. (2016). Basement–Cover decoupling and progressive
2733 exhumation of metamorphic sediments at hot rifted margin. Insights from the Northeastern
2734 Pyrenean analog. *Tectonophysics*, 686, 82-97.
2735
2736

2737
2738 Collombet, M., J. C. Thomas, A. Chauvin, P. Tricart, J. P. Bouillin, and J. P. Gratier (2002),
2739 Counterclockwise rotation of the western Alps since the Oligocene: New insights from
2740 paleomagnetic data, *Tectonics*, 21(4), 14-1-14–15, doi:10.1029/2001TC901016.
2741
2742

2743
2744 Cotillon, P. 1968. Le Crétacé Inférieur De L'arc Subalpin De Castellane Entre L'asse Et Le Var:
2745 Stratigraphie Et Sédimentologie. PhD Thesis, University of Lyon
2746
2747

2748
2749 Coward, M., and D. Dietrich (1989), Alpine tectonics - an overview, *Geol. Soc. London, Spec.*
2750 *Publ.*, 45(1), 1–29, doi:10.1144/GSL.SP.1989.045.01.01.
2751
2752

2753
2754 Cowie, P.A., Scholz, C.H. (1992). Growth of faults by accumulation of seismic slip. *Journal of*
2755 *Geophysical Research* 97, 11085-11095.
2756
2757

2758
2759 Curnelle, R., Dubois, P. (1986). Évolution mésozoïque des grands bassins sédimentaires Français;
2760 bassins de Paris, d'Aquitaine et du Sud-Est. *Bulletin de la Société Géologique de France*, 2,
2761 529-546.
2762
2763

2764
2765 d'Atri, A., F. Piana, L. Barale, C. Bertok, and L. Martire (2016), Geological setting of the southern
2766
2767
2768
2769
2770
2771
2772
2773

2774
2775 termination of Western Alps, *Int. J. Earth Sci.*, 105(6), 1831–1858, doi:10.1007/s00531-015-
2776 1277-9.
2777
2778

2779 Daignières, M., Séguret, M., Specht, M., and the ECORS Team. (1994). The Arzacq-western
2780 Pyrenees ECORS deep seismic profile. In *Hydrocarbon and petroleum geology of France*, pp.
2781 199-208, Springer Berlin Heidelberg.
2782
2783
2784

2785 De Graciansky, P.-C., R. Busnardo, R. Doublet, and J. Martinod (1987) Tectogenese distensive
2786 d'age cretace inferieur aux confins des Baronnies (Chaines subalpines meridionales); liaison
2787 avec le rifting atlantique; consequences sur la tectonique alpine, *Bulletin de la Société*
2788 *géologique de France*, 3, 1211-1214.
2789
2790
2791
2792
2793

2794 De Graciansky, P.-C. Lemoine M., 1988. Early Cretaceous extensional tectonics in the
2795 southwestern French Alps: a consequence of North-Atlantic rifting during Tethyan spreading.
2796 *Bulletin de la Société géologique de France*, 4, 733-737.
2797
2798
2799

2800 de Saint Blanquat, M., Brunel, M., Mattauer, M. (1986). Les zones de cisaillements du massif nord
2801 Pyrénéen du Saint-Barthelemy, témoins probables del'extension crustale d'âge crétaé.
2802 *Académie des Sciences, Comptes Rendus*, 303, 1339-1344.
2803
2804
2805
2806

2807 de Saint Blanquat, M., Lardeaux, J.M., Brunel, M. (1990). Petrological arguments for high
2808 temperature extensional deformation in the Pyrenean Variscan crust (Saint Barthélémy
2809 massif, Ariège, France), *Tectonophysics*, 177, 245-262.
2810
2811
2812

2813 Debroyas, E. J. (1990), Le flysch noir albo-cénomanié témoin de la structuration albienne à
2814 sénonienne de la zone nord-Pyrénéenne en Bigorre (Hautes Pyrénées, France), *Bulletin de la*
2815 *Société géologique de France*, 6, 273–286.
2816
2817
2818
2819

2820 Dercourt, J. et al. (1986), Geological evolution of the tethys belt from the atlantic to the pamirs
2821 since the LIAS, *Tectonophysics*, 123(1–4), 241–315, doi:10.1016/0040-1951(86)90199-X.
2822
2823

2824 Destro, N. (1995). Release fault: A variety of cross fault in linked extensional fault systems, in the
2825 Sergipe-Alagoas Basin, NE Brazil. *Journal of Structural Geology*, 17, 615-629.
2826
2827

2828 Deville, E., Mascle, A., Lamiriaux, C., Le Bras, A., 1994. Tectonic styles, re-evaluation of plays in
2829
2830
2831
2832

2833
2834 southeastern France. *Oil Gas Journal*. 92, 53-58
2835

2836 Dewey, J. F., M. L. Helman, S. D. Knott, E. Turco, and D. H. W. Hutton (1989), Kinematics of the
2837
2838 western Mediterranean, *Geol. Soc. London, Spec. Publ.*, 45(1), 265–283,
2839
2840 doi:10.1144/GSL.SP.1989.045.01.15.
2841

2842 Dinarès-Turell, J., Garcia-Senz, J. (2000). Remagnetization of Lower Cretaceous limestones from
2843
2844 the southern Pyrenees and relation to the Iberian plate geodynamic evolution. *Journal of*
2845
2846 *Geophysical Research: Solid Earth*, 105, 19405-19418.
2847

2848 Doglioni, C., E. Gueguen, F. Sàbat, and M. Fernandez (1997), The Western Mediterranean
2849
2850 extensional basins and the Alpine orogen, *Terra Nov.*, 9(3), 109–112, doi:10.1046/j.1365-
2851
2852 3121.1997.d01-18.x.
2853

2854 Dumont, T., T. Simon-Labric, C. Authemayou, and T. Heymes (2011), Lateral termination of the
2855
2856 north-directed Alpine orogeny and onset of westward escape in the Western Alpine arc:
2857
2858 Structural and sedimentary evidence from the external zone, *Tectonics*, 30(5), n/a-n/a,
2859
2860 doi:10.1029/2010TC002836.
2861

2862 Dumont, T., S. Schwartz, S. Guillot, T. Simon-Labric, P. Tricart, and S. Jourdan (2012), Structural
2863
2864 and sedimentary records of the Oligocene revolution in the Western Alpine arc, *J. Geodyn.*,
2865
2866 56–57, 18–38, doi:10.1016/j.jog.2011.11.006.
2867

2868 Ellenberger, F. 1967. Les interférences de l'érosion et de la tectonique tangentielle tertiaire dans
2869
2870 le Bas-Languedoc (principalement dans l'arc de Saint-Chinian). Note sur les charriages
2871
2872 cisailants, *Rev. Géogr. phys. Géol. dyn.*, 9, 87-142
2873

2874 Faccenna, C. et al. (2014), Mantle dynamics in the Mediterranean, *Rev. Geophys.*, 52(3), 283–332,
2875
2876 doi:10.1002/2013RG000444.
2877

2878 Falvey, D.A. (1974). The development of continental margins in plate tectonic theory. *Journal of*
2879
2880 the Australian Petroleum Exploration Association, 14, 95-106.
2881

2882 Faulds, J.E., Varga, R.J. (1998). The role of accommodation zones and transfer zones in the
2883
2884 regional segmentation of extended terranes. *Geological Society of America Special Papers*,
2885
2886
2887
2888
2889
2890
2891

2892
2893 323, 1-46.
2894

2895 Ferrer, O., Roca, E., Benjumea, B., Muñoz, J. A., Ellouz, N., & MARCONI Team. (2008). The
2896
2897 deep seismic reflection MARCONI-3 profile: Role of extensional Mesozoic structure during
2898
2899 the Pyrenean contractional deformation at the eastern part of the Bay of Biscay. *Marine and*
2900
2901 *Petroleum Geology*, 25, 714-730.
2902

2903
2904 Ford, M., Duchene, S., Gasquet, D., Vanderhaeghe, O. (2006). Two-phase orogenic convergence in
2905
2906 the external and internal SW Alps. *J. Geol. Soc. London.*, 163, 815–826, doi:10.1144/0016-
2907
2908 76492005-034.
2909

2910 Fortané, A., Duée, G., Lagabrielle, Y., Coutelle, A. (1986). Lherzolites and the western “Chainons
2911
2912 béarnais”(French Pyrenees): Structural and paleogeographical pattern. *Tectonophysics*, 129,
2913
2914 81-98.
2915

2916 Frizon de Lamotte, D., Raulin, C., Mouchot, N., Wrobel-Daveau, J.-C., Blanpied, C., Ringenbach,
2917
2918 J.-C. (2011). The southernmost margin of the Tethys realm during the Mesozoic and
2919
2920 Cenozoic: Initial geometry and timing of the inversion processes, *Tectonics*, 30, TC3002,
2921
2922 doi:10.1029/2010TC002691.
2923
2924

2925 Froitzheim, N., D. Plašienka, and R. Schuster (2008), Alpine tectonics of the Alps and Western
2926
2927 Carpathians, *Geol. Cent. Eur.*, 2, 1141–1232.
2928

2929 Fry, N. (1989). Southwestward thrusting and tectonics of the western Alps. Geological Society,
2930
2931 London, Special Publications, 45, 83-109.
2932

2933 Galdeano, A., Moreau, M.G., Pozzi, J.P., Berthou, P. Y., Malod, J.A. (1989). New paleomagnetic
2934
2935 results from Cretaceous sediments near Lisboa (Portugal) and implications for the rotation of
2936
2937 Iberia. *Earth and Planetary Science Letters*, 92, 95-106.
2938
2939

2940 García-Lasanta, C., Oliva-Urcia, B., Román-Berdiel, T., Casas, A.M., Hirt, A.M. (2014).
2941
2942 Understanding the Mesozoic kinematic evolution in the Cameros basin (Iberian Range, NE
2943
2944 Spain) from magnetic subfabrics and mesostructures. *Journal of Structural Geology*, 66, 84-
2945
2946 101.
2947
2948
2949
2950

- 2951
2952 García-Mondéjar, J., Agirrezabala, L.M., Aranburu, A., Fernández-Mendiola, P.A., Gómez-Pérez,
2953 I., López-Horgue, M., Rosales, I. (1996). Aptian-Albian tectonic pattern of the Basque-
2954 Cantabrian Basin (Northern Spain). *Geological Journal*, 31, 13-45
2955
2956
2957
2958 García-Mondéjar, J., 1996. Plate reconstruction of the Bay of Biscay. *Geology* 24, 635-638.
2959
2960
2961 García-Senz, J. (2002). Cuencas extensivas del Cretácico Inferior en los Pirineos centrales.
2962 Formación y subsecuente inversión. PhD Thesis, Universitat de Barcelona.
2963
2964
2965 Gattacceca, J., A. Deino, R. Rizzo, D. S. Jones, B. Henry, B. Beaudoin, and F. Vadeboin (2007),
2966 Miocene rotation of Sardinia: New paleomagnetic and geochronological constraints and
2967 geodynamic implications, *Earth Planet. Sci. Lett.*, 258(3–4), 359–377,
2968 doi:10.1016/j.epsl.2007.02.003.
2969
2970
2971
2972
2973
2974 Gawthorpe, R. L., & Hurst, J. M. (1993). Transfer zones in extensional basins: their structural style
2975 and influence on drainage development and stratigraphy. *Journal of the Geological Society*,
2976 150(6), 1137-1152.
2977
2978
2979
2980 Gibbs, A. D. (1984). Structural evolution of extensional basin margins. *Journal of the Geological*
2981 *Society*, 141(4), 609-620.
2982
2983
2984 Goffé, B., and C. Chopin (1986), High-pressure metamorphism in the Western Alps: zoneography
2985 of metapelites, chronology and consequences, *Schweizerische Mineral. und Petrogr.*
2986 *Mitteilungen*, 66(1–2), 41–52.
2987
2988
2989
2990
2991 Gong, Z., Langereis, C.G., Mullender, T.A.T. (2008). The rotation of Iberia during the Aptian and
2992 the opening of the Bay of Biscay. *Earth and Planetary Science Letters*, 273, 80-93.
2993
2994
2995
2996
2997
2998
2999
3000
3001
3002
3003
3004
3005
3006
3007
3008
3009

- 3010
3011 Granado, P., Tavani, S., Carrera, N., Muñoz, J.A. (In Press). Deformation pattern around the
3012
3013 Conejera Fault blocks (Asturian Basin, North Iberian Margin). *Geologica Acta*.
3014
- 3015 Guyonnet-Benaize, C., Lamarche, J., Masse, J.P., Villeneuve, M., Viseur, S. (2010). 3D structural
3016
3017 modelling of small-deformations in poly-phase faults pattern. Application to the Mid-
3018
3019 Cretaceous Durance uplift, Provence (SE France). *Journal of Geodynamics*, 50, 81-93.
3020
- 3021 Handy, M. R., S. M. Schmid, R. Bousquet, E. Kissling, and D. Bernoulli (2010), Reconciling plate-
3022
3023 tectonic reconstructions of Alpine Tethys with the geological–geophysical record of spreading
3024
3025 and subduction in the Alps, *Earth-Science Reviews*, 102, 121–158,
3026
3027 doi:10.1016/j.earscirev.2010.06.002.
3028
3029
- 3030 Henuy, J. (2003) - Sédimentation carbonatée et silicoclastique sous contrôle tectonique, le bassin
3031
3032 Sud-Provençal et sa plate-forme carbonatée au Turonien moyen au Coniacien moyen.
3033
3034 Evolutions séquentielle, diagénétique, paleogéographique. Thèse de Doctorat de l'Université
3035
3036 de Provence, Marseille, 252 p.
3037
3038
- 3039 Hibsich, C., D. Kandel, C. Montenat, and P. O. d'Estevou (1992), Evenements tectoniques cretaces
3040
3041 dans la partie meridionale du bassin subalpin (massif Ventoux-Lure et partie orientale de l'arc
3042
3043 de Castellane, SE France); implications geodynamiques, *Bull. la Soc. Geol. Fr.*, 163(2), 147–
3044
3045 158.
3046
- 3047 Hippolyte, J.-C., J. Angelier, F. Bergerat, D. Nury, and G. Guieu (1993), Tectonic-stratigraphic
3048
3049 record of paleostress time changes in the Oligocene basins of the Provence, southern France,
3050
3051 *Tectonophysics*, 226(1–4), 15–35, doi:10.1016/0040-1951(93)90108-V.
3052
3053
- 3054 Homberg, C., J. Schnyder, and M. Benzaggagh (2013), Late Jurassic-Early Cretaceous faulting in
3055
3056 the Southeastern French basin: does it reflect a tectonic reorganization?, *Bull. la Soc. Geol.*
3057
3058 *Fr.*, 184(4–5), 501–514, doi:10.2113/gssgfbull.184.4-5.501.
3059
- 3060 Huismans, R. S., Podladchikov, Y.Y., Cloetingh, S. (2001). Transition from passive to active
3061
3062 rifting: Relative importance of asthenospheric doming and passive extension of the
3063
3064 lithosphere. *Journal of Geophysical Research: Solid Earth*, 106, 11271-11291.
3065
3066
3067
3068

- 3069
3070 Huismans, R., Beaumont, C. (2011). Depth-dependent extension, two-stage breakup and cratonic
3071
3072 underplating at rifted margins. *Nature*, 473, 74-78.
3073
- 3074 Jammes, S., G. Manatschal, L. Lavier, and E. Masini (2009), Tectonosedimentary evolution related
3075
3076 to extreme crustal thinning ahead of a propagating ocean: Example of the western Pyrenees,
3077
3078 *Tectonics*, 28(4), n/a-n/a, doi:10.1029/2008TC002406.
3079
- 3080
3081 Jammes, S., Lavier, L., Manatschal, G. (2010). Extreme crustal thinning in the Bay of Biscay and
3082
3083 the Western Pyrenees: From observations to modeling. *Geochemistry, Geophysics,*
3084
3085 *Geosystems*, 11, DOI: 10.1029/2010GC003218
3086
- 3087 Johnson, J. A., and C. A. Hall (1989), Tectono-stratigraphic model for the Massif D'Igountze-
3088
3089 Mendibelza, western Pyrenees, *J. Geol. Soc. London.*, 146(6), 925–932,
3090
3091 doi:10.1144/gsjgs.146.6.0925.
3092
- 3093
3094 Jolivet, L., C. Gorini, J. Smit, and S. Leroy (2015), Continental breakup and the dynamics of rifting
3095
3096 in back-arc basins: The Gulf of Lion margin, *Tectonics*, 34(4), 662–679,
3097
3098 doi:10.1002/2014TC003570.
3099
- 3100 Kerckhove, C. (1969), La “zone du Flysch” dans les nappes de l’Embrunais-Ubaye (Alpes
3101
3102 occidentales), *Géologie Alp.*, 45, 5–204.
3103
- 3104 Kim, Y.S., Sanderson, D.J. (2005). The relationship between displacement and length of faults: a
3105
3106 review. *Earth-Science Reviews* 68, 317-334.
3107
- 3108 Kooi, H., Cloetingh, S., Burrus, J. (1992). Lithospheric necking and regional isostasy at extensional
3109
3110 basins 1. Subsidence and gravity modeling with an application to the Gulf of Lions margin
3111
3112 (SE France). *Journal of Geophysical Research: Solid Earth*, 97, 17553-17571.
3113
- 3114
3115 Lacombe, O., and L. Jolivet (2005), Structural and kinematic relationships between Corsica and the
3116
3117 Pyrenees-Provence domain at the time of the Pyrenean orogeny, *Tectonics*, 24(1), n/a-n/a,
3118
3119 doi:10.1029/2004TC001673.
3120
- 3121 Lacroix, A. (1895), *Les phénomènes de contact de la lherzolite et de quelques ophites des Pyrénées*,
3122
3123 Librairie polytechnique, Baudry et cie.
3124
3125
3126
3127

- 3128
3129 Lagabrielle, Y., and J.-L. Bodinier (2008), Submarine reworking of exhumed subcontinental mantle
3130 rocks: field evidence from the Lherz peridotites, French Pyrenees, *Terra Nova*, 20(1), 11–21,
3131 doi:10.1111/j.1365-3121.2007.00781.x.
3132
3133
3134
3135 Lagabrielle, Y., Labaume, P., & de Saint Blanquat, M. (2010). Mantle exhumation, crustal
3136 denudation, and gravity tectonics during Cretaceous rifting in the Pyrenean realm (SW
3137 Europe): Insights from the geological setting of the lherzolite bodies. *Tectonics*, 29(4).
3138
3139
3140
3141
3142 Lamarche, J., Lavenu, A.P.C., Gauthier, B.D.M., Guglielmi, Y., & Jayet, O. (2012). Relationships
3143 between fracture patterns, geodynamics and mechanical stratigraphy in carbonates (South-
3144 East Basin, France). *Tectonophysics*, 581, 231–245.
3145
3146
3147
3148
3149 Lanaja, J. M. (1987), *Contribución de la exploración petrolífera al conocimiento de la geología de*
3150 *España*, IGME.
3151
3152
3153 Larrasoaña, J. C., Parés, J. M., Millán, H., Del Valle, J., & Pueyo, E. L. (2003). Paleomagnetic,
3154 structural, and stratigraphic constraints on transverse fault kinematics during basin inversion:
3155 The Pamplona Fault (Pyrenees, north Spain). *Tectonics*, 22(6).
3156
3157
3158
3159 Lemoine, 1984; M. Lemoine; La marge occidentale de la Tethys ligure et des Alpes occidentales.
3160 G. Boillot (Ed.), *Les Marges Continentales Autour de la France*, Masson Edition, Paris
3161 (1984), pp. 155–182
3162
3163
3164
3165 Lemoine, M., Bas, T., Arnaud-Vanneau, A., Arnaud, H., Dumont, T., Gidon, M., Bourbon, M., de
3166 Graciansky, P.-C., Rudkiewicz, J.-L., Megard-Galli, J., Tricart, P. (1986). The continental
3167 margin of the Mesozoic Tethys in the Western Alps. *Marine and petroleum geology*, 3(3),
3168 179-199.
3169
3170
3171
3172
3173
3174 Lemoine, M., P. C. De Graciansky, and P. Tricart (2000), *De l'océan à la chaîne de montagnes:*
3175 *tectonique des plaques dans les Alpes*, Editions scientifiques GB.
3176
3177
3178
3179 Lepvrier, C., Martínez-García, E. (1990). Fault development and stress evolution of the post-
3180 Hercynian Asturian Basin (Asturias and Cantabria, northwestern Spain). *Tectonophysics*, 184,
3181 345-356.
3182
3183
3184
3185
3186

- 3187
3188 Liati A, Froitzheim N (2006) Assessing the Valais ocean, Western Alps: U-Pb SHRIMP zircon
3189
3190 geochronology of eclogite in the Balma unit, on top of the Monte Rosa nappe. *Eur J Mineral*
3191
3192 18(3):299–308
3193
- 3194 Lister, G.S., Etheridge, M.A., and Symonds, P.A., 1991, Detachment models for the formation of
3195
3196 passive continental margins: *Tectonics*, v. 10, p. 1038-1064
3197
- 3198 López-Mir, B., Muñoz, J.A., García-Senz, J. (2015). Extensional salt tectonics in the partially
3199
3200 inverted Cotiella post-rift basin (south-central Pyrenees): structure and evolution.
3201
3202 *International Journal of Earth Sciences*, 104, 419-434.
3203
3204
- 3205 Louis, L., Robion, P., David, C., Frizon de Lamotte, D. (2006). Multiscale anisotropy controlled by
3206
3207 folding: the example of the Chaudrons fold (Corbieres, France). *Journal of Structural*
3208
3209 *Geology*, 28, 549-560.
3210
- 3211 Malusà, M. G., Faccenna, C., Garzanti, E., Polino, R. (2011). Divergence in subduction zones and
3212
3213 exhumation of high pressure rocks (Eocene Western Alps). *Earth and Planetary Science*
3214
3215 *Letters*, 310, 21-32.
3216
3217
- 3218 Mata, M.P., Casas, A.M., Canals, A., Gil, A., Pocovi, A. (2001). Thermal history during Mesozoic
3219
3220 extension and Tertiary uplift in the Cameros Basin, northern Spain. *Basin Research*, 13, 91-
3221
3222 111.
3223
- 3224 Mameli, P., Mongelli, G., Oggiano, G., Dinelli, E. (2007). Geological, geochemical and
3225
3226 mineralogical features of some bauxite deposits from Nurra (Western Sardinia, Italy): insights
3227
3228 on conditions of formation and parental affinity. *International Journal of Earth Sciences*, 96,
3229
3230 887-902.
3231
3232
- 3233 Manatschal G, Müntener O. (2009) A type sequence across an ancient magma-poor ocean-continent
3234
3235 transition: the example of the western Alpine Tethys ophiolites. *Tectonophysics* 473(1–2):4–
3236
3237 19
3238
- 3239 Manatschal, G. (2004). New models for evolution of magma-poor rifted margins based on a review
3240
3241 of data and concepts from West Iberia and the Alps. *International Journal of Earth Sciences*,
3242
3243
3244
3245

3246
3247 93, 432-466.
3248

3249 Manatschal, G., Lavier, L., Chenin, P. (2015). The role of inheritance in structuring hyperextended
3250 rift systems: Some considerations based on observations and numerical modeling. *Gondwana*
3251 *Research*, 27, 140-164.
3252
3253
3254

3255 Martire, L., C. Bertok, A. D'atri, E. Perotti, and F. Piana (2014), Selective dolomitization by
3256 syntaxial overgrowth around detrital dolomite nuclei: a case from the Jurassic of the Ligurian
3257 Briançonnais (Ligurian Alps), *J. Sediment. Res.*, 84(1), 40–50.
3258
3259

3260 Masini, E., G. Manatschal, J. Tugend, G. Mohn, and J.-M. Flament (2014), The tectono-
3261 sedimentary evolution of a hyper-extended rift basin: the example of the Arzacq–Mauléon rift
3262 system (Western Pyrenees, SW France), *Int. J. Earth Sci.*, 103(6), 1569–1596,
3263 doi:10.1007/s00531-014-1023-8.
3264
3265
3266
3267
3268
3269

3270 Masse, J. P., and J. Philip. (1976), Paléogéographie et tectonique du Crétacé moyen en Provence:
3271 révision du concept d'isthme durancien. *Revue de Géographie physique et de Géologie*
3272 *dynamique*, 18.1, 49-66.
3273
3274
3275
3276

3277 Masse, J. P., Villeneuve, M., Leonforte, E., & Nizou, J. (2009). Block tilting of the North Provence
3278 early Cretaceous carbonate margin: stratigraphic, sedimentologic and tectonic data. *Bulletin*
3279 *de la société géologique de France*, 180(2), 105-115.
3280
3281
3282

3283 Mató, E., Saula, E., Picart, J., Solà, J., Montaner, J., Serra, J., Caus, E. (1995a). Geological map of
3284 Catalunya 1:25000. Sheet 296-2-1. Institut Cartogràfic i Geològic de Catalunya. Barcelona.
3285
3286

3287 Mató, E., Saula, E., Montaner, J., Solà, J., Caus, E., Serra, J. (1995b). Geological map of
3288 Catalunya 1:25000. Sheet 297-1-2. Institut Cartogràfic i Geològic de Catalunya. Barcelona.
3289
3290

3291 Mauffret, A., and M. Gennesseaux (1989), Compression, décrochements et distension sur le
3292 pourtour méditerranéen nord-occidental, *Comptes rendus l'Académie des Sci. Série 2,*
3293 *Mécanique, Phys. Chim. Sci. l'univers, Sci. la Terre*, 308(10), 961–967.
3294
3295
3296
3297

3298 Mazzoli, S., and M. Helman (1994), Neogene patterns of relative plate motion for Africa-Europe:
3299 some implications for recent central Mediterranean tectonics, *Geol. Rundschau*, 83(2), 464–
3300
3301
3302
3303
3304

3305
3306 468, doi:10.1007/BF00210558.
3307

3308 McKenzie, D. (1978). Some remarks on the development of sedimentary basins. *Earth and*
3309 *Planetary science letters*, 40(1), 25-32.
3310

3311
3312 Mencos, J., Carrera, N., Muñoz, J.A. (2015). Influence of rift basin geometry on the subsequent
3313 postrift sedimentation and basin inversion: The Organyà Basin and the Bóixols thrust sheet
3314 (south central Pyrenees). *Tectonics*, 34, 1452-1474, doi: 10.1002/2014TC003692.
3315
3316

3317
3318 Merle, O. (1982), Mise en place séquentielle de la Nappe du Parapaillon en Embrunais-Ubaye
3319 (Flysch à Helminthoïdes, Alpes occidentales), *Comptes Rendus l'Académie des Sci. Paris*,
3320 294, 603–606.
3321
3322

3323
3324 Michard, A., Martinotti, G., (2002) The Eocene unconformity of the Brianconnais domain in the
3325 French-Italian Alps, revisited (Marguareis massif, Cuneo); a hint for a Late Cretaceous-
3326 Middle Eocene frontal bulge setting. *Geodinamica Acta*, 15, 289-301
3327
3328
3329

3330
3331 Michard, A., D. Avigad, B. Goffé, and C. Chopin (2004), The high-pressure metamorphic front of
3332 the south Western Alps (Ubaye-Maira transect, France, Italy), *Schweiz. Miner. Petrogr. Mitt*,
3333 84, 215–235.
3334
3335
3336

3337
3338 Mohn, G., G. Manatschal, O. Müntener, M. Beltrando, and E. Masini (2010), Unravelling the
3339 interaction between tectonic and sedimentary processes during lithospheric thinning in the
3340 Alpine Tethys margins, *Int. J. Earth Sci.*, 99(S1), 75–101, doi:10.1007/s00531-010-0566-6.
3341
3342
3343

3344
3345 Molliex, S., O. Bellier, M. Terrier, J. Lamarche, G. Martelet, and N. Espurt (2011), Tectonic and
3346 sedimentary inheritance on the structural framework of Provence (SE France): Importance of
3347 the Salon-Cavaillon fault, *Tectonophysics*, 501(1–4), 1–16, doi:10.1016/j.tecto.2010.09.008.
3348
3349
3350

3351
3352 Molnar, P. (1988). Continental tectonics in the aftermath of plate tectonics. *Nature*, 335, 131-137.
3353

3354
3355 Montenat, C., C. Hibsich, J. C. Perrier, F. Pascaud, and P. de Bretizel (1997), Tectonique cassante
3356 d'âge Crétacé inférieur dans l'arc de Nice (Alpes-Maritimes, France), *Géologie Alp.*, 73, 59–
3357
3358
3359 66.
3360
3361
3362
3363

- 3364
3365 Morley, C. K., Nelson, R. A., Patton, T. L., & Munn, S. G. (1990). Transfer zones in the East
3366 African rift system and their relevance to hydrocarbon exploration in rifts (1). *AAPG Bulletin*,
3367 74(8), 1234-1253.
3368
3369
3370
3371 Mouthereau, F., P.-Y. Filleaudeau, A. Vacherat, R. Pik, O. Lacombe, M. G. Fellin, S. Castellort, F.
3372 Christophoul, and E. Masini (2014), Placing limits to shortening evolution in the Pyrenees:
3373 Role of margin architecture and implications for the Iberia/Europe convergence, *Tectonics*,
3374 33(12), 2283–2314, doi:10.1002/2014TC003663.
3375
3376
3377
3378
3379
3380 Muñoz, J.A. (1992). Evolution of a continental collision belt: ECORS-Pyrenees crustal balanced
3381 cross-section. In: McClay (Ed.), *Thrust Tectonics*. Chapman & Hall, London, 235-246.
3382
3383
3384 Muñoz, J. A. (2002). The Pyrenees. In: *The Geology of Spain*, W. Gibbons and M. T. Moreno
3385 (eds.), pp. 370-385, Geological Society, London, U. K.
3386
3387
3388
3389 Nirrengarten, M., Manatschal, G., Tugend, J., Kuszniir, N.J. Sauter, D. (2017). Nature and origin of
3390 the J-magnetic anomaly offshore Iberia–Newfoundland: implications for plate
3391 reconstructions. *Terra Nova*, 29, 20-28.
3392
3393
3394
3395 Neres, M., Font, E., Miranda, J. M., Camps, P., Terrinha, P., Mirão, J. (2012). Reconciling
3396 Cretaceous paleomagnetic and marine magnetic data for Iberia: New Iberian paleomagnetic
3397 poles. *Journal of Geophysical Research: Solid Earth*, 117, B06102.
3398
3399
3400
3401 Olivet, J. L. (1996), La cinématique de la plaque ibérique, *Bull. Cent. Rech. Explor. Prod. Elf*
3402 *Aquitaine*, 20(1), 131–195.
3403
3404
3405
3406 Oliva-Urcia, B., Román-Berdiel, T., Casas, A.M., Pueyo, E.L., Osácar, C. (2010). Tertiary
3407 compressional overprint on Aptian-Albian extensional magnetic fabrics, North Pyrenean
3408 Zone. *Journal of Structural Geology*, 32, 362-376
3409
3410
3411
3412 Oliva-Urcia, B., Casas, A.M., Soto, R., Villalaín, J.J., Kodama, K. (2011). A transtensional basin
3413 model for the Organyà basin (central southern Pyrenees) based on magnetic fabric and brittle
3414 structures. *Geophysical Journal International*, 184, 111-130.
3415
3416
3417
3418 Oliva-Urcia, B., Román-Berdiel, T., Casas, A.M., Bógalo, M. F., Osácar, M. C., García-Lasanta, C.
3419
3420
3421
3422

- 3423
3424 (2013). Transition from extensional to compressional magnetic fabrics in the Cretaceous
3425 Cabuérniga basin (North Spain). *Journal of Structural Geology*, 46, 220-234.
3426
3427
3428 Omodeo-Salé, S., Salas, R., Guimerà, J., Ondrak, R., Mas, R., Arribas, J., Suárez-Ruiz, I., Martínez,
3429 L. (2017). Subsidence and thermal history of an inverted Late Jurassic-Early Cretaceous
3430 extensional basin (Camerós, North-central Spain) affected by very low to low-grade
3431 metamorphism. *Basin Research*, 51, 156-174, doi:10.1111/bre.12142
3432
3433
3434
3435
3436
3437 Passchier, C. W., (1984), Mylonite dominated footwall geometry in a shear zone, central Pyrénées,
3438
3439 *Geological Magazine*, 121, 429-436.
3440
3441
3442
3443
3444
3445
3446
3447
3448
3449
3450
3451
3452
3453
3454
3455
3456
3457
3458
3459
3460
3461
3462
3463
3464
3465
3466
3467
3468
3469
3470
3471
3472
3473
3474
3475
3476
3477
3478
3479
3480
3481
- Pedreira, D., Afonso, J. C., Pulgar, J. A., Gallastegui, J., Carballo, A., Fernández, M., García-Castellanos, D., Jiménez-Munt, I., Semprich, J. and García-Moreno, O. (2015). Geophysical-petrological modeling of the lithosphere beneath the Cantabrian Mountains and the North-Iberian margin: geodynamic implications, *Lithos*, 230(C), 46–68.
<http://doi.org/10.1016/j.lithos.2015.04.018>
- Philip, J. (1970) - Les formations calcaires à rudistes du Crétacé supérieur provençal et rhodanien. Thèse de Doctorat d'Etat, Marseille, 433 p.
- Philip, J., Masse, J. L., Machhour, L. (1987). L'évolution paleogeographique et structurale du front de chevauchement nord-toulonnais (Basse-Provence occidentale, France). *Bulletin de la Société géologique de France*, 3, 541-550.
- Pi, E., Solà, J., Montaner, J., Picart, J., Samsó, J.M., Calvet, F., Mato, E., Pujades, J., Saula, E., Caus, E. Berastegui, X. (1997). Geological map of Catalunya 1:25000. Sheet 258-1-1. Institut Cartogràfic i Geològic de Catalunya. Barcelona.
- Piana, F., A. Musso, C. Bertok, A. D'Atri, L. Martire, E. Perotti, D. Varrone, and G. Martinotti (2009), New data on post-Eocene tectonic evolution of the external Ligurian Briançonnais (Western Ligurian Alps), *Boll. della Soc. Geol. Ital.*, 128(2), 353–366, doi:10.3301/IJG.2009.128.2.353.
- Piana, F., S. Battaglia, C. Bertok, A. D'atri, A. Ellero, L. Leoni, L. Martire, and E. Perotti (2014),

- 3482
3483 Illite (KI) and chlorite (AI) “crystallinity” indices as a constraint for the evolution of the
3484 External Briançonnais Front in Western Ligurian Alps (NW Italy), *Ital. J. Geosci.*, 133(3),
3485 445–454, doi:10.3301/IJG.2014.21.
3486
3487
3488
3489 Puigdefàbregas, C., Souquet, P. (1986). Tecto-sedimentary cycles and depositional sequences of the
3490 Mesozoic and Tertiary from the Pyrenees. *Tectonophysics*, 129, 173-203.
3491
3492
3493 Pujadas, J., Casas, M. Muñoz, J.A., Sabat, F. (1989). Thrust tectonics and Paleogene syntectonic
3494 sedimentation in the Emporda area, southeastern Pyrenees. *Geodinamica Acta*, 3, 195-206.
3495
3496
3497 Rat, P. (1988), The Basque-Cantabrian basin between the Iberian and European plates: Some facts
3498 but still many problems, *Rev. la Soc. geológica España*, 1(3–4), 327–348.
3499
3500
3501 Rehault, J. P., J. Mascle, and G. Boillot (1984), Evolution géodynamique de la Méditerranée depuis
3502 l’Oligocene, *Mem. Soc. Geol. Ital*, 27, 85–96.
3503
3504
3505 Riedel, W., 1929. Zur mechanik geologischer brucherscheinungen, *Zentralblatt für Mineralogie.*
3506
3507
3508
3509
3510
3511 Geologie und Paläontologie 1929B, 354–368.
3512
3513 Roca, E., J. A. Muñoz, O. Ferrer, and N. Ellouz (2011), The role of the Bay of Biscay Mesozoic
3514 extensional structure in the configuration of the Pyrenean orogen: Constraints from the
3515 MARCONI deep seismic reflection survey, *Tectonics*, 30(2), n/a-n/a,
3516
3517
3518
3519
3520
3521
3522
3523
3524
3525
3526
3527
3528
3529
3530
3531
3532
3533
3534
3535
3536
3537
3538
3539
3540
- Rosenbaum, G., Lister, G. S. (2005). The Western Alps from the Jurassic to Oligocene: spatio-temporal constraints and evolutionary reconstructions. *Earth-Science Reviews*, 69(3-4), 281-306.
- Roure, F., Choukroune, P., Berastegui, X., Muñoz, J. A., Villien, A., Matheron, P., Bareyt, M., Seguret, M., Camara, P., Deramond, J. (1989). ECORS deep seismic data and balanced cross sections: Geometric constraints on the evolution of the Pyrenees. *Tectonics*, 8, 41-50, doi: 10.1029/TC008i001p00041
- Rouvier, H., Henry, B., Le Goff, M. (2012). Mise en évidence par le paléomagnétisme de rotations régionales dans la virgation des Corbières (France). *Bulletin de la Société géologique de*

- 3541
3542 France, 183, 409-424.
3543
3544 Royden, L., Keen, C.E. (1980). Rifting process and thermal evolution of the continental margin of
3545
3546 eastern Canada determined from subsidence curves. *Earth and Planetary Science Letters*, 51,
3547
3548 343-361.
3549
3550 Salardon, R., Carpentier, C., Bellahsen, N., Pironon, J., France-Lanord, C. (2017). Interactions
3551
3552 between tectonics and fluid circulations in an inverted hyper-extended basin: Example of
3553
3554 mesozoic carbonate rocks of the western North Pyrenean Zone (Chaînons Béarnais,
3555
3556 France). *Marine and Petroleum Geology*, 80, 563-586.
3557
3558
3559 Salas, R., Guimerà, J., Mas, R., Martín-Closas, C., Meléndez, A., Alonso, A. (2001). Evolution of
3560
3561 the Mesozoic central Iberian Rift System and its Cainozoic inversion (Iberian chain). In Peri-
3562
3563 Tethys memoir, 6: Peri-Tethyan Rift/Wrench Basins and Passive Margins (eds P. A. Ziegler,
3564
3565 W. Cavazza, A. H. F. Robertson & S. Crasquin-Soleau), *Mémoires de Muséum National*
3566
3567 *d'Histoire Naturelle*, 186, 145-186.
3568
3569
3570 Salas, R., Casas, A. (1993). Mesozoic extensional tectonics, stratigraphy and crustal evolution
3571
3572 during the Alpine cycle of the eastern Iberian basin. *Tectonophysics*, 228, 33-55.
3573
3574
3575 Saula, E., Mató, E., Montaner, J., Solà, J., Picart, J., Agustí, J., Lienas, M., Moya, S., Serra, J.,
3576
3577 Caus, E. (1994). Geological map of Catalunya 1:25000. Sheet 296-2-2. Institut Cartogràfic i
3578
3579 Geològic de Catalunya. Barcelona.
3580
3581
3582 Saura, E., Ardèvol i Oró, L., Teixell, A., Vergés, J. (2016). Rising and falling diapirs, shifting
3583
3584 depocenters, and flap overturning in the Cretaceous Sopeira and Sant Gervàs subbasins
3585
3586 (Ribagorça Basin, southern Pyrenees). *Tectonics*, 35, 638-662.
3587
3588
3589 Schlunegger, F., Kissling, E. (2015). Slab rollback orogeny in the Alps and evolution of the Swiss
3590
3591 Molasse basin. *Nature communications*, 6, 8605.
3592
3593
3594 Schmid, S. M., Kissling, E. (2000), The arc of the western Alps in the light of geophysical data on
3595
3596 deep crustal structure. *Tectonics* 19, 62-85.
3597
3598
3599 Schmid, S. M., O. A. Pfiffner, N. Froitzheim, G. Schönborn, and E. Kissling (1996), Geophysical-

- 3600 geological transect and tectonic evolution of the Swiss-Italian Alps, *Tectonics*, 15(5), 1036–
3601 1064, doi:10.1029/96TC00433.
3602
3603
3604
3605 Schmid, S. M., B. Fügenschuh, E. Kissling, and R. Schuster (2004), Tectonic map and overall
3606 architecture of the Alpine orogen, *Eclogae Geol. Helv.*, 97(1), 93–117, doi:10.1007/s00015-
3607 004-1113-x.
3608
3609
3610
3611 Sengör, A. M., Burke, K. (1978). Relative timing of rifting and volcanism on Earth and its tectonic
3612 implications. *Geophysical Research Letters*, 5, 419-421.
3613
3614
3615
3616 Septfontaine, M., 1995. Large scale progressive unconformities in Jurassic strata of the Prealps S of
3617 lake Geneva. Interpretation as synsedimentary inversion structures; paleotectonic
3618 implications. *Eclogae Geol. Helv.* 88, 553–576
3619
3620
3621
3622 Séranne, M. (1999), The Gulf of Lion continental margin (NW Mediterranean) revisited by IBS: an
3623 overview, *Geol. Soc. London, Spec. Publ.*, 156(1), 15–36,
3624 doi:10.1144/GSL.SP.1999.156.01.03.
3625
3626
3627
3628 Séranne, M., A. Benedicto, P. Labaum, C. Truffert, and G. Pascal (1995), Structural style and
3629 evolution of the Gulf of Lion Oligo-Miocene rifting: role of the Pyrenean orogeny, *Mar. Pet.*
3630 *Geol.*, 12(8), 809–820, doi:10.1016/0264-8172(95)98849-Z.
3631
3632
3633
3634 Sibuet, J.-C., S. P. Srivastava, and W. Spakman (2004), Pyrenean orogeny and plate kinematics, *J.*
3635 *Geophys. Res. Solid Earth*, 109(B8), doi:10.1029/2003JB002514.
3636
3637
3638
3639 Souque, C., Robion, P., Frizon de Lamotte, D., 2002. Cryptic magnetic fabric of tectonic origin
3640 revealed by heating of sedimentary samples from the Corbières, France. *Physics and*
3641 *Chemistry of the Earth*, 27, 1253–1262.
3642
3643
3644
3645 Soto, R., Casas-Sainz, A.M., Villalain, J.J., Gil-Imaz, A., Fernández-González, G., Del Río, P.,
3646 Calvo, M., Mochales, T. (2008). Characterizing the Mesozoic extension direction in the northern
3647 Iberian Plate margin by anisotropy of magnetic susceptibility (AMS). *Journal of the Geological*
3648 *Society of London* 165, 1007-1018.
3649
3650
3651
3652
3653
3654
3655
3656
3657
3658

- 3659
3660 Manivit H., Peybernès B. (1985). Le groupe du Flysch noir (albo-cénomanién) dans les
3661 Pyrénées. *Bull. Centres Rech. Explor. Prod. Elf-Aquitaine*, 9, 183-252
3662
3663
3664 Stampfli, G. M., Mosar, J., Marquer, D., Marchant, R., Baudin, T., Borel, G. (1998). Subduction
3665 and obduction processes in the Swiss Alps. *Tectonophysics*, 296(1-2), 159-204.
3666
3667
3668 Stampfli, G. M., & Borel, G. D. (2002). A plate tectonic model for the Paleozoic and Mesozoic
3669 constrained by dynamic plate boundaries and restored synthetic oceanic isochrons. *Earth and*
3670 *Planetary Science Letters*, 196(1), 17-33.
3671
3672
3673 Stampfli, G. M., & Hochard, C. (2009). Plate tectonics of the Alpine realm. *Geological Society,*
3674 *London, Special Publications*, 327(1), 89–111. <http://doi.org/10.1144/SP327.6>
3675
3676
3677 Sylvester, A. G. (1988). Strike-slip faults. *Geological Society of America Bulletin*, 100, 1666-1703.
3678
3679
3680 Tassone, A., Roca, E., Muñoz, J.A., Cabrera, L., Canals, M. (1994). Evolución del sector
3681 septentrional del margen continental catalán durante el Cenozoico. *Acta geológica hispánica,*
3682 *29*, 3-37.
3683
3684
3685
3686
3687
3688 Tavani, S., Mencos, J., Bausà, J., Muñoz, J.A. (2011). The fracture pattern of the Sant Corneli
3689 Bóixols oblique inversion anticline (Spanish Pyrenees). *Journal of Structural Geology*, 33,
3690 1662-1680.
3691
3692
3693
3694 Tavani, S., Muñoz, J.A., (2012). Mesozoic rifting in the Basque–Cantabrian Basin (Spain):
3695 inherited faults, transversal structures and stress perturbation. *Terra Nova*, 24, 70-76.
3696
3697
3698
3699 Tavani, S., and P. Granado (2015), Along-strike evolution of folding, stretching and breaching of
3700 supra-salt strata in the Plataforma Burgalesa extensional forced fold system (northern Spain),
3701 *Basin Res.*, 27(4), 573–585, doi:10.1111/bre.12089.
3702
3703
3704
3705 Tchalenko, J. S. (1970), Similarities between Shear Zones of Different Magnitudes, *Geol. Soc. Am.*
3706 *Bull.*, 81(6), 1625, doi:10.1130/0016-7606(1970)81[1625:SBSZOD]2.0.CO;2.
3707
3708
3709
3710 Teixell, A. (1998). Crustal structure and orogenic material budget in the west central Pyrenees,
3711 *Tectonics*, 17, 395-406, doi:10.1029/98TC00561
3712
3713
3714
3715
3716
3717

- 3718
3719 revisited: Inferences from a new kinematic scenario. *Comptes Rendus Geoscience*, 348, 257-
3720
3721 267.
3722
- 3723 Thinon, I., Réhault, J.P., Fidalgo-González, L. (2002). The syn-rift sedimentary cover of the North
3724 Biscay Margin (bay of Biscay): From new reflection seismic data. *Bulletin de la Société*
3725
3726 *Géologique de France*, 173, 515-522.
3727
3728
- 3729 Thinon, I., Matias, L., Réhault, J.P., Hirn, A., Fidalgo-González, L., Avedik, F. (2003). Deep
3730 structure of the Armorican Basin (Bay of Biscay): A review of Norgasis seismic reflection
3731 and refraction data. *Journal of the Geological Society of London*, 160, 99-116.
3732
3733
3734
3735
- 3736 Thomas, J. C., M. E. Claudel, M. Collombet, P. Tricart, A. Chauvin, and T. Dumont (1999), First
3737 paleomagnetic data from the sedimentary cover of the French Penninic Alps: evidence for
3738 Tertiary counterclockwise rotations in the Western Alps, *Earth Planet. Sci. Lett.*, 171(4), 561–
3739 574, doi:10.1016/S0012-821X(99)00182-X.
3740
3741
3742
3743
- 3744 Tugend, J., G. Manatschal, N. J. Kusznir, E. Masini, G. Mohn, and I. Thinon (2014), Formation and
3745 deformation of hyperextended rift systems: Insights from rift domain mapping in the Bay of
3746 Biscay-Pyrenees, *Tectonics*, 33(7), 1239–1276, doi:10.1002/2014TC003529.
3747
3748
3749
3750
- 3751 Tugend, J., Manatschal, G., Kusznir, N. (2015). Spatial and temporal evolution of hyperextended
3752 rift systems: Implication for the nature, kinematics, and timing of the Iberian-European plate
3753 boundary. *Geology*, 43, 15-18.
3754
3755
3756
- 3757 van der Beek, P.A., Cloetingh, S., Andriessen, P.A.M., 1994. Extensional basin formation
3758 mechanisms and vertical motion of rift flanks: constraints from tectonic modelling and
3759 fission-track thermochronology. *Earth Planet. Sci. Lett.* 121, 417 – 433.
3760
3761
3762
3763
- 3764 van der Voo, R. (1969). Paleomagnetic evidence for the rotation of the Iberian Peninsula,
3765 *Tectonophysics*, 7, 5-56.
3766
3767
- 3768 Vanossi, M. (1969). La serie Brianzese del Salto del Lupo (Liguria occidentale): osservazioni
3769 sedimentologico-stratigrafiche. *Atti Ist. Geol. Univ. Pavia*, 20, 3-16.
3770
3771
- 3772 Vanossi, M. (1972). Rilevamento geologico ed analisi strutturale delle dorsali del M. Mongioie e
3773
3774
3775
3776

3777
3778 del M. Cimone. *Atti Ist. Geol. Univ. Pavia*, 23, 29-71.
3779

3780 Vauchez, A., Clerc, C., Bestani, L., Lagabrielle, Y., Chauvet, A., Lahfid, A., Mainprice, D. (2013).
3781

3782 Preorogenic exhumation of the North Pyrenean Agly massif (Eastern Pyrenees France).
3783

3784 *Tectonics*, 32(2), 95-106.
3785

3786 Vergés, J., García-Senz, J. (2001). Mesozoic evolution and Cainozoic inversion of the Pyrenean rift.
3787

3788 *Mémoires du Muséum national d'histoire naturelle*, 186, 187-212.
3789

3790 Vergés, J., M. Fernández, and A. Martínez (2002), The Pyrenean orogen: pre-, syn-, and post-
3791

3792 collisional evolution, *J. Virtual Explor.*, 8, 57–76.
3793

3794 Vielzeuf, D. and Kornprobst, J. (1984). Crustal splitting and the emplacement of Pyrenean
3795

3796 lherzolites and granulites, *Earth Planet. Science Lett.*, 67, 87–96.
3797

3798 Vissers, R.L. M., and P. T. Meijer (2012), Mesozoic rotation of Iberia: Subduction in the
3799

3800 Pyrenees?, *Earth-Science Rev.*, 110(1–4), 93–110, doi:10.1016/j.earscirev.2011.11.001.
3801

3802 Vissers, R. L., van Hinsbergen, D. J., Van Der Meer, D. G., Spakman, W. (2016). Cretaceous slab
3803

3804 break-off in the Pyrenees: Iberian plate kinematics in paleomagnetic and mantle reference
3805

3806 frames. *Gondwana Research*, 34, 49-59.
3807

3808 Wilson, J.T., 1965, A new class of faults and their bearing on continental drift, *Nature*, 207, 343-
3809

3810 347.
3811

3812 Ziegler, P.A., Cloetingh, S. (2004). Dynamic processes controlling evolution of rifted basins. *Earth-
3813*

3814 *Science Reviews*, 64, 1-50.
3815
3816
3817
3818
3819
3820
3821
3822
3823
3824
3825
3826
3827
3828
3829
3830
3831
3832
3833
3834
3835

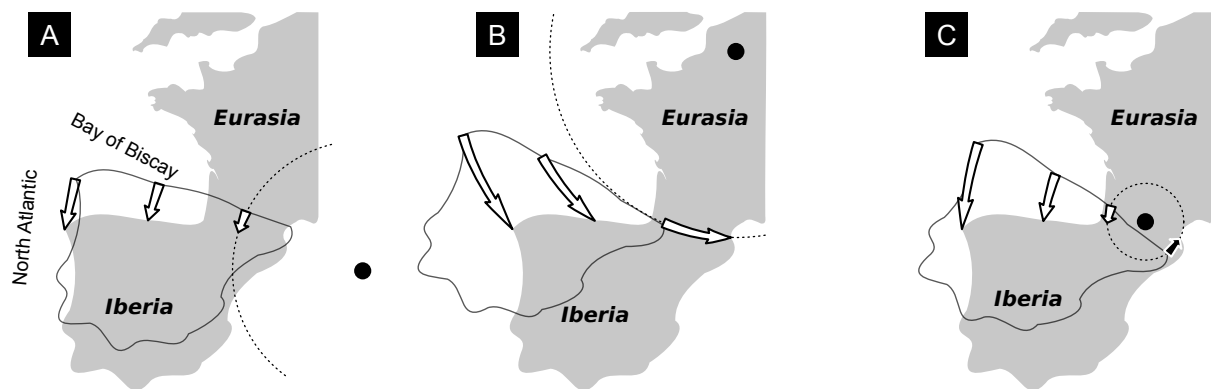


Figure 1 (Two columns)

Kinematic models proposed in the early 70's to explain the opening of the Bay of Biscay. The motion of Iberia with respect to fixed Eurasia is described by its rigid rotation about an Euler's pole located: (A) to the east of Iberia, (B) near Paris, (C) in the Pyrenean mountain range. Modified from Choukroune et al. (1973).

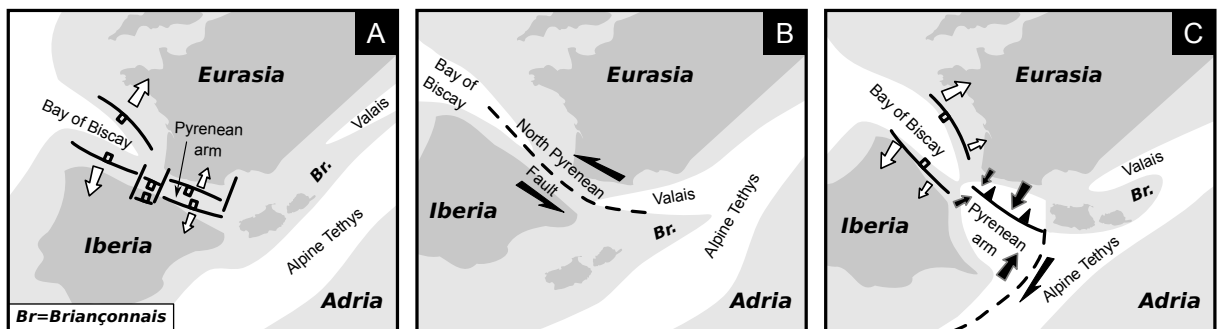


Figure 2 (Two columns)

Reconstructions of the Iberia-Eurasia margin and surrounding regions at the mid-Cretaceous time. (A) rift-perpendicular scenario, after Manatschal and Müntener (2009). (B) Strike-slip scenario, after Stampfli and Borel (2002). (C) Scissor scenario, after Advokaat et al., (2014).

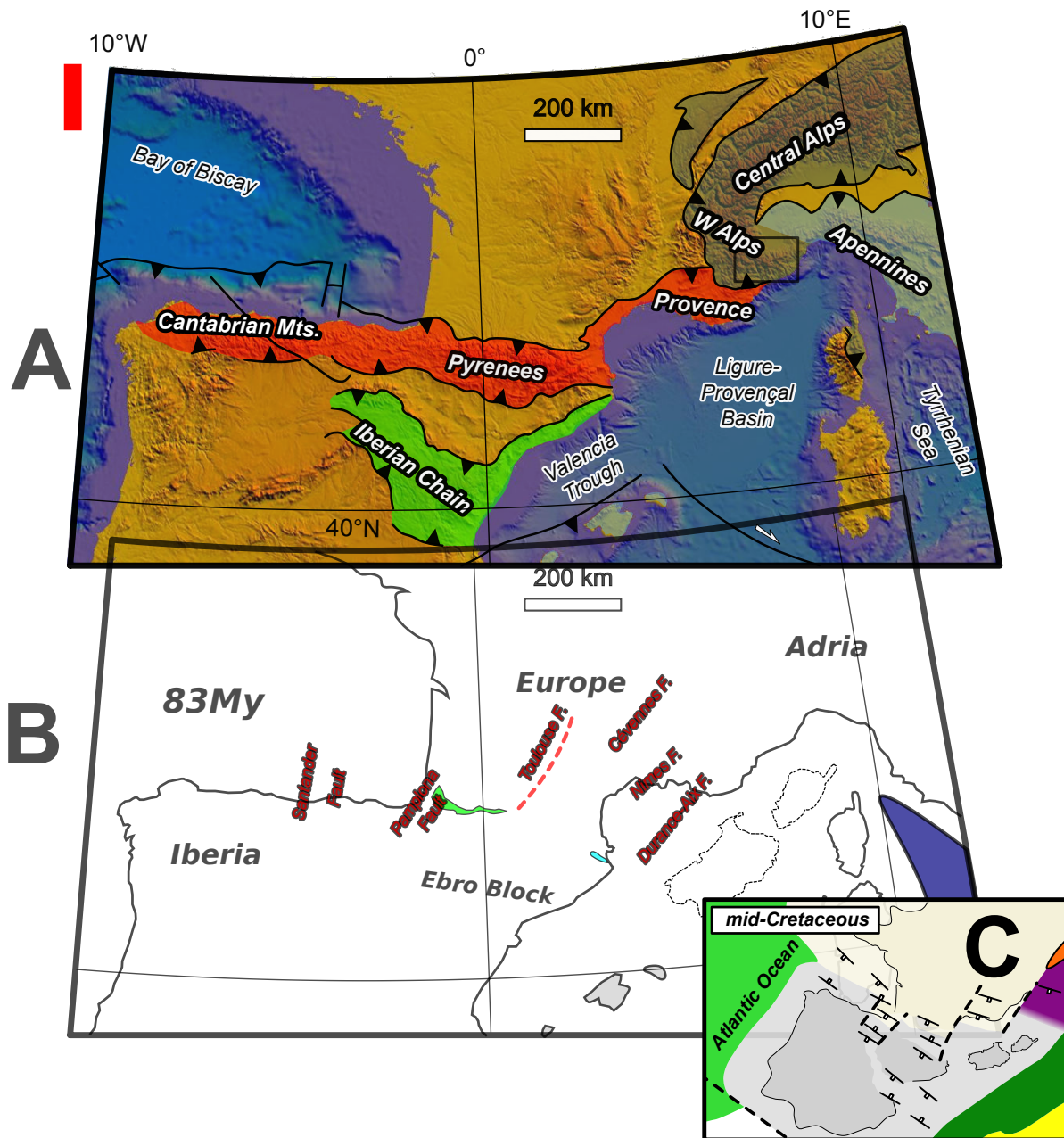


Figure 3 (Two columns)

Tectonic map of the westernmost Europe, with Late Cretaceous - Cenozoic belts and basins (A), and Mesozoic domains (B), with focus on the architecture of the Bay of Biscay – Pyrenean rift system. The distribution of Mesozoic domains is modified after Tugend et al. (2015) for the Bay of Biscay-Pyrenean area, and from Handy et al., (2010) for the Alps-Apennines area. The position of the Corsica-Sardinia block before the opening of the Ligure-Provençal basin is from Bache et al., (2010). (C) Reconstruction of the Iberia-Eurasia margin and surrounding domains in the mid-Cretaceous, modified from Manatschal and Müntener (2009)

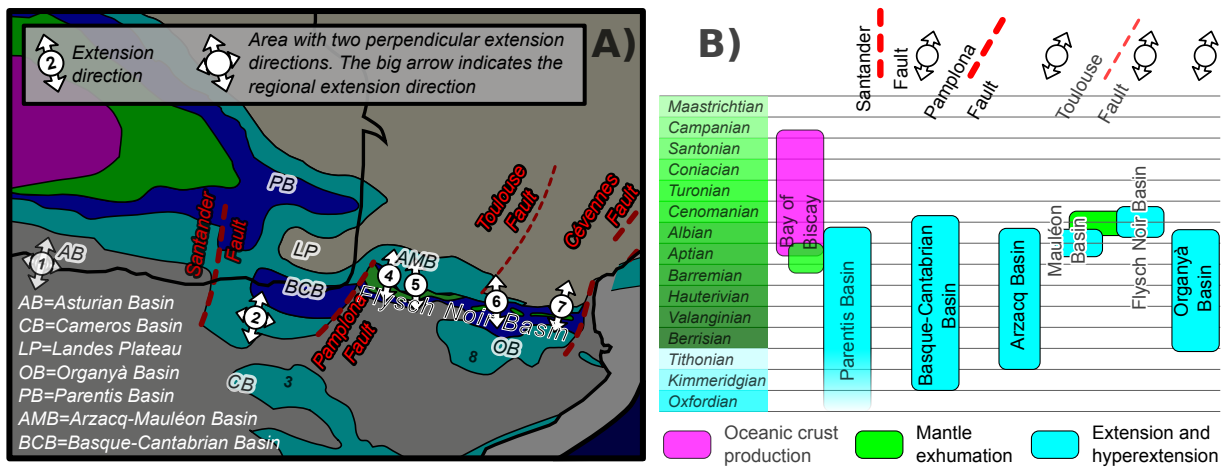


Figure 4 (Two columns)

Crataceous extensional structures in the Pyrenean Arm. (A) Detail of the map in figure 3b in the Pyrenean area, with orientation of Crataceous extension indicated. (B) Table illustrating the timing of major events and the direction of extensional structures in the different domains of the Pyrenean Arm and surrounding areas. References cited in the text and/or indicated in the figure are: Tugend et al. (2014) for the age of the oceanic crust in the Bay of Biscay. Thinon et al. (2003) and Roca et al. (2011) for the age of mantle exhumation in the Bay of Biscay. Ferrer et al. (2008) for the age of extension and hyperextension in the Parentis Basin. García-Mondéjar et al. (1986) and Rat (1988) for the age of extension in the Basque-Cantabrian Basin. Biteau et al. (2006) for the age of extension in the Arzacq Basin. Jammes et al. (2009), Lagabrielle et al. (2010), and Masini et al. (2014) for the age of hyperextension and mantle exhumation in the Mauléon Basin. Souquet et al. (1985) and Debros (1990) for the age of extension and hyperextension in the Flysch Noir Basin. Dinarès-Turell and García-Senz (2000) and García-Senz (2002) for the age of extension in the Organyà basin. Granado et al. (In press) for the extension direction (meso-structural data) in the Asturian basin (indicated as site 1). Soto et al. (2008) and Oliva-Urcia et al. (2013) (AMS data), and Tavani and Muñoz (2012) (meso- and macro-structural data) for the extension direction in the Basque-Cantabrian basin (indicated as site 2). Soto et al. (2008) and García-Lasanta et al. (2014) (AMS), and Mata et al. (2001) (meso-structural data) for the extension direction in the Cameros basin (indicated as site 3). Lagabrielle et al. (2010) for the extension direction (meso-structural data) in the Mauléon extensional detachment (indicated as site 4). Salardon et al. (2017) (meso-structural data) and Olivia-Urcia et al. (2010) (AMS) for the extension direction in the Mauléon basin (indicated as site 5). Passchier (1984) and de Saint Blanquat et al. (1986 and 1990) for the extension direction (meso-structural data) in the Saint Barthélémy massif extensional detachment (indicated as site 6). Vauchez et al. (2013) for the extension direction (meso-structural data) in the Agly massif extensional detachment (indicated as site 7). Gong et al. (2009) and Oliva-Urcia et al. (2011) (AMS data), and Tavani et al. (2011) (meso- and macro-structural data) for the extension direction in the Organyà basin (indicated as site 8).

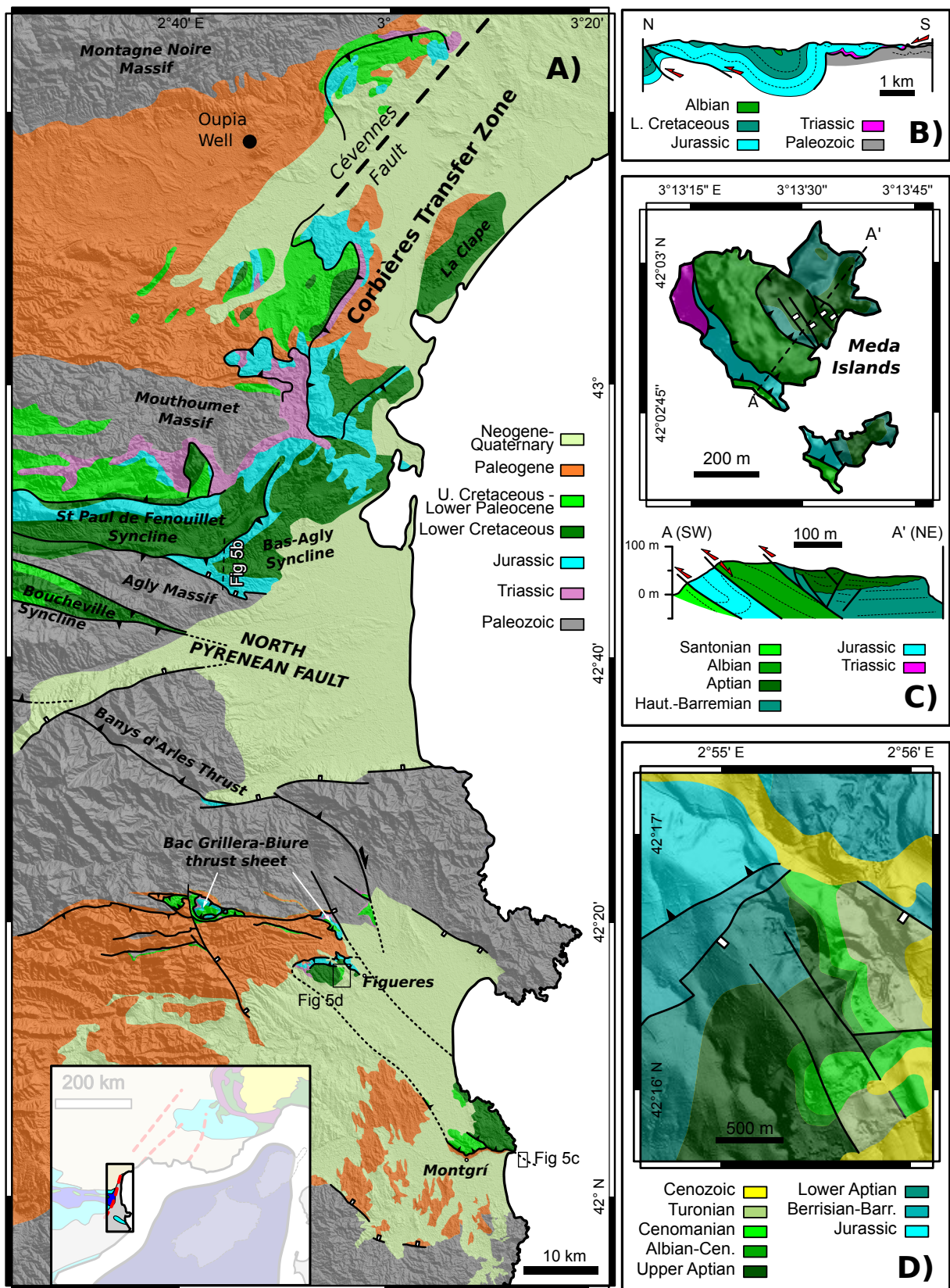


Figure 5
 (A) Geological map of the eastern Pyrenees. (B) Cross section across the Bas Agly syncline (after Vauchez et al., 2013). (C) Cross section across the Meda Islands of the Montgrí area (after Mató et al., 1995b). (D) Geological map of the Figueres area.

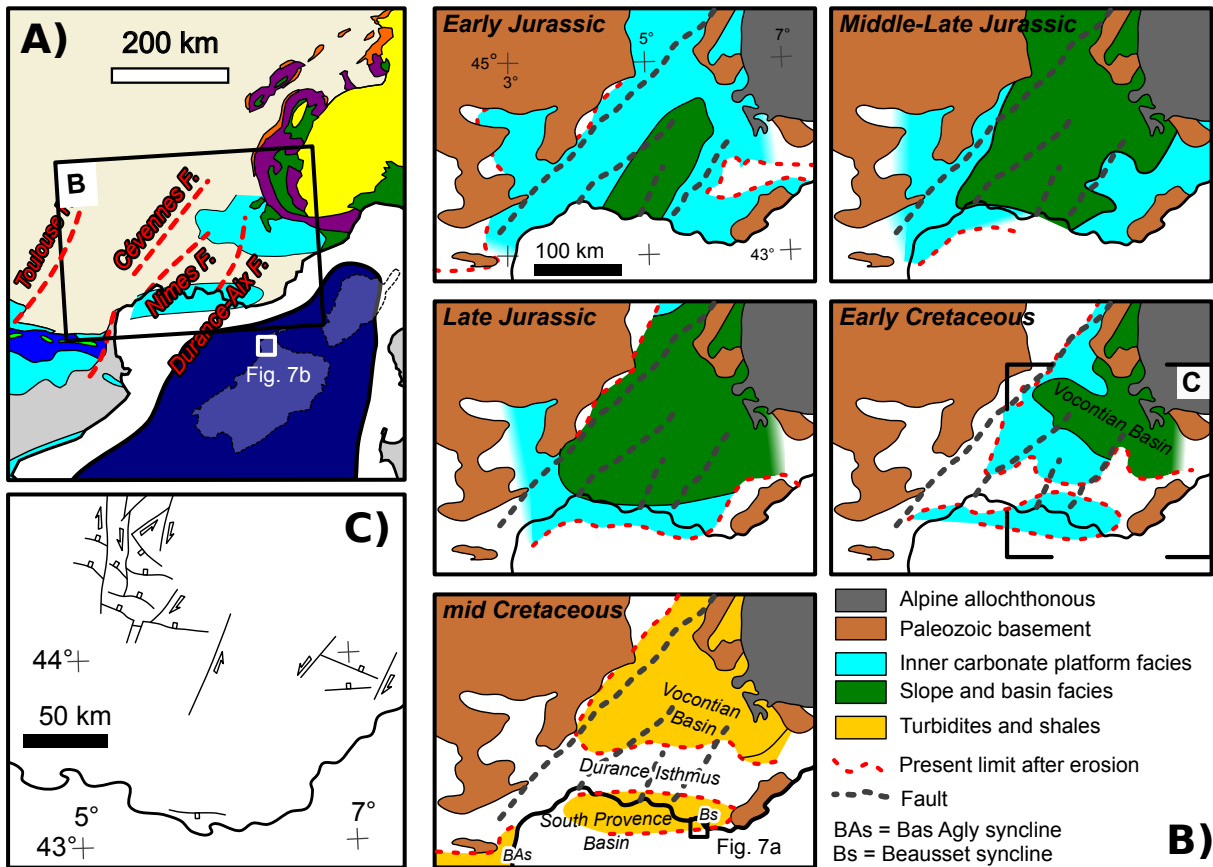


Figure 6 (Two columns)

(A) Detail of the map in figure 3b, showing the location of the Late Jurassic - Cretaceous extensional structures developed on the European margin of the Alpine Tethys, and presently exposed in the central and western Alps, in the Provence region of the Pyrenean System, and in Sardinia (B) Facies distribution in the SE Basin of France, from Triassic to mid-Cretaceous (after Curnelle and Dubois, 1986). (C) Simplified Early Cretaceous structural scheme of the SE Basin of France, with major faults indicated (after de Graciansky and Lemoine, 1988).

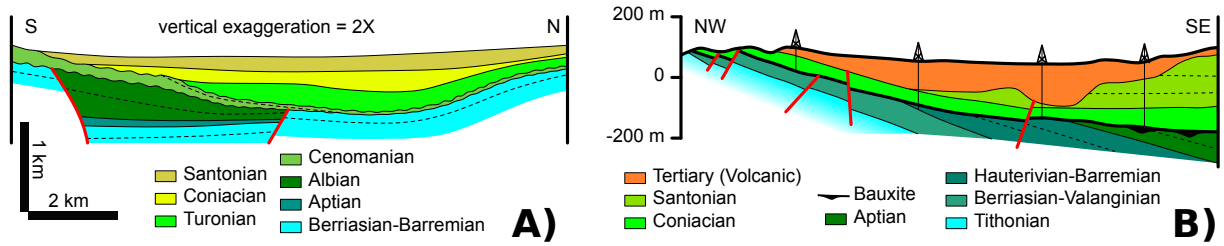


Figure 7 (Two columns)

(A) Schematic cross-section of the southern margin of the South Provence basin (after Philip et al. (1987)). (B) Cross-section of the Olmedo area in Sardinia (after Mameli et al. 2007).

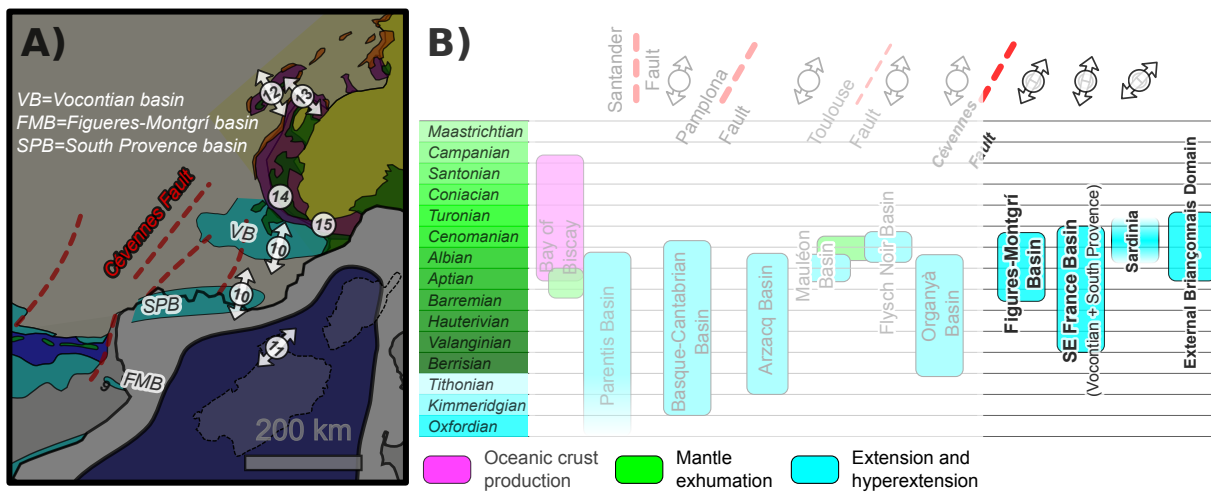


Figure 8 (Two columns)

Cretaceous extensional structures in eastern Pyrenees and SE France basin. (A) Detail of the map in figure 3b in the area, with orientation of Cretaceous extension indicated. (B) Table illustrating the timing of major events and the direction of extensional structures in the different domains, with data from the Bay of Biscay - Pyrenean Arm in transparency. References cited in the text and/or indicated in the figure are: Saula et al. (1994) and Mató et al. (1995a, 1995b) for the age of extension in the Figueres-Montgrí basin. Guyonnet-Benaize et al. (2010) and Masse et al. (2009) for the age of extension in the Vocontian and South Provence basins. Mameli et al. (2007) for the age of extension in the Olmedo area of Sardinia. Mató et al. (1995b) for the extension direction (syn-sedimentary faults orientation) in the Figueres-Montgrí (indicated as site 9). Guyonnet-Benaize et al. (2010), Lamarche et al. (2012), and Homberg et al. (2013) (meso-structures), and de Graciansky and Lemoine (1988) (major faults) for the extension direction in the Vocontian and South Provence basins (both indicated as site 10). Mameli et al. (2007) (orientation of an extensional fold) for the extension direction in the Olmedo area of Sardinia (indicated as site 11). Septfontaine (1995) for the age and direction (orientation of major fault) of extension in the Helvetic domain (indicated as site 12). Cardello and Mancktelow (2014) for the age and direction (meso- and macro-structures) of extension in the Helvetic domain (indicated as site 13), notice that this could be a gravitational-structure. Chaulieu (1992), Claudel et al. (1997), and Claudel and Dumont (1999) for the age of extension in the external Briançonnais Domain of the Western Alps (indicated as site 14).

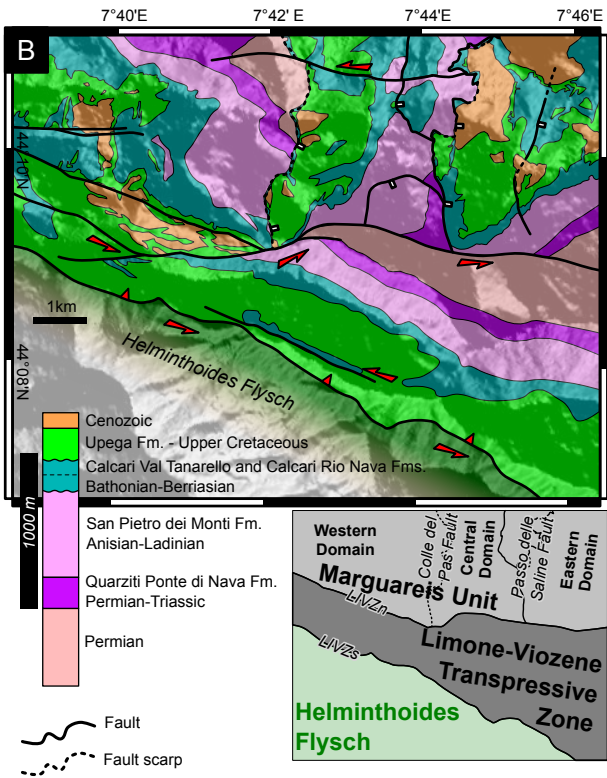
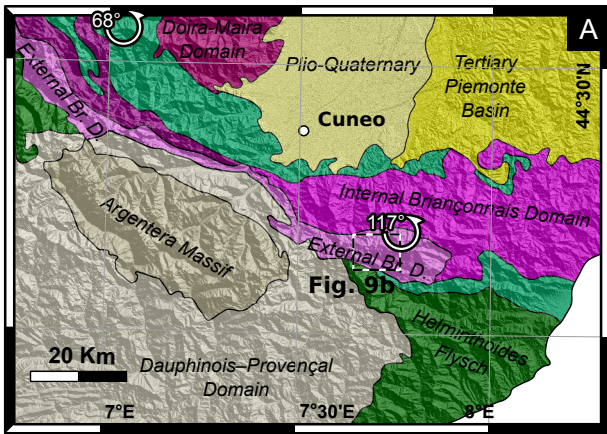


Figure 9 (Single column)

Geological maps of the Marguareis area. (A) Map of the western Alps (modified from d’Atri et al., 2015), with inset showing the location of figure 9b. The arrows indicate counter-clockwise rotations about vertical axes (from Collombet et al., 2002). (B) Map of the Marguareis area (from Bertok et al., Submitted), with structural scheme.

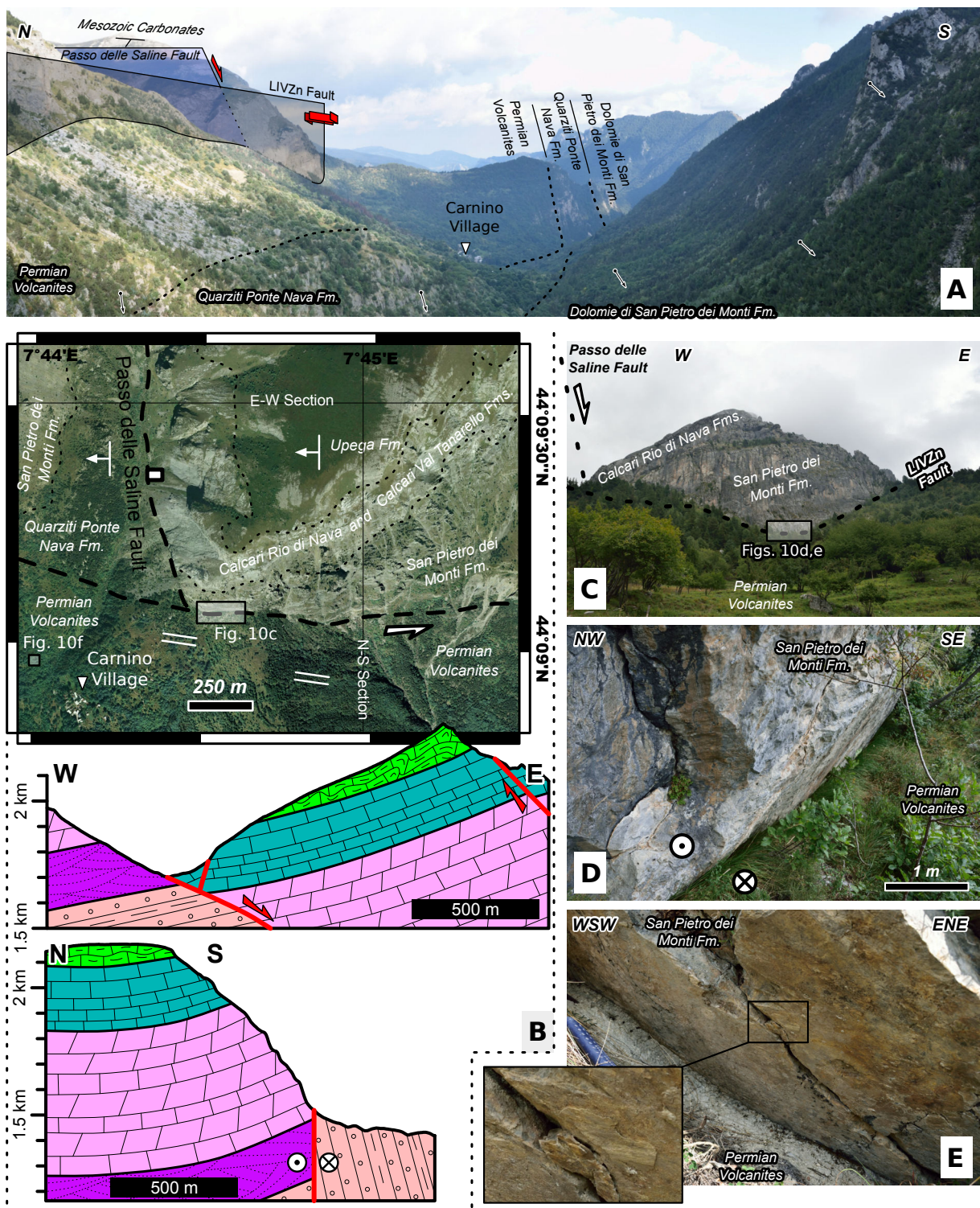


Figure 10 (Two columns)

Limone-Viozene northern (LIVZn) Fault in the eastern portion of the study area. (A) Panoramic view, from the west, of the LIVZn Fault, showing south-dipping Permo-Triassic rocks exposed in the southern block, and Triassic to Jurassic carbonates of the northern block, faulted by the Passo delle Saline Fault. (B) Orthophoto with structural scheme of the area and location of photographs and E-W and N-S oriented geological cross-sections (C) Panoramic view of the northern block of the LIVZn Fault: W-dipping Triassic and Jurassic carbonates are in the hanging-wall of the E-Dipping Passo delle Saline Fault, which abut onto the LIVZn Fault. (D) Principal displacement zone of the LIVZn Fault, with Permian Volcanites and Triassic dolostones in the southern and northern block, respectively. (E) Detail of the fault, showing calcite slicken-fibers indicating a left-lateral kinematics.

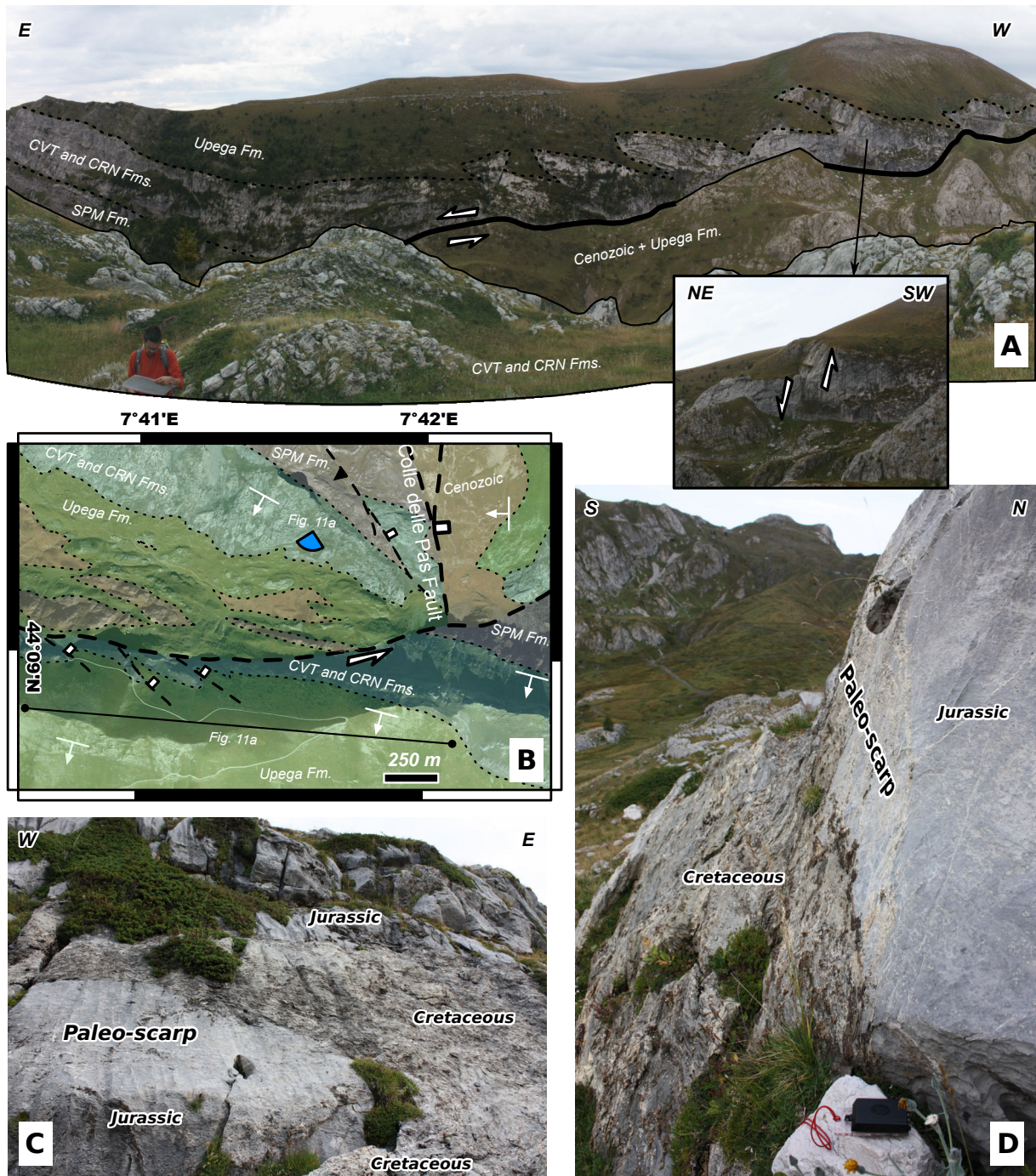


Figure 11 (Two columns)

Details of the LIVZn Fault in the western portion of the study area. (A) View from the north of the fault (for location of the photograph see Fig. 11b), with inset photograph showing a NW-SE striking normal fault in the southern block of the fault. (B) Orthophoto with structural scheme of the area and location of photographs. (C) and (D) E-W striking faults palaeoescarpment in Jurassic carbonates covered by patches of mid-Cretaceous sediments.

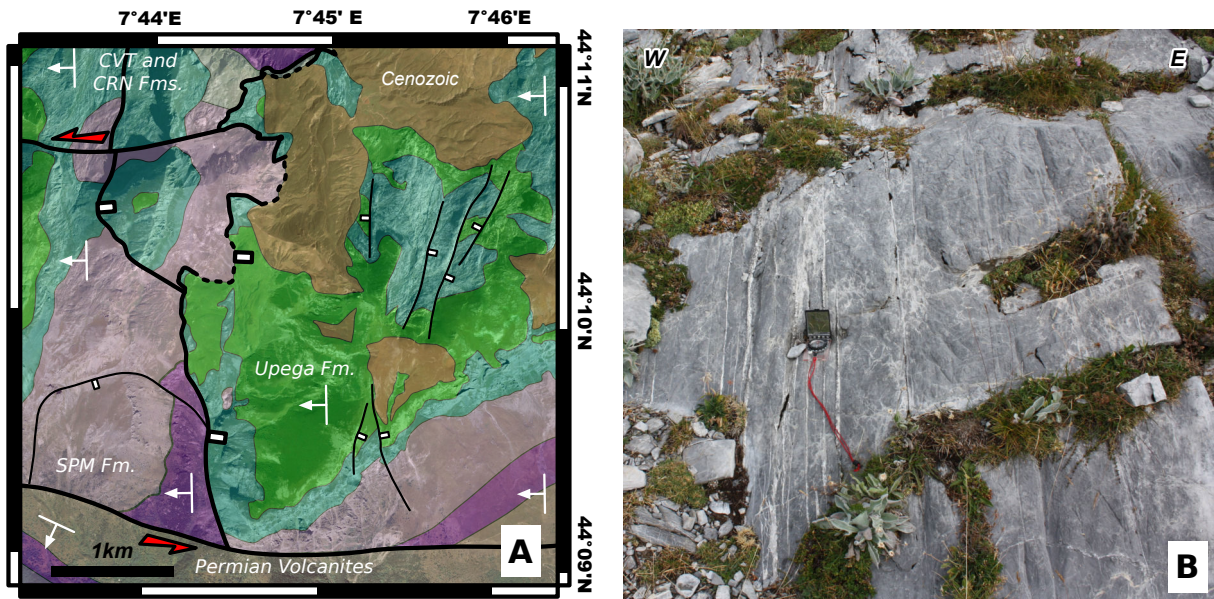


Figure 12 (Two columns)

(A) Orthophoto with structural scheme of the Passo delle Saline Fault area, showing hundreds of meters long N-S striking extensional faults.
 (B) N-S striking veins affecting Jurassic carbonates.

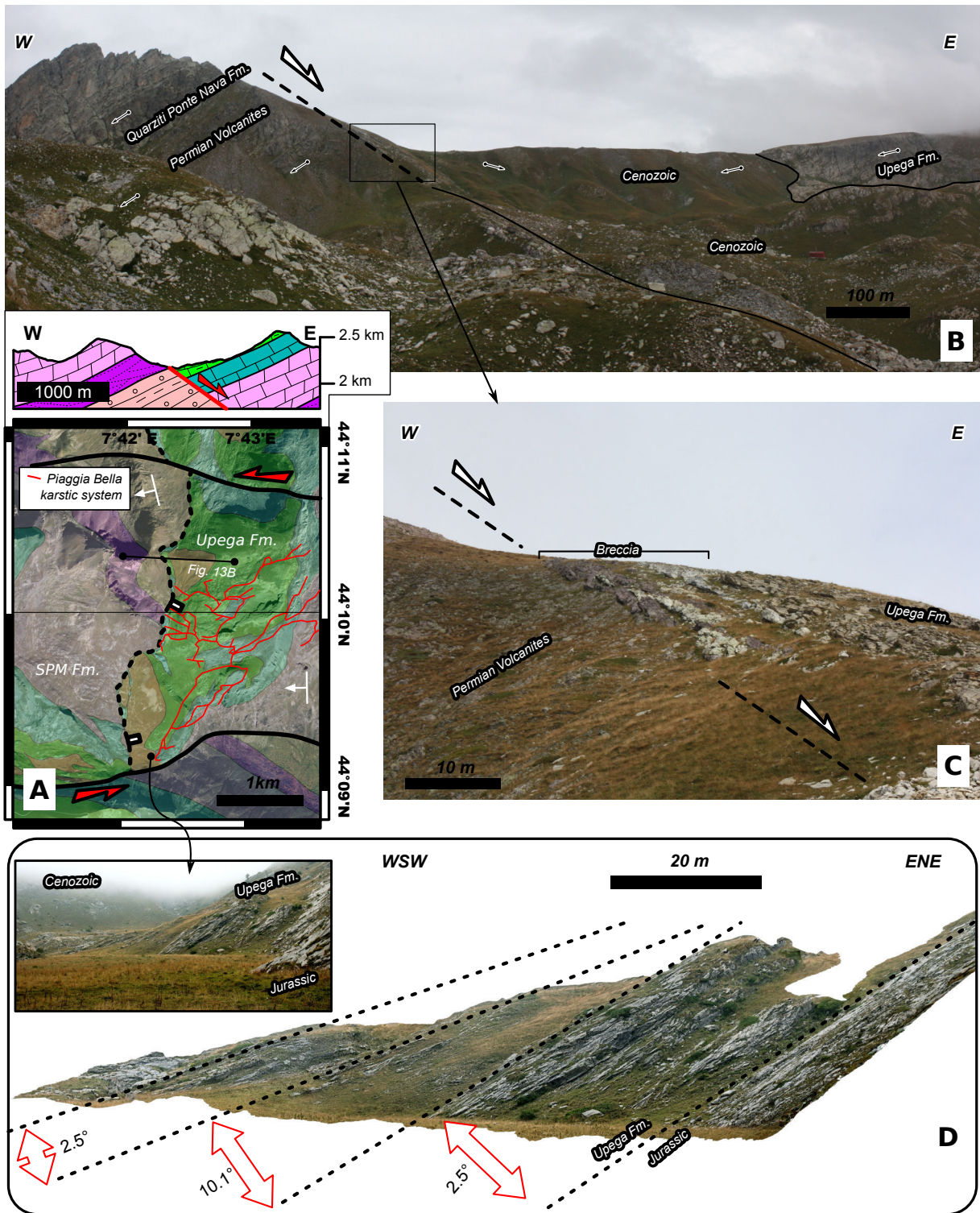


Figure 13 (Two columns)

(A) Orthophoto with structural scheme of the Colle del Pas Fault area and geological cross-section. (B) View from the south of the fault, with W-dipping Permo-Triassic rock in the footwall and sub-horizontal to slightly W-dipping Upper Cretaceous and Cenozoic rocks in the hanging-wall. (C) Detail of the fault showing Permian volcanites underlying a 5-m thick breccia, which in turn is overlapped by Upper Cretaceous marls of the Upega Fm.. (D) Three-dimensional virtual outcrop model of the lower portion of the Upega Fm, built by means of multi-view photographs (see Tavani et al., 2016 details). The model is seen in orthographic view along a direction perpendicular to beddings, thus representing a distortion-free properly oriented cross-section of the outcrop, and shows a growth wedge of 15° in the lowermost portion of the Upega Fm.

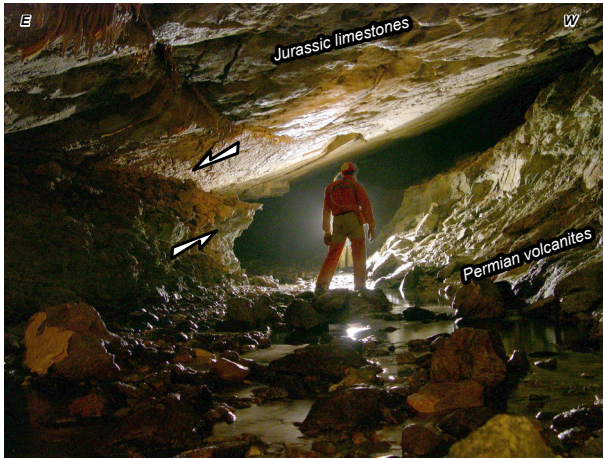


Figure 14 (Single column)
Photograph of Colle del Pas Fault plane as seen in the Piaggia Bella Karstic system.

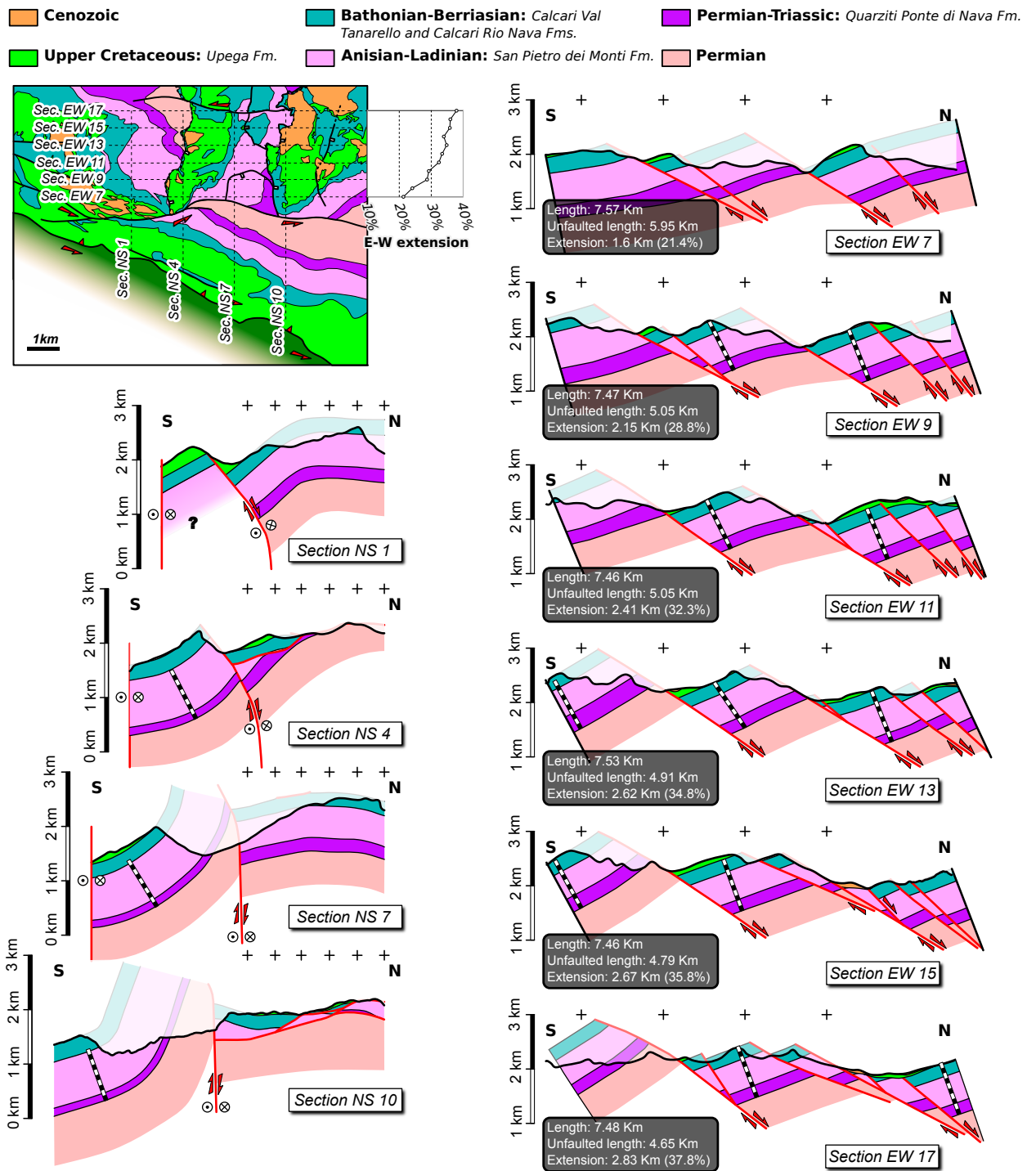


Figure 15 (Two columns)
E-W and N-S oriented cross-sections across the Marguareis extensional system. See text for details.

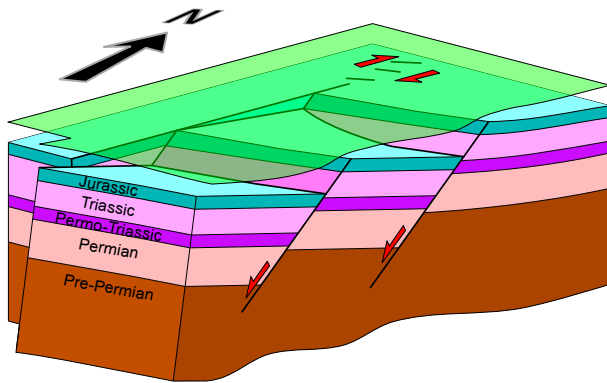


Figure 16 (Single column)
3D scheme illustrating the geometry of the Marguareis Extensional System at early Late Cretaceous.

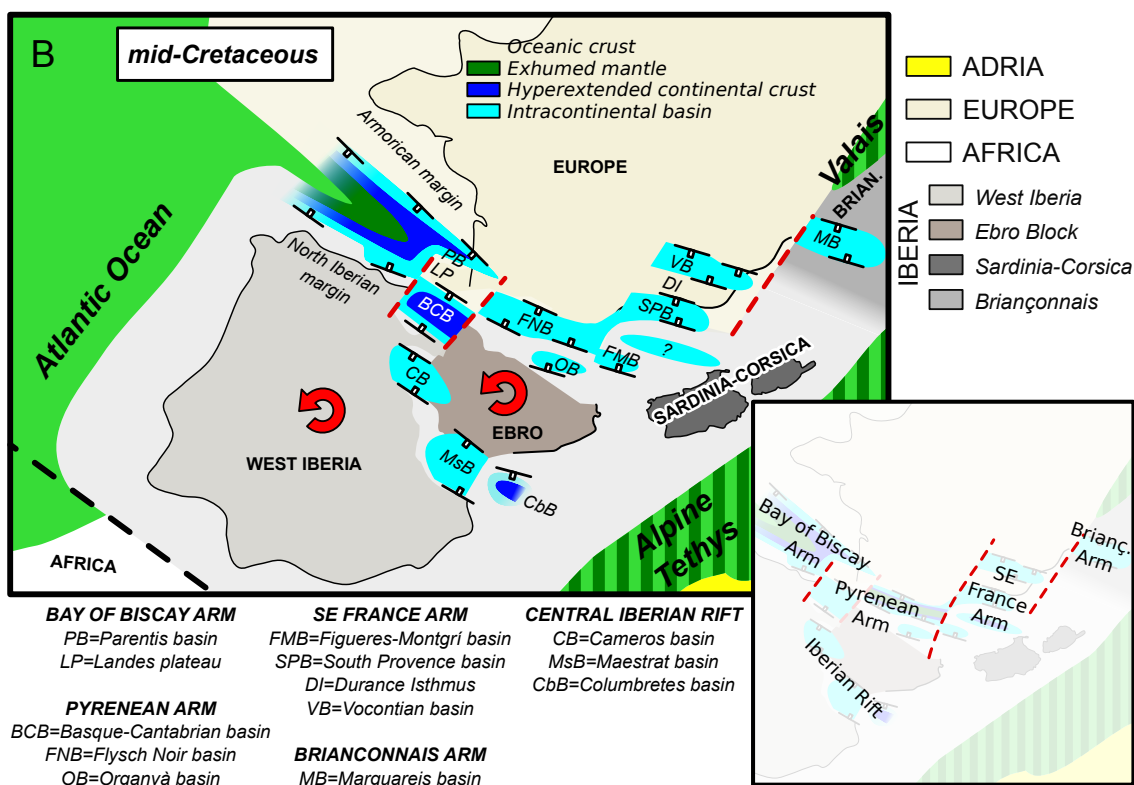
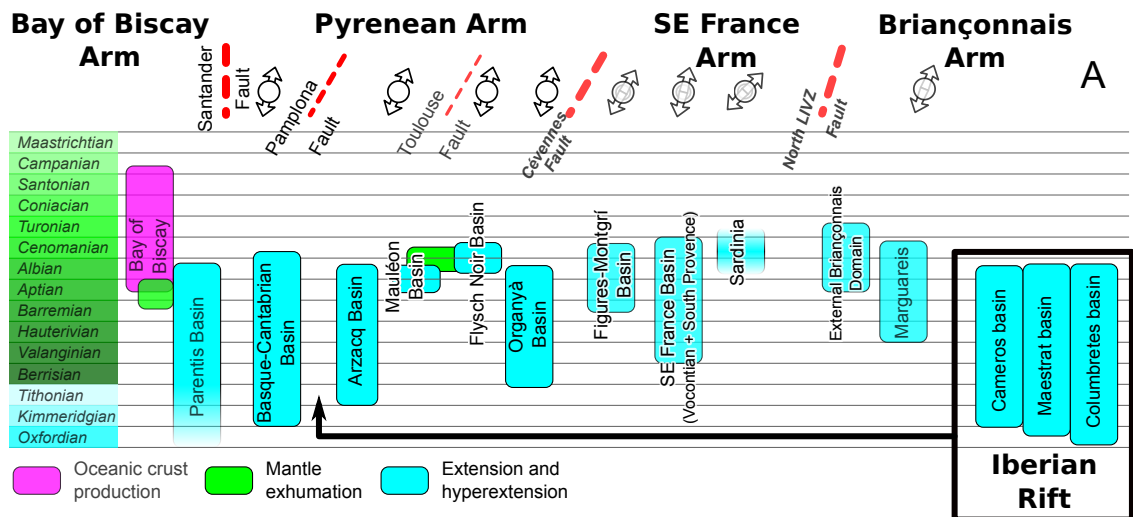


Figure 17
 (A) Table illustrating the timing of major events and the direction of extensional structures in the different domains of the study area. (B) Reconstruction of the Iberia-Eurasia margin and surrounding areas in the mid-Cretaceous times, with major basins, transform faults, and crustal domains indicated.